

**Integral Test of JENDL-3.3 Based on Shielding Benchmarks  
Shielding Integral Test Working Group (FY2006-2010)  
Japanese Nuclear Data Committee**

---

Nuclear Science and Engineering Center

Nuclear Science Research Institute  
Sector of Nuclear Science Research

JAEA  
Research

本レポートは国立研究開発法人日本原子力研究開発機構が不定期に発行する成果報告書です。  
本レポートの入手並びに著作権利用に関するお問い合わせは、下記あてにお問い合わせ下さい。  
なお、本レポートの全文は日本原子力研究開発機構ホームページ (<https://www.jaea.go.jp>)  
より発信されています。

国立研究開発法人日本原子力研究開発機構 研究連携成果展開部 研究成果管理課  
〒319-1195 茨城県那珂郡東海村大字白方 2 番地4  
電話 029-282-6387, Fax 029-282-5920, E-mail:ird-support@jaea.go.jp

This report is issued irregularly by Japan Atomic Energy Agency.  
Inquiries about availability and/or copyright of this report should be addressed to  
Institutional Repository Section,  
Intellectual Resources Management and R&D Collaboration Department,  
Japan Atomic Energy Agency.  
2-4 Shirakata, Tokai-mura, Naka-gun, Ibaraki-ken 319-1195 Japan  
Tel +81-29-282-6387, Fax +81-29-282-5920, E-mail:ird-support@jaea.go.jp

## Integral Test of JENDL-3.3 Based on Shielding Benchmarks

Shielding Integral Test Working Group (FY2006-2010)  
Japanese Nuclear Data Committee  
Nuclear Science and Engineering Center

Nuclear Science Research Institute, Sector of Nuclear Science Research,  
Japan Atomic Energy Agency  
Tokai-mura, Naka-gun, Ibaraki-ken

(Received December 25, 2018)

Integral tests of neutron and photon production data in cross-section libraries based on the Japanese Evaluated Nuclear Data Library, Version 3.3 (JENDL-3.3) have been performed by using shielding benchmarks. An evaluation scheme for shielding benchmark analysis established in the Japanese Nuclear Data Committee (JNDC) was applied to the integral test for 28 materials in 22 medium-heavy nuclei and the compounds such as Lithium, Oxygen, LiF, TEFLON:(CF<sub>2</sub>)<sub>n</sub>, Sodium, Aluminum, Li<sub>2</sub>AlO<sub>3</sub>, LiAlO<sub>2</sub>, Silicon, SiC, Titanium, Li<sub>2</sub>TiO<sub>3</sub>, Vanadium, Chromium, Manganese, Iron, Cobalt, Nickel, SS304, Copper, Arsenic, Selenium, Zirconium, Li<sub>2</sub>ZrO<sub>3</sub>, Niobium, Molybdenum, Tungsten and Mercury. Calculations were made by using a continuous-energy Monte Carlo code MCNP and multi-group discrete ordinates codes ANISN, DORT and TORT. Calculations with JENDL-3.2, ENDF/B-VI, EFF-2, FENDL-1 and FENDL-2 were also made for comparison. The results of JENDL-3.3 were generally satisfactory and the cross-section libraries generated with JENDL-3.3 were validated to shielding applications for fission and fusion reactors.

Keywords: JENDL-3.3, Shielding, Integral Test, Validation, Fission and Fusion Reactors

---

The member of the Shielding Integral Test Working Group in Japanese Nuclear Data Committee (FY2006-2010) related to this report is listed as follows:

Naoki YAMANO (Tokyo Tech, Leader), Chihiro ICHIHARA (Kyoto Univ.), Kotaro UEKI (ARTECH), Yoshihiro MATSUMOTO (NUSTEC), Fujio MAEKAWA (JAEA), Chikara KONNO (JAEA), Yasushi HOSHIAI (CRC), Kenji SASAKI (MFBR), Morio TAKEMURA (KHI), Takeo NISHITANI (JAEA), Satoshi SATO (QST), Shigetaka MAEDA (JAEA) and Yasushi OHKAWACHI (JAEA)

## 遮蔽ベンチマークによる JENDL-3.3 の積分テスト

シグマ委員会 Shielding 積分テストワーキンググループ (2006-2010 年度)

日本原子力研究開発機構 原子力科学研究所  
原子力基礎工学研究センター

(2018 年 12 月 25 日)

評価済核データライブラリ JENDL-3.3 における中性子及びガンマ線生成データの積分テストを遮蔽ベンチマークにより実施した。シグマ委員会で確立した積分ベンチマーク解析に対する評価手法を用いて、22 種の中重核及び化合物（リチウム、酸素、フッ化リチウム、テフロン、ナトリウム、アルミニウム、 $\text{Li}_2\text{AlO}_3$ 、 $\text{LiAlO}_2$ 、ケイ素、炭化ケイ素、チタン、 $\text{Li}_2\text{TiO}_3$ 、バナジウム、塩素、マンガン、鉄、コバルト、ニッケル、SS304、銅、ヒ素、セレン、ジルコニウム、 $\text{Li}_2\text{ZrO}_3$ 、ニオブ、モリブデン、タンクスティン、水銀）からなる 28 物質のベンチマークテストが行われた。

遮蔽ベンチマーク計算は、連続エネルギーモンテカルロコード MCNP や多群離散座標コード ANISN、DORT や TORT を使って実施された。積分ベンチマーク結果の比較のために、JENDL-3.2、ENDF/B-VI、EFF-2、FENDL-1、FENDL-2 を使って同様の計算を実施した。これらにより、JENDL-3.3 は遮蔽評価に対し、全体的に十分な性能を有しており、JENDL-3.3 から計算した断面積ライブラリは核分裂炉や核融合炉への遮蔽応用に有効であることを確認した。

---

本レポートの執筆に携わったシグマ委員会 Shielding 積分テストワーキンググループ (2006-2010 年度) の委員は以下の通りである。

山野直樹 (東工大、リーダー)、市原千博 (京都大)、植木紘太郎 (ARTECH)、松本誠弘 (NUSTEC)、前川藤夫 (原子力機構)、今野力 (原子力機構)、星合康嗣 (CRC)、佐々木研治 (MFBR)、竹村守雄 (KHI)、西谷健夫 (原子力機構)、佐藤聰 (量研)、前田茂貴 (原子力機構)、大川内靖 (原子力機構)

原子力科学研究所：〒319-1195 茨城県那珂郡東海村大字白方 2-4

## Contents

<b>1. Introduction .....</b>	1
<b>2. Integral Test Method .....</b>	1
2.1    Method for Integral Validation .....	1
2.2    Benchmark Problems .....	2
2.2.1    OKTAVIAN .....	2
2.2.2    FNS .....	4
2.2.3    SDT of ORNL .....	7
2.2.4    JASPER.....	7
2.2.5    ASPIS.....	8
2.2.6    KfK .....	8
2.2.7    IPPE .....	8
2.2.8    NIST.....	9
2.2.9    ORNL.....	10
2.3    Cross-Section Processing and Library Generation .....	11
<b>3. Results .....</b>	11
3.1    Lithium and LiF .....	11
3.2    TEFLON: $(CF_2)_n$ .....	11
3.3    Oxygen .....	12
3.4    Sodium .....	12
3.5    Aluminum, $Li_2AlO_3$ and $LiAlO_2$ .....	12
3.6    Silicon and SiC .....	12
3.7    Titanium and $Li_2TiO_3$ .....	13
3.8    Vanadium.....	13
3.9    Chromium.....	13
3.10    Manganese.....	13
3.11    Iron .....	13
3.12    Cobalt .....	14
3.13    Nickel and SS304.....	14
3.14    Copper .....	15
3.15    Arsenic .....	15
3.16    Selenium .....	15
3.17    Zirconium and $Li_2ZrO_3$ .....	15
3.18    Niobium.....	15
3.19    Molybdenum .....	16
3.20    Tungsten .....	16
3.21    Mercury .....	16
<b>4. Discussion .....</b>	60
<b>5. Conclusion .....</b>	60
<b>Acknowledgments .....</b>	60
<b>References .....</b>	60
<b>Appendix A .....</b>	65

## 目 次

1. 序論 .....	1
2. 積分テスト手法 .....	1
2.1 積分的検証手法 .....	1
2.2 ベンチマーク問題 .....	2
2.2.1 OKTAVIAN .....	2
2.2.2 FNS .....	4
2.2.3 ORNL の SDT .....	7
2.2.4 JASPER .....	7
2.2.5 ASPIS .....	8
2.2.6 KfK .....	8
2.2.7 IPPE .....	8
2.2.8 NIST .....	9
2.2.9 ORNL .....	10
2.3 断面積処理とライブラリ作成 .....	11
3. 結果 .....	11
3.1 リチウムとフッ化リチウム .....	11
3.2 テフロン .....	11
3.3 酸素 .....	12
3.4 ナトリウム .....	12
3.5 アルミニウム、 $\text{Li}_2\text{AlO}_3$ 、 $\text{LiAlO}_2$ .....	12
3.6 ケイ素と炭化ケイ素 .....	12
3.7 チタンと $\text{Li}_2\text{TiO}_3$ .....	13
3.8 バナジウム .....	13
3.9 クロム .....	13
3.10 マンガン .....	13
3.11 鉄 .....	13
3.12 コバルト .....	14
3.13 ニッケルと SS304 .....	14
3.14 銅 .....	15
3.15 ヒ素 .....	15
3.16 セレン .....	15
3.17 ジルコニウムと $\text{Li}_2\text{ZrO}_3$ .....	15
3.18 ニオブ .....	15
3.19 モリブデン .....	16
3.20 タングステン .....	16
3.21 水銀 .....	16
4. 議論 .....	60
5. 結論 .....	60
謝辞 .....	60
参考文献 .....	60
付録 A .....	65

## Table List

<b>Table 2.1</b>	Shielding benchmark problems adopted in the integral test of JENDL-3.3 .....	2
<b>Table 2.2</b>	Detailed description of sample piles of the OKTAVIAN benchmark experiment .....	5
<b>Table 2.3</b>	Parameters of the experimental setup of the IPPE measurement .....	9
<b>Table 2.4</b>	Uncertainties of the IPPE experimental data .....	9
<b>Table 2.5</b>	Specifications of Bonner ball detectors .....	11
<b>Table 3.1</b>	Calculated results and C/E values of the ORNL iron experiments (JENDL-3.3) .....	42
<b>Table 3.2</b>	Calculated results and C/E values of the ORNL iron experiments (JENDL-3.2) .....	43
<b>Table 3.3</b>	Calculated results and C/E values of the ORNL iron experiments (ENDF/B-VI) .....	44
<b>Table 3.4</b>	Calculated results and C/E values of the ORNL stainless steel experiments (JENDL-3.3).....	45
<b>Table 3.5</b>	Calculated results and C/E values of the ORNL stainless steel experiments (JENDL-3.2).....	45
<b>Table 3.6</b>	Calculated results and C/E values of the ORNL stainless steel experiments (ENDF/B-VI).....	45
<b>Table A-1.1</b>	Neutron source for Cr and Nb samples.....	65
<b>Table A-1.2</b>	Neutron source for Li, CF, Si and Co samples .....	67
<b>Table A-1.3</b>	Neutron source for LiF, Mn, Cu, Mo and W samples .....	68
<b>Table A-1.4</b>	Neutron source for Ti, As, Se and Zr samples .....	69
<b>Table A-1.5</b>	Neutron source for Al sample .....	71

## Figure List

<b>Fig. 2.1</b>	A schematic configuration of NIST benchmark experiment .....	10
<b>Fig. 3.1</b>	Results of OKTAVIAN Lithium benchmark. ....	17
<b>Fig. 3.2</b>	Results of OKTAVIAN LiF benchmark. ....	17
<b>Fig. 3.3</b>	Results of OKTAVIAN TEFILON benchmark. ....	17
<b>Fig. 3.4</b>	Results of FNS Oxygen benchmark. ....	18
<b>Fig. 3.5</b>	Results of JASPER IVFS-IC/Pb benchmark. ....	19
<b>Fig. 3.6</b>	Results of JASPER IHX-IB/Pb benchmark. ....	19
<b>Fig. 3.7</b>	Results of Sodium SDT4 benchmark. ....	20
<b>Fig. 3.8</b>	Results of OKTAVIAN Aluminum benchmark. ....	20
<b>Fig. 3.9</b>	Results of FNS $\text{Li}_2\text{AlO}_3$ benchmark at 76.2 mm depth. ....	21
<b>Fig. 3.10</b>	Results of FNS $\text{Li}_2\text{AlO}_3$ benchmark at 177.8 mm depth. ....	21
<b>Fig. 3.11</b>	Results of FNS $\text{Li}_2\text{AlO}_3$ benchmark at 279.4 mm depth. ....	22
<b>Fig. 3.12</b>	Results of IPPE Al benchmark from 12 cm radius. ....	22
<b>Fig. 3.13</b>	Photon flux of FNS $\text{LiAlO}_2$ benchmark. ....	23
<b>Fig. 3.14</b>	Results of OKTAVIAN Silicon benchmark. ....	24
<b>Fig. 3.15</b>	Results of FNS Silicon Carbide benchmark at 12.7cm depth. ....	24
<b>Fig. 3.16</b>	Results of FNS Silicon Carbide benchmark at 27.9 cm depth. ....	25
<b>Fig. 3.17</b>	Results of FNS Silicon Carbide benchmark at 43.2 cm depth. ....	25
<b>Fig. 3.18</b>	Results of FNS Silicon Carbide benchmark at 58.4 cm depth. ....	26
<b>Fig. 3.19</b>	Results of OKTAVIAN Titanium benchmark (1). ....	26
<b>Fig. 3.20</b>	Results of OKTAVIAN Titanium benchmark (2). ....	27
<b>Fig. 3.21</b>	Photon flux of OKTAVIAN Titanium benchmark. ....	27
<b>Fig. 3.22</b>	Photon flux of FNS $\text{Li}_2\text{TiO}_3$ benchmark. ....	28
<b>Fig. 3.23</b>	Results of FNS Vanadium benchmark at 7.6 cm depth. ....	28
<b>Fig. 3.24</b>	Results of FNS Vanadium benchmark at 17.8 cm depth. ....	29
<b>Fig. 3.25</b>	Photon flux of FNS Vanadium benchmark at 7.6 cm depth. ....	29
<b>Fig. 3.26</b>	Photon flux of FNS Vanadium benchmark at 17.8 cm depth. ....	30

<b>Fig. 3.27</b>	Results of OKTAVIAN Chromium benchmark (1).....	30
<b>Fig. 3.28</b>	Results of OKTAVIAN Chromium benchmark (2).....	31
<b>Fig. 3.29</b>	Photon flux of OKTAVIAN Chromium benchmark.....	31
<b>Fig. 3.30</b>	Results of OKTAVIAN Manganese benchmark.....	32
<b>Fig. 3.31</b>	Results of SDT1 Iron benchmark for 20.32 cm transmission .....	32
<b>Fig. 3.32</b>	Results of SDT1 Iron benchmark for 30.48 cm transmission .....	32
<b>Fig. 3.33</b>	Results of KfK Iron benchmark for 15 cm sphere. ....	33
<b>Fig. 3.34</b>	Results of KfK Iron benchmark for 20 cm sphere. ....	33
<b>Fig. 3.35</b>	Results of KfK Iron benchmark for 25 cm sphere. ....	33
<b>Fig. 3.36</b>	Results of KfK Iron benchmark for 30 cm sphere. ....	33
<b>Fig. 3.37</b>	Results of KfK Iron benchmark for 35 cm sphere. ....	33
<b>Fig. 3.38</b>	Results of KfK Iron benchmark for 40 cm sphere. ....	33
<b>Fig. 3.39</b>	Results of IPPE Iron benchmark. ....	34
<b>Fig. 3.40</b>	Results of NIST Iron benchmark.....	34
<b>Fig. 3.41</b>	Results of ASPIS Iron benchmark at 22.54 cm depth. ....	34
<b>Fig. 3.42</b>	Results of ASPIS Iron benchmark at 56.83 cm depth. ....	35
<b>Fig. 3.43</b>	Results of ASPIS Iron benchmark at 85.41 cm depth. ....	35
<b>Fig. 3.44</b>	Results of ASPIS Iron benchmark at 113.98 cm depth. ....	36
<b>Fig. 3.45</b>	Results of FNS Iron benchmark at 11 cm in depth.....	36
<b>Fig. 3.46</b>	Results of FNS Iron benchmark at 21 cm in depth. ....	37
<b>Fig. 3.47</b>	Results of FNS Iron benchmark at 31 cm depth. ....	37
<b>Fig. 3.48</b>	Results of FNS Iron benchmark at 41 cm depth. ....	38
<b>Fig. 3.49</b>	Results of FNS Iron benchmark at 61 cm depth. ....	38
<b>Fig. 3.50</b>	Results of FNS Iron benchmark at 81 cm depth (1).....	39
<b>Fig. 3.51</b>	Results of FNS Iron benchmark at 81 cm depth (2).....	39
<b>Fig. 3.52</b>	Photon flux of KfK Iron benchmark for 25 cm sphere. ....	39
<b>Fig. 3.53</b>	Photon flux of KfK Iron benchmark for 35 cm sphere. ....	39
<b>Fig. 3.54</b>	Photon flux of FNS Iron benchmark at 30 cm in depth. ....	40
<b>Fig. 3.55</b>	Photon flux of FNS Iron benchmark at 70 cm in depth. ....	40
<b>Fig. 3.56</b>	Results of OKTAVIAN Cobalt benchmark (1).....	40
<b>Fig. 3.57</b>	Results of OKTAVIAN Cobalt benchmark (2).....	41
<b>Fig. 3.58</b>	Results of IPPE Nickel benchmark. ....	41
<b>Fig. 3.59</b>	Results of FNS Copper benchmark at 7.6 cm in depth. ....	46
<b>Fig. 3.60</b>	Results of FNS Copper benchmark at 38 cm in depth. ....	46
<b>Fig. 3.61</b>	Results of FNS Copper benchmark at 53.2 cm in depth. ....	47
<b>Fig. 3.62</b>	Results of OKTAVIAN Copper benchmark. ....	47
<b>Fig. 3.63</b>	Results of OKTAVIAN Arsenic benchmark.....	48
<b>Fig. 3.64</b>	Results of OKTAVIAN Selenium benchmark.....	49
<b>Fig. 3.65</b>	Results of OKTAVIAN Zirconium benchmark.....	49
<b>Fig. 3.66</b>	Results of FNS Li <sub>2</sub> ZrO <sub>3</sub> benchmark at 76 mm in depth. ....	50
<b>Fig. 3.67</b>	Results of FNS Li <sub>2</sub> ZrO <sub>3</sub> benchmark at 177 mm in depth. ....	50
<b>Fig. 3.68</b>	Results of FNS Li <sub>2</sub> ZrO <sub>3</sub> benchmark at 279 mm in depth. ....	51
<b>Fig. 3.69</b>	Results of FNS Li <sub>2</sub> ZrO <sub>3</sub> benchmark at 380 mm in depth. ....	51
<b>Fig. 3.70</b>	Results of FNS Li <sub>2</sub> ZrO <sub>3</sub> benchmark at 10.16 cm in depth. ....	51
<b>Fig. 3.71</b>	Results of OKTAVIAN Niobium benchmark.....	52
<b>Fig. 3.72</b>	Results of gamma-ray spectrum in the OKTAVIAN Niobium benchmark. ....	52
<b>Fig. 3.73</b>	Results of the OKTAVIAN Molybdenum benchmark.....	53
<b>Fig. 3.74</b>	Results of the FNS Tungsten benchmark. ....	54
<b>Fig. 3.75</b>	Results of gamma-ray spectrum of the FNS Tungsten benchmark. ....	54

<b>Fig. 3.76</b>	Results of gamma-ray spectrum of the OKTAVIAN Tungsten benchmark. ....	55
<b>Fig. 3.77</b>	Results of OKTAVIAN Tungsten benchmark. ....	56
<b>Fig. 3.78</b>	Results of FNS Mercury benchmark. ....	57
<b>Fig. 3.79</b>	Results of gamma-ray heating rate in the FNS Tungsten benchmark. ....	57
<b>Fig. 4.1</b>	Calculated spectra with the modified Manganese data in the JENDL-3.2 library. ....	58
<b>Fig. 4.2</b>	General dependence of the partial cross section to the energy spectra, which was performed with MCNP-4A with artificial libraries modified from FSXLIB-J3R2. ....	59

This is a blank page.

## 1. Introduction

The Japanese Evaluated Nuclear Data Library, Version 3.3<sup>1)</sup> (JENDL-3.3) was released in May 2002. The Shielding Integral Test Working Group in the Japanese Nuclear Data Committee (JNDC) was in charge of validation work for JENDL-3.3 through shielding benchmark tests. For the shielding benchmark tests, a point-wise cross-section library, FSXLIB-J3R3<sup>2)</sup> for a continuous-energy Monte Carlo code, MCNP<sup>3)</sup> and a multi-group library, MATXS-J33<sup>2)</sup> for deterministic Sn codes were produced by the Japan Atomic Energy Agency (JAEA: former Japan Atomic Energy Research Institute (JAERI)). In order to validate the cross-section libraries based on JENDL-3.3, integral tests with shielding benchmarks were performed for 28 materials in 22 medium-heavy nuclei and the compounds such as Lithium, Oxygen, LiF, TEFLON:(CF<sub>2</sub>)<sub>n</sub>, Sodium, Aluminum, Li<sub>2</sub>AlO<sub>3</sub>, LiAlO<sub>2</sub>, Silicon, SiC, Titanium, Li<sub>2</sub>TiO<sub>3</sub>, Vanadium, Chromium, Manganese, Iron, Cobalt, Nickel, SS304, Copper, Arsenic, Selenium, Zirconium, Li<sub>2</sub>ZrO<sub>3</sub>, Niobium, Molybdenum, Tungsten and Mercury. An evaluation scheme<sup>4)</sup> of the shielding integral test for nuclear data evaluation, which was established in JNDC was adopted in the present study.

Chapter 2 describes the integral test method used in the integral validation, brief descriptions of adopted shielding benchmark problems and the cross-section processing schemes.

Chapter 3 shows the validation results on each shielding benchmark and the problems for each nuclide and the issues to be solved are summarized in Chapter 4. The concluding remarks are described in Chapter 5.

## 2. Integral Test Method

### 2.1 Method for Integral Validation

For the integral test of cross sections by using shielding benchmarks, we should select appropriate benchmark problems of different types that include various source conditions (e.g. fission and 14MeV D-T neutron sources) and simple geometry types (e.g. slab, cylinder or sphere with thin or thick layer). Detailed experimental conditions that are explicitly described for dimension, material composition, instrument and the associated error estimation are also required.

In the present study, we selected a number of spectrum measurements listed in **Table 2.1** that were characterized as having high sensitivity to the nuclear data of interest. For calculation, we selected a continuous-energy Monte Carlo code MCNP-4C<sup>3)</sup> and multi-group discrete ordinates codes ANISN<sup>5)</sup>, DORT<sup>6)</sup> and TORT<sup>7)</sup> because these transport codes were used in conventional shielding calculations. A systematic analysis method<sup>4)</sup> was applied to specify the accuracy and to find problems definitely for typical reactions of nuclear data when discrepancy was found between the calculation results and measurements. Calculations based on JENDL-3.2<sup>8)</sup>, ENDF/B-VI<sup>9)</sup>, EFF-2<sup>10)</sup>, FENDL-1<sup>11)</sup> and FENDL-2<sup>12)</sup> were also performed for comparison of nuclear data.

**Table 2.1** Shielding benchmark problems adopted in the integral test of JENDL-3.3

Nuclide/Compound	Benchmark Experiments
Lithium	OKTAVIAN
LiF and TEFLON: $(CF_2)_n$	OKTAVIAN
Oxygen	FNS
Sodium	SDT4, JASPER(IVFS-IC/Pb.9, IHX-IB/Pb)
Aluminum, $Li_2AlO_3$ and $LiAlO_2$	OKTAVIAN, FNS, IPPE
Silicon and SiC	OKTAVIAN, FNS
Titanium and $Li_2TiO_3$	OKTAVIAN, FNS
Vanadium	FNS
Chromium	OKTAVIAN
Manganese	OKTAVIAN
Iron	SDT1, FNS, ASPIS, KfK, IPPE, NIST
Cobalt-59	OKTAVIAN
Nickel, Stainless steel (SS304)	IPPE, ORNL
Copper	OKTAVIAN, FNS
Arsenic	OKTAVIAN
Selenium	OKTAVIAN
Zirconium and $Li_2ZrO_3$	OKTAVIAN, FNS
Niobium	OKTAVIAN
Molybdenum	OKTAVIAN
Tungsten	OKTAVIAN, FNS
Mercury	FNS

## 2.2 Benchmark Problems

### 2.2.1 OKTAVIAN

The leakage neutron spectra from 15 kinds of sample spheres were measured for the purpose of benchmark experiment<sup>13-16)</sup>. The spectra were measured with a time-of-flight (TOF) method using an intense neutron source OKTAVIAN<sup>17)</sup>.

#### (1) Neutron source

The neutron TOF measurement was conducted at OKTAVIAN, which was an intense 14 MeV neutron source facility of Faculty of Engineering, Osaka University. The major constituents of this facility are a 400 kV Cockcroft-Walton type high voltage generator, a duoplasmatron ion source, a post-acceleration nanosecond beam bunching system and tritium neutron producing targets. We used the pulsed beam line of OKTAVIAN, which was capable of producing neutron pulses as narrow as 2 ns of pulse width. The average current during the experiment was 20  $\mu$ A with 500 kHz repetition rate and the average neutron yield was about  $10^9$  n/sec by adopting a 370 GBq tritium neutron producing target.

#### (2) Experimental setup

All samples were in powder or granite form and the purity of the samples ranges between 99 and 99.99 %. The hydrogen and the moisture content for several samples were measured by using a heat conductance

detector and a Karl-Fischer type detector. Both were proved to have negligible effect to the experimental results by the Monte Carlo calculation using MCNP-4A<sup>18)</sup>.

The samples were contained in a spherical vessel to form sample piles. The samples, Li, TEFLO: (CF<sub>2</sub>)<sub>n</sub>, Al, Ti, Cr, Co, As, Se and W, were contained in spherical shells, the outer diameters of which were 39.9 cm. This sphere was made of stainless steel, the thickness of which was 0.2 cm and was equipped with a central void, the inner diameter of which was 10.0 cm and a re-entrant hole for introducing a deuteron beam, the inner diameter of which was 11 cm.

The LiF, Mn, Cu, Zr and Mo samples were contained in 61.0 cm outer diameter spheres made of mild steel. The spherical shell was equipped with a beam hole, the inner diameter of which was 5 cm. The wall thickness was 0.5 cm for the sphere section and 0.3 cm for the beam hole section, respectively.

Si sample was contained in a stainless steel sphere, the outer diameter and thickness of which were 60.0 cm and 0.5 cm, respectively. A 20 cm diameter central void and an 11 cm diameter beam hole similar to those for 40 cm spheres were equipped.

Nb powder was contained in a stainless steel sphere the outer diameter and thickness of which were 28.0 cm and 0.3 cm, respectively.

The details of the samples are described in **Table 2.2**.

### (3) Measurement<sup>13-16)</sup>

Deuteron beam was introduced to the center of the spherical sample pile through a beam duct and bombarded the tritium target to generate 14 MeV neutrons through the T(d,n)<sup>4</sup>He reaction. In this series of measurements, we used a 370-GBq gas-in-metal type tritium target, in which tritium gas was absorbed in a thin evaporated titanium layer on a 3.2 cm diameter and 0.05 cm thick copper backing plate. This target was accommodated in a stainless steel housing.

Neutrons leaking from the outer surface of a spherical sample pile were detected with a liquid scintillation counter composed of an NE-213 scintillator, the diameter and the length of which are 12.7 cm and 5.1 cm, respectively, and an RCA-8854 photomultiplier tube. This was located about 11 m from the center of the pile and 55 degrees horizontally and -5 degrees vertically with respect to the deuteron beam axis, respectively.

A pre-collimator, which consisted of iron and polyethylene, was placed between the sample pile and the detector to reduce the background neutrons scattered by the walls and other structural materials.

Neutron signals from the liquid scintillation counter were discriminated from  $\gamma$ -ray signals by using the pulse shape discrimination technique. To cover neutron energy down to 0.1 MeV, two identical pulse shape discriminating circuits were used in parallel with different gain settings of the delay line amplifiers.

Total leakage neutron spectrum was derived from the time distribution of neutrons reaching to the detector surface. In order to obtain the absolute value, 0.2 mm thick Nb activation foils were set so as to surround the target assembly and irradiated both with and without the sample pile. Then the gamma-rays from the <sup>92m</sup>Nb generated through the <sup>93</sup>Nb(n,2n) reaction were counted using a pure Ge detector. The monitor values with sample piles can be different from those without sample piles because of reflected neutrons. We calculated this effect with MCNP-4A and estimated that the difference was about 1 %.

By using these run-to-run monitor values and the integrated value of source neutron spectrum measured with a TOF setup, the absolute neutron spectrum, *i.e.* the energy distribution of the total leakage current from the surface of the sample, was derived as followings.

Total leakage current  $J(E)$  is defined as

$$J(E) = 4\pi R^2 \int_0^1 f(R, \mu, E) 2\pi\mu d\mu, \quad (1)$$

where  $R$  is an outer radius of a sample pile,  $f(R, \mu, E)$  is an angular flux, and  $\mu$  is a cosine of angle between radial vector and direction viewing the detector. If we assume that the distribution of the source neutrons is

isotropic, the angular flux at the outer surface of the sample pile becomes independent of the surface position. The energy distribution of the neutrons reaching to the detector surface is described as,

$$D(E) = \int_0^1 f(R, \mu, E) \frac{S_d}{(F_p - \mu R)^2} 2\pi R^2 \mu d\mu, \quad (2)$$

where  $S_d$  is a cross sectional area of the detector, and  $F_p$  is a flight path. Since  $F_p$  is much larger than the maximum value of  $\mu R$ ,  $F_p - \mu R$  in Eq. (2) can be replaced by  $F_p$ . Then  $D(E)$  can be related to the  $J(E)$  as,

$$D(E) = \frac{S_d}{4\pi F_p^2} J(E), \quad (3)$$

In the TOF measurement for the source run, *i.e.* the measurement without a sample pile, the energy distribution of the neutrons reaching to the detector,  $Q(E)$  (1/MeV·source neutron) is defined as,

$$Q(E) = \frac{S_d}{4\pi F_p^2} q(E), \quad (4)$$

where  $q(E)$  is the energy distribution of the source neutrons normalized as the integral over whole energy becomes unity.  $J(E)$  can be reduced by using  $D(E)$  and Eq. (4) as,

$$J(E) = \frac{D(E)}{\int_0^{15} Q(E) dE}. \quad (5)$$

Detection efficiency for the scintillation counter was obtained with a Monte Carlo code, O5S<sup>19)</sup> above 0.1 MeV, and was assured by two kinds of experimental values described below.

The efficiency between 0.1 MeV and 0.83 MeV was determined by a TOF measurement of the leakage neutron spectrum from a 30 cm diameter spherical pile of graphite. Graphite data required in deriving the efficiency were taken from ENDF/B-V<sup>20)</sup>. The efficiency error from inconsistency among nuclear data for graphite was estimated to be about 3 %. The uncertainty from the statistical error was less than 5 % between 0.4 and 0.83 MeV, around 10 % between 0.2 and 0.4 MeV and larger than 10 % below 0.2 MeV, respectively.

The efficiency between 0.83 and 8.2 MeV was determined from the measurement of fission neutron spectrum of <sup>252</sup>Cf which was assumed to be a Maxwellian spectrum with T=1.42 MeV. The efficiency error introduced primarily from the shape of the <sup>252</sup>Cf fission neutron spectrum was estimated to be around 3 % between 0.83 and 5 MeV and less than 10 % between 5 and 8.2 MeV judging from the difference of the fission spectra between the Maxwellian and that obtained by Mannhart<sup>21)</sup>.

## 2.2.2 FNS

A series of JAERI-FNS benchmark experiments were conducted by a pulsed beam line of the intense 14 MeV neutron source facility at Fusion Neutronics Source (FNS) at JAEA<sup>22)</sup>. Two types of experiments with D-T neutrons have been performed for 25 years at FNS. One is a Time-of-flight (TOF) experiment<sup>23)</sup> and the other is an in-situ experiment<sup>24)</sup>. Angular neutron spectra leaking from thinner cylindrical slabs of lithium oxide and liquid-oxygen were measured by NE-213 scintillator from the energy range between 100 keV and 14 MeV. Leakage neutron spectra were measured at several angles from 0 to 66.8 degrees with respect to the deuteron beam direction. Details of the experiments are described in references<sup>25-31)</sup>. Numerical data of the measured spectra are also given in references<sup>32, 33)</sup>.

The in-situ experiment was performed with a cylindrical assembly placed in front of the D-T neutron source of FNS. Neutron spectra inside of slabs of LiAlO<sub>2</sub>, Li<sub>2</sub>AlO<sub>3</sub>, Li<sub>2</sub>TiO<sub>3</sub>, SiC, Vanadium, Iron, Copper, Li<sub>2</sub>ZrO<sub>3</sub>, Tungsten and Mercury were measured by using several detectors from the neutron energy range

**Table 2.2** Detailed description of sample piles of the OKTAVIAN benchmark experiment

Sample		Diameter (cm)	Weight (kg)	Apparent density (g/cm <sup>3</sup> )	Sample thickness		Chemical composition			Date of measurement	Neutron source
Element	Description				cm	mfp*					
Al	Powder 80 % 0.2 - 1.0 mm	39.9	32.8	1.22	9.8	0.5	Al >99.7 % Cu <0.01 %	<0.20 %	Si <0.15 %	Dec. 22, 1988	Appendix A-1.5
	Si granular	60.0	138.1	1.29	20.0	1.1	Si >99.9 %			Mar. 13, 1987	
Ti	Powder 10 - 20 mesh	39.9	41.2	1.54	9.8	0.5	Ti >99.4 % Cl 0.084 % N 0.002 % H <0.003 %	Fe 0.084 % O 0.061 % Mn 0.002 %	Mg 0.029 % C 0.006 % Si <0.01 %	Aug. 31, 1988	A-1.4
	Cr powder	39.9	99.7	3.72	9.8	0.7	Cr >99.78 % C 0.021 %	Fe 0.16 % Si 0.007 %		Aug. 21, 1986	
Mn	Powder	61.0	490.5	4.37	27.5	3.4	Mn 99.95 % C 0.005 %	S 0.022 % Si 0.002 %	Fe 0.020 %	Jul. 8, 1987	A-1.3
	Powder 300 mesh	39.9	52.0	1.94	9.8	0.5	Co >99.50 % Si 0.04 % Mn 0.02 %	Ni 0.15 % Ca 0.03 % Cu 0.01 %	Fe 0.12 % C 0.03 %	Mar. 12, 1987	
Cu	Powder 100 mesh	61.0	675.0	6.01	27.5	4.7	Cu 99.993 %	S 10 ppm	As 0.6 ppm	Jul. 8, 1987	A-1.3
	Powder 60 - 200 mesh	28.0	47.7	4.39	11.2	1.1	Nb >99.8 %	Ta 0.1 %	O 0.07 %	Aug. 21, 1986	
Mo	Powder 4.2 µm	61.0	241.3	2.15	27.5	1.5	Mo >99.9 %	H <sub>2</sub> O < 0.03 %		Jul. 9, 1987	A-1.3
	W powder	39.9	118.6	4.43	9.8	0.8	W >99.9 %	O 230 ppm	Fe 45 ppm	Jul. 9, 1987	

\* mean free path

between 1 eV and 14 MeV. Detectors were inserted in the assembly at several positions along the central axis of the cylinder. Details of the experiments are described in references<sup>32, 34-49)</sup>.

The secondary gamma-rays were also measured from LiAlO<sub>2</sub>, Li<sub>2</sub>TiO<sub>3</sub>, Vanadium, Iron, Li<sub>2</sub>ZrO<sub>3</sub>, Tungsten and Mercury.

### (1) Neutron source

Positive deuteron ions were extracted from an ion source with 50 kV voltage, and bent by an analyzing magnet to get single charged ion beam. The deuterons were accelerated by 300 kV to 350 kV voltage of the total energy. The deuteron beam was introduced to the first target room and bombarded to a tritium-titanium metal target. The beam current was controlled between 20 nA and 2 mA according to the measurement conditions. The maximum neutron yield was about  $3 \times 10^{11}$  n/s for whole solid angle at beam current of 2 mA.

A pair of neutron and alpha-particle is generated associating with the D-T reaction. The absolute neutron yield can be determined by counting the number of the associated alpha-particles. Two systems of alpha-particle monitor<sup>50, 51)</sup> with silicon surface barrier solid state detectors are equipped in a beam drift tube. The absolute neutron yield can be determined with accuracy of 2 % by the alpha monitor. A long counter and a <sup>232</sup>Th fission counter are also settled as relative neutron yield monitors. The long counter is about 10 times more sensitive than the alpha counters. When counts of the alpha monitors are not enough, the long counter calibrated to the alpha counters is used to determine the neutron yield.

Source neutron spectrum emitting from the target was calculated by MORSE-DD<sup>52)</sup>, simulating the real target structure as precise as possible. The calculated spectrum for 0-degree to the direction of the d+ beam is normalized to the yield per unit solid angle, and then multiplied by  $4\pi$ . Hence the energy integration of the spectrum with energy results 1.1261. The reasons why the value is more than unity are follows: i) Emitted neutrons are slightly enhanced to forward direction by D-T reaction kinematics, and ii) number of neutrons is multiplied by (n, 2n) reactions with structural materials of the target. The spectrum of the target gamma-rays generated by interaction of neutrons and structural materials of the target was calculated by MCNP-3B<sup>53)</sup>. Since the gamma-ray emission is almost isotropic, an integrated spectrum for whole solid angle was given. The energy integral of the spectrum is 0.1637, i.e., 0.1637 photons are emitted isotropically, following one D-T reaction. When the experiment is analyzed, the source neutron spectrum and the gamma-ray spectrum have to be given by normalizing the total number of the source neutrons or photons to 1.1261 and 0.1637, respectively.

### (2) Experimental setup

The size of experimental assembly is different in each experiment as follows:

- Lithium oxide: 200.0 mm thickness, Liquid-oxygen: 200.0 mm thickness.

As a typical configuration of the in-situ experiment the shape of most of the experimental assemblies is a quasi-cylinder. The effective diameter of the assembly is 630 mm. The thickness of the experimental assemblies is different in each experiment as follows:

- LiAlO<sub>2</sub>: 101.6 mm thickness, Li<sub>2</sub>AlO<sub>3</sub>: 279.4 mm thickness, SiC: 584.0 mm thickness,
- Li<sub>2</sub>TiO<sub>3</sub>: 279.4 mm thickness, Vanadium: 178.0 mm thickness, Iron: 810.0 mm thickness,
- Copper: 532.0 mm thickness, Li<sub>2</sub>ZrO<sub>3</sub>: 380.0 mm thickness, Tungsten: 380.0 mm thickness,
- Mercury: 140.0 mm thickness.

### (3) Measurement

In the TOF measurement, angular neutron spectra leaking from a thin cylindrical slab were measured by an NE-213 scintillator from the energy range between 100 keV and 14 MeV. In the in-situ experiment, neutron energy spectra, reaction rates of dosimetry reactions, gamma heating rates were measured inside the experimental assembly. Details of the measured quantities and the techniques are described in reference<sup>22)</sup>.

### 2.2.3 SDT of ORNL

SDT1 and SDT4 benchmarks named as the Broomstick experiments were adopted to investigate the effect of minima in the neutron total cross sections in the MeV energy range<sup>54-56)</sup>.

#### (1) Neutron source

The neutron source of the Broomstick experiment was a collimated beam with a diameter of 3.5 in. from the Tower Shielding Reactor II of Oak Ridge National Laboratory ORNL. To reduce air-scattering effects the reactor and detector were shielded with lead and water and the reactor beam and detector acceptance were tightly collimated.

#### (2) Experimental setup

The iron sample is a cylinder form of 4 in. in diameter and placed so that its axis coincides with the axis of the neutron beam. The distance from the neutron source to the sample is 50 ft. and the detector is placed at a position 50 ft. from the sample. The sodium sample is a cylinder approximately 4 in. in diameter with stainless-steel container.

#### (3) Measurement

The detector is a nominal 2 in. × 2 in. NE-213 scintillator. The unfolding of the pulse-height distributions was accomplished using a FERDOR code. The uncollided transmitted neutron spectra through two samples of iron, one 8-in. thick and the other 12-in. thick (density of 0.0847 atoms/barn·cm) were measured. The error in the unfolding is such that the spectrum lies somewhere within the darkened area within 68% confidence limits. The uncollided transmitted neutron spectra through ~2 ft. of sodium (density of 0.0254 atoms/barn·cm) were measured. The error in the unfolding is such that the spectrum lies somewhere within the darkened area within 68% confidence limits. In addition, an estimated 5-10% error is included in the absolute measurements due to power calibration.

### 2.2.4 JASPER

A series of JASPER experiments were performed as a US and Japan Shielding Program for Experimental Research of FBR shielding mockups. Various types of benchmark experiments were conducted for simulating FBR shield. In this study, we selected two typical sodium benchmarks because the material configuration was rather simple and thick enough to investigate deep penetration. Selected benchmarks were JASPER IVFS-IC/Pb.9 (197.4 cm thick sodium) and JASPER IHX-IB/Pb (231.3 cm thick sodium) benchmarks<sup>57, 58)</sup> to check deep penetration profile.

#### (1) Neutron source

Neutron source of the JASPER experiment was the collimated beam with a diameter of  $15\frac{7}{64}$  in. and  $17\frac{3}{32}$  in. from the Tower Shielding Reactor II of ORNL. To reduce air-scattering effects the reactor and detector were shielded with lead and Lithium-paraffin (IVFS-IC) or concrete (IHX-IB) and the reactor beam was tightly collimated.

#### (2) Experimental setup

The sodium sample is a rectangular form with stainless-steel container and placed so that its axis coincides with the axis of the neutron beam. The detector is placed at the behind of the sample.

#### (3) Measurement

Neutron spectrum between 800 keV and 15 MeV on the centerline at 25 cm behind lead shield was measured by using an NE-213 counter with an unfolding code FERD. Spherical proton recoil counters, filled

with hydrogen to pressures of 1, 3, and 10 atmospheres, were also used to measure neutron flux between 50 keV and 1 MeV using the SPEC-4 code.

The measurements with each detector were referenced to the reactor power (watts) using the data from two fission chambers positioning along the reactor centerline as a basis. Bonner ball counters from 3 to 12 in. were also used to measure reaction rates.

### **2.2.5 ASPIS**

The ASPIS experiment<sup>59)</sup> was designed for providing information of benchmark quality for testing of data and calculation methods for deep-penetration profile by natural iron shielding material.

(1) Neutron source

Fission neutrons generated from a low-power natural uranium converter plate (ASPIIS) driven by the source reactor NESTOR were used as a large thin rectangular source. The ASPIIS plate was placed at the interface of graphite moderator and extensive iron shield (137.16 cm effective thickness).

(2) Experimental setup

The iron sample is placed with a rectangular form of 137.16 cm in effective thickness so that its axis coincides with the axis of the neutron source. The detector is placed at each depth from 22.14 to 113.98 cm in the iron slab.

(3) Measurement

Measurements were made for the axial attenuation profiles with three threshold detectors of  $^{103}\text{Rh}(n,n')$ ,  $^{103\text{m}}\text{Rh}$ ,  $^{115}\text{In}(n,n')$ ,  $^{115\text{m}}\text{In}$ , and  $^{32}\text{S}(n,p)$ ,  $^{32}\text{P}$  and one Cd-covered Au activation foil. The neutron spectra were measured by spectrometers at four positions in the iron shield using an unfolding code RADAK.

### **2.2.6 KfK**

The KfK experiment<sup>60, 61)</sup> was provided for measuring leakage neutron energy spectra from six kinds of iron spheres from 15 cm to 40 cm in diameter. The gamma-ray energy spectra were also measured for both 25 and 35 cm spheres in diameter.

(1) Neutron source

A  $^{252}\text{Cf}$  neutron source was located at the center of the sphere. The energy spectrum of source neutrons was measured and evaluated using spectrometers.

(2) Experimental setup

The iron spheres used in the experiments were constructed with pure iron (C: 0.07w/o, Mn: 0.05w/o, P: 0.009w/o, S: 0.007w/o). The diameters of the iron spheres were 15, 20, 25, 30, 35 and 40 cm, respectively.

(3) Measurement

Three proton recoil counters and a  $^3\text{He}-\text{Si}$  diode detector were used for the measurement. In the measurement with the proton recoil counters, the background was estimated using a shadow cone. Neutron energy spectra were obtained using the unfolding technique with the SPEC4 code. In the measurement for  $^3\text{He}-\text{Si}$  diode counter, the measured data were corrected by  $\text{Si}(n,d)$ ,  $\text{Si}(n,p)$  reaction rates and the background subtraction. Neutron energy spectra were also obtained with the Bluhm unfolding technique<sup>62)</sup>.

### **2.2.7 IPPE**

The IPPE experiment<sup>63)</sup> was provided for measuring leakage neutron energy spectra with TOF method from Be, Al, Fe, Ni, Pb, LiPb and Bi spheres from 5 cm to 14 cm in thickness. We adopted Al, Fe and Ni experiments in this benchmark test.

### (1) Neutron source

The neutron source was generated by the  $T(d,n)$  reaction using the KG-3 Cockcroft-Walton accelerator with an RF electromagnetic discharge ion source. The maximum deuteron beam was 250 keV and the mean beam current was 1  $\mu$ A. The beam spot diameter was 5 mm and the neutron yield was  $10^8$  n/s. The source assembly was designed with (a)  $\phi 28$  mm TiT target and (b)  $\phi 11$  mm TiT target inside thin Al holder. The angular distribution of the 14 MeV source neutron yield was measured by: (1) simultaneous irradiation of ten Al foils located at 10 cm distance around the target, and counting the induced activity of  $^{24}\text{Na}$  by the  $\beta$ - $\gamma$  technique, and (2) measuring of the neutron yield by the TOF method.

### (2) Experimental setup

The parameters of these experiments are listed in **Table 2.3**. The hole in the sphere was used for input of neutron source.

**Table 2.3** Parameters of the experimental setup of the IPPE measurement

Source	Element	Radius (cm)		Sphere thickness (cm)	Hole diameter (cm)	number density ( $10^{22}/\text{cm}^3$ )	Angles (degree)	Target type
		out	in					
$T(d,n)$	Be	11.0	6.0	5.0	5.0	12.36	0, 30, 60	a
	Al	12.0	4.5	7.5	6.2	5.966	0, 40, 75	b
	Fe	12.0	4.5	7.5	6.2	8.734	0, 40, 75	a
	Ni	12.0	4.5	7.5	6.2	9.016	0, 40, 75	b
	Pb	12.0	4.5	7.5	5.0	3.30	0, 30, 60	a
	LiPb	20.0	6.0	14.0	5.0	2.76-Pb 0.565-Li	40	b
	Bi	12.0	3.0	9.0	5.0	2.82	0, 60, 95	a

### (3) Measurement

The leakage neutron energy spectra from the shells were measured by a scintillation detector at 3.7 m flight path. The background was measured with 1 m long iron shadow bar, the number of source neutron was determined by measuring  $\alpha$ -associated particles.

In the experiments, the estimated errors were listed in **Table 2.4**. These errors include the uncertainty of standard cross-sections as well as the deviations of different runs during the calibrations and measurements.

**Table 2.4** Uncertainties of the IPPE experimental data

Component	Value
Statistics	1 - 4 %
Absolute normalization	3 %
Detector efficiency	5 %
Correction calculation	2 %
Total	6 - 7 %

### 2.2.8 NIST

The experiment was performed at the National Institute of Standards and Technology as a means of checking the degree to which the iron inelastic scattering cross section in ENDF/B-VI resolved the well-known discrepancy between predicted and observed neutron transport<sup>64)</sup>.

### (1) Neutron source

A  $^{252}\text{Cf}$  spontaneous fission neutron source was located at the center of sphere.

## (2) Experimental setup

A schematic configuration of the experiment is shown in **Fig. 2.1**. The iron sphere of 50.7 cm in diameter was used as a sample.

## (3) Measurement

The leakage neutron spectrum from the iron sphere was measured using a rotating neutron spectrometer (ROSPEC) over an energy range of 50 keV to 4.5 MeV.

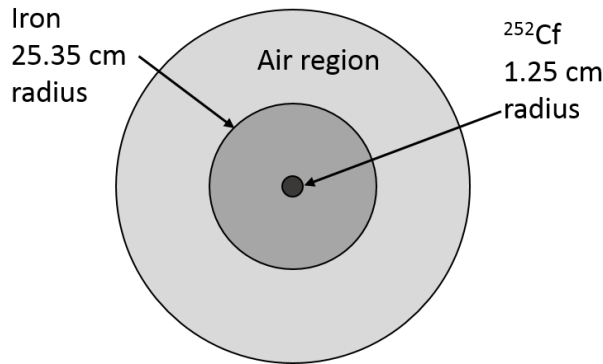


**Fig. 2.1** A schematic configuration of NIST benchmark experiment.

## 2.2.9 ORNL

A series of deep-penetration neutron transmission measurements through iron slabs up to 36 in. thick and stainless steel slabs up to 18 in. thick were performed at the Tower Shielding Facility (TSF) of ORNL using a collimated beam from the reactor neutrons as the source<sup>65)</sup>. These measurements were made at various positions behind 60-in. square slabs, so that the effect of side leakage of neutrons was negligible even for a 36-in. thick sample of iron, since the beam was tightly collimated.

### (1) Neutron source

Neutrons of the TSR-II reactor were extracted from the collimators. The energy spectrum of source neutrons were absolutely determined by the spectrometer measurements for the centerline point located on the exit plane of the collimator for the energy region between 100 eV and 10 MeV. The accuracy of the incident spectrum was estimated to be within 10 % above 200 keV and within 20 % below 200 keV.

### (2) Experimental setup

This collimator was used for all the measurements except those made behind 18 in. of stainless steel. The measurements behind 18 in. stainless steel were made using the reactor collimator.

The thickness, density and composition of the individual slabs used in the experiment were accurately determined. The calculation models based on the experimental conditions were the same as the previous analysis report<sup>65)</sup>.

### (3) Measurement

Measurements for the transmitted neutron energy spectra were made behind 12-in.-thick iron and 18-in.-thick stainless steel, covering the energy range above 80 keV, by using two types of spectrometers as follows: a) NE-213 scintillator which determined energy spectra in the energy range between 800 keV and 15 MeV, b) Benjamin proton recoil spectrometer which determined energy spectra in the energy range between 80 keV and 1.5 MeV.

A set of three spherical BF<sub>3</sub> detectors surrounded by various thickness of polyethylene (0.5 to 4 in.) and an outside shell of cadmium was also used to obtain integral flux behind iron and stainless steel. These

“Bonner ball” detectors have response functions with peak in a different range in neutron energy. The descriptions of each Bonner ball are given in **Table 2.5**.

These measurements show that the tightly collimated source could be represented as a virtual point anisotropic source located 68 in. inside the collimator from the edge of the iron collar (point S' shown in Fig. 17 of reference 65), with a uniform beam intensity over a diameter of about 6-1/2 in. at the mouth of the collimator and zero elsewhere.

**Table 2.5** Specifications of Bonner ball detectors

Standard Bonner ball designation	Polyethylene thickness (inch)	Polyethylene density (g/cm <sup>3</sup> )	Diameter of ball (inch)	Displacement of center of detection from geometric center (inch)*
3	0.515	0.951	3.09	0.9
6	1.91	0.925	5.88	1.8
10	3.90	0.951	9.86	3.0

\* The detection of this displacement is toward the center of gravity of the hemispherical surface upon which the neutrons are incident.

### 2.3 Cross-Section Processing and Library Generation

The analyses for the selected benchmarks were performed by using two versions of a three-dimensional continuous-energy Monte Carlo transport code, MCNP-4A and MCNP-4C2. The libraries used in the MCNP calculations were FSXLIB-J3R3<sup>3)</sup> processed from JENDL-3.3<sup>1)</sup>, FSXLIB-J3R2<sup>67)</sup> from JENDL-3.2<sup>8)</sup>, the processed library<sup>68)</sup> from ENDF/B-VI<sup>9)</sup> and the processed library<sup>69)</sup> from EFF-2.4<sup>70)</sup>. These libraries were generated by using the NJOY<sup>71)</sup> code.

In the calculation of some benchmark problems, the Sn transport codes ANISN<sup>5)</sup>, DORT<sup>6)</sup> and TORT<sup>7)</sup> were also used with 175 group library processed from MATXS-J33<sup>3)</sup> library using the TRANXS-2.15<sup>72)</sup> code.

## 3. Results

### 3.1 Lithium and LiF

In **Fig. 3.1**, the measured and calculated neutron spectra with FSXLIB-J3R3 (JENDL-3.3), FSXLIB-J3R2 (JENDL-3.2) and ENDF/B-VI (release 2) from a 40 cm diameter Li sphere of the OKTAVIAN experiment are depicted.

Except the energy region between 5 and 10 MeV, where considerable underestimation with all nuclear data is observed, all the calculations predict the experiment within a few percent differences. As the fraction of the partial spectrum stated above is relatively small, the all nuclear data studied can be considered adequate.

The measured and the calculated spectra with JENDL-3.3, JENDL-3.2 and ENDF/B-VI from a 61 cm LiF sphere are shown in **Fig. 3.2**. Though the partial spectrum above 2 MeV energy range is satisfactorily predicted by every calculation, the difference between measured and calculated values is large below 2 MeV. The cause of this difference is not yet clear. Because in the case of the Li sample, the agreement between measurement and calculations is fairly good below 2 MeV, the cross section values of fluorine could be the primary cause for the disagreement.

### 3.2 TEFLON: (CF<sub>2</sub>)<sub>n</sub>

In **Fig. 3.3**, the measured and calculated spectra with FSXLIB-J3R3, FSXLIB-J3R2 and ENDF/B-VI (release 2) from a 40 cm TEFLON: (CF<sub>2</sub>)<sub>n</sub> of the OKTAVIAN experiment are depicted. All the calculations underestimate the experiment by more than 30 % and the difference among the calculations using three nuclear data is not large. The nuclear data of fluorine could be one of the reasons for this large difference. However, other causes should be further examined.

### 3.3 Oxygen

A JAERI-FNS benchmark result for liquid oxygen measured at 0 degree from 20 cm penetration is shown in **Fig. 3.4**. The neutron spectrum calculated with JENDL-3.3 shows a good agreement with the experiment, and it is improved compared with JENDL-3.2.

### 3.4 Sodium

For thick neutron penetration problems, JASPER IVFS-IC/Pb.9 and IHX-IB/Pb benchmarks are shown in **Figs. 3.5** and **3.6**, respectively. The results with JENDL-3.3 indicate a good agreement with both the measurements, while the results with ENDF/B-VI show overestimation compared with experiments in the energy range below 1.5 MeV. The difference is attributed to the inelastic reactions, based on the sensitivity analysis. The calculation results of MCNP-4C and DORT are consistent with each other and the tendency of the penetrated neutron energy spectra is the same between the IVFS-IC/Pb.9 and the IHX-IB/Pb benchmarks.

The SDT4 benchmark called Broomstick experiment, which was performed to check the effect of minima in the neutron total cross sections in the MeV energy range was analyzed. The result for 60.56 cm thick sodium is shown in **Fig. 3.7**. The neutron spectrum calculated with JENDL-3.3 shows a good agreement with the experiment, and it is the same as that with JENDL-3.2.

### 3.5 Aluminum, $\text{Li}_2\text{AlO}_3$ and $\text{LiAlO}_2$

In **Fig. 3.8**, the measured spectrum and the calculated spectra with FSXLIB-J3R3, FSXLIB-J3R2, ENDF/B-VI (release 2) and EFF-2.4 from a 40 cm Al spherical sample of the OKTAVIAN experiment are shown. All the calculations can predict the experiment almost satisfactorily. The prediction with EFF-2.4 is slightly better above 1.5 MeV than those with other data files except the lower energy region below 500 keV. JENDL-3.2 and EFF-2.4 show overestimation slightly between 300 keV and 500 keV compared with JENDL-3.3.

The FNS benchmark results for lithium aluminate ( $\text{Li}_2\text{AlO}_3$ ) measured at 76.2mm, 177.8 mm and 279.4 mm depths are shown in **Figs. 3.9** through **3.11**, respectively. The neutron spectra calculated with JENDL-3.3, JENDL-3.2 and FENDL-2 show almost the same tendency. Neutron flux below 10 keV is underestimated in the three libraries. The IPPE benchmark result for the aluminum sphere of 12 cm in radius (7.5 cm thickness) is shown in **Fig. 3.12**. Photon flux measurement of FNS for  $\text{LiAlO}_2$  from 10.16 cm penetration is shown in **Fig. 3.13** previously. The photon peaks from the discrete inelastic reactions are well reproduced with JENDL-3.3, while a peak at 6 MeV is underestimated in JENDL-3.2.

### 3.6 Silicon and SiC

The measured spectrum and the calculated spectra with JENDL-3.3, JENDL-3.2, ENDF/B-VI (release 5) and EFF-2.4 from a 60 cm Si sphere of the OKTAVIAN experiment are shown in **Fig. 3.14**. All the calculations predict the experiment well in general. However, the evaluation of ENDF/B-VI (release 5) gives the best prediction within 10 % agreement except the lowest energy region (i.e., 0.1 to 1 MeV), though the JENDL-3.3, JENDL-3.2 and EFF-2.4 can predict the experiment almost satisfactorily, the neutron energy spectra between 4.5 and 8 MeV underestimate the experiment result. The C/E values between 5 and 10 MeV have about 20 % discrepancies. The discrete inelastic cross section has a large dependence to the partial energy spectrum in this energy region<sup>16)</sup>. Since the discrete inelastic cross section values in the ENDF/B-VI are considered larger than those in the other three nuclear data, it might be proper to adjust the inelastic cross section values in the JENDL-3.3, JENDL-3.2 and EFF-2.4.

The FNS benchmark results for silicon carbide measured at 12.7, 27.9, 43.2 and 58.4 cm depth are shown in **Figs. 3.15** through **3.18**, respectively. The neutron spectra calculated with JENDL-3.3 and JENDL-3.2 show almost the same tendency. Neutron flux around 20 keV is underestimated in both libraries. The calculation results of MCNP-4C and TORT are consistent with each other.

### 3.7 Titanium and $\text{Li}_2\text{TiO}_3$

The measured spectrum and JENDL-3.3, JENDL-3.2, ENDF/B-VI (release 2) and EFF-2.4 calculations from a 40 cm Ti sphere of the OKTAVIAN experiment are shown in **Fig. 3.19**. Though the partial spectra including the elastic peak calculated with four data files predict the measured values within 20 %, the other parts of the calculated spectra differ from the experiment by up to 56 %.

**Fig. 3.20** compares the measured spectra with those of JENDL-3.3, JENDL-3.2 and ENDF/B-VI for OKTAVIAN Ti 40 cm sphere benchmark, where the ANISN and MCNP-4C calculations are shown. The calculations with JENDL-3.3 and JENDL-3.2 predict the experiment with fair agreement above 3 MeV, whereas, below 3 MeV, these calculations overestimate the measurement. It appears that in the JENDL-3.3 calculations the difference of the calculated spectra between ANISN and MCNP-4C is negligible. This implies that the anisotropy has very small effect to the formation of the spectrum. The ENDF/B-VI underestimates the experiment between 3 and 10 MeV and overestimates below 3 MeV. However, below 1 MeV the overestimation is not as severe as those with the other nuclear data. The cause of those discrepancies is not yet clarified.

The photon flux measurement of OKTAVIAN for Titanium from 40 cm sphere is shown in **Fig. 3.21**. The photon flux measurement of FNS for  $\text{Li}_2\text{TiO}_2$  from 10.16 cm penetration is shown in **Fig. 3.22**. The photon peaks from the discrete inelastic reactions are well reproduced with JENDL-3.3, while a peak at 6 MeV is underestimated in JENDL-3.2.

### 3.8 Vanadium

**Figures 3.23** and **3.24** show the neutron benchmarks performed by FNS. Neutron flux calculated with JENDL-3.3 shows underestimation below 1 keV, while it becomes better compared with JENDL-3.2 as shown in **Fig. 3.23**. On the contrary, a good agreement is generally obtained between 0.1 and 1 MeV. **Figures 3.25** and **3.26** show the photon benchmarks performed by FNS. For photon production data, JENDL-3.3 is slightly improved from JENDL-3.2.

### 3.9 Chromium

The measured spectrum and JENDL-3.3, JENDL-3.2, ENDF/B-VI (release 2) and EFF-2.4 calculations of the OKTAVIAN 40 cm sphere experiment are shown in **Fig. 3.27**. The general agreement between the calculated and measured spectra is satisfactory. The difference of JENDL-3.3 calculations between ANISN and MCNP-4C calculations is negligible as shown in **Fig. 3.28**. EFF-2.4, however, overestimates the experiment by 24 %, presumably caused by too low values of the discrete inelastic cross sections or the problem of the energy distribution of secondary neutrons as discussed in the previous paper<sup>13)</sup>.

The photon flux measurement of OKTAVIAN for Chromium from 40 cm sphere is shown in **Fig. 3.29**. The photon flux is well reproduced with JENDL-3.3, while FENDL-1 shows better performance beyond 5 MeV.

### 3.10 Manganese

The measured spectrum and JENDL-3.3, JENDL-3.2, ENDF/B-VI (release 2) and EFF-2.4 calculations of the leakage spectra from a 61 cm Manganese sphere of the OKTAVIAN experiment are shown in **Fig. 3.30**. Except the minor difference around 10 MeV, the calculations with all the nuclear data, JENDL-3.3, JENDL-3.2, ENDF/B-VI (release 2) and EFF-2.4 can predict the experiment with an excellent agreement.

### 3.11 Iron

The SDT1 benchmark called Broomstick experiment, which was performed to check the effect of minima in the neutron total cross sections in the MeV energy range, was analyzed. The results for 20.32 and 30.48 cm thick iron are shown in **Figs. 3.31** and **3.32**, respectively. The neutron spectrum calculated with

JENDL-3.3 shows a good agreement with the experiment, and it is similar to that with JENDL-3.2.

For relatively thin neutron transmission benchmarks, we selected KfK, IPPE and NIST experiments from iron spheres with a  $^{252}\text{Cf}$  source in the center. The results are shown in **Figs. 3.33** through **3.38** for the KfK iron sphere from 15 to 40 cm in diameter. Neutron spectrum calculated with MCNP-4C shows good agreement except for resonance minima below 400 keV, but a good agreement is generally obtained between calculation and measurement. **Fig. 3.39** shows the result of the IPPE iron sphere of 12 cm in radius (7.5 cm thickness). **Fig. 3.40** shows the result of the NIST iron sphere of 50.7 cm in diameter. The result with JENDL-3.3 is similar to that with JENDL-3.2, however the result with JENDL-3.3 shows slightly larger than that with ENDF/B-VI in the energy range between 1.6 and 2 MeV. This tendency also appears in the KfK benchmark.

For relatively thick neutron penetration benchmarks, we adopted the ASPIS and FNS experiments. **Figs. 3.41** through **3.44** show comparisons between the calculated results and the ASPIS measurements from 22.54 cm to 113.98 cm depth of iron slabs. **Figs. 3.45** through **3.51** indicate comparisons between the calculated results with MCNP-4C/DORT and the FNS measurements from 11 cm to 81 cm depth of the large iron cylinder. In these benchmarks, neutron fluxes calculated with JENDL-3.3 in the energy range between 0.7 and 1 MeV are slightly underestimated compared with the experiments. On the contrary, the results with ENDF/B-VI are much better in this energy region. The two calculation results with DORT and MCNP-4C show the same flux profile, so that we recommend some consideration should be made in this energy range. For lower energy region below the 24 keV s-wave resonance, JENDL-3.3 slightly indicates overestimation compared with measurement as shown in **Fig. 3.51**. The calculation to experimental (C/E) ratio integrated over between 1 and 1000 eV is relatively large in JENDL-3.3, whereas the C/E deviations with JENDL-3.3 for the other energy region at each measured position are relatively smaller than those with another libraries.

The results of the ORNL iron benchmark experiments are shown in **Tables 3.1** through **3.3** for JENDL-3.3, JENDL-3.2 and ENDF/B-VI, respectively. The C/E values of the Bonner balls with JENDL-3.3 for the iron slab of 30.81 cm in thickness range from 0.96 to 1.26, for the iron slab of 62.001 cm in thickness range from 0.91 to 1.28, and for the iron slab of 92.862 cm range from 0.82 to 1.32, respectively. The C/E values of the NE-213 spectrometer with JENDL-3.3 for the iron slab of 10.287 cm in thickness range from 1.09 to 1.29, for the iron slab of 30.81 cm in thickness range from 0.93 to 1.10, respectively. The C/E value of the Benjamin spectrometer with JENDL-3.3 for the iron slab of 31.115 cm in thickness is 1.05. These C/E values are similar to those with JENDL-3.2 and ENDF/B-VI.

For photon production benchmarks, we employed the KfK and FNS measurements. The results with JENDL-3.3 indicate good agreement with measurements as shown in **Figs. 3.52** through **3.55**, and the results are better than those with JENDL-3.2.

### 3.12 Cobalt

The measured and calculated spectra with JENDL-3.3, JENDL-3.2, ENDF/B-VI (release 2) and EFF-2.4 from the 40 cm Co sphere of the OKTAVIAN experiment are shown in **Fig. 3.56**. Though the elastic scattering peak around 14 MeV can be well predicted by every nuclear data, all the calculations underestimate the experiment by more than 30 %. The cause for the discrepancy has not been clarified. The difference of JENDL-3.3 calculations between the ANISN and MCNP-4C calculations is negligible as shown in **Fig. 3.57**.

### 3.13 Nickel and SS304

**Figure 3.58** shows the leakage neutron spectrum from the nickel sphere of 12 cm in radius (7.5 cm thickness) of the IPPE benchmark. The result is generally acceptable, and no problem is found. The results of the ORNL stainless steel benchmark experiments are shown in **Tables 3.4** through **3.6** for JENDL-3.3, JENDL-3.2 and ENDF/B-VI, respectively. The C/E values of the Bonner balls with JENDL-3.3 for the SS304 slab of 30.91 cm in thickness range from 0.99 to 1.26. The C/E value of the Benjamin spectrometer with JENDL-3.3 for the SS304 slab of 30.91 cm in thickness is 1.07. These C/E values are similar to those with

JENDL-3.2 and ENDF/B-VI.

### 3.14 Copper

**Figures 3.59 through 3.61** show the comparison between calculation and measurement for the FNS Copper experiment. The results of JENDL-3.3 are in good agreement with the experiments except below 1 keV for the FNS benchmark.

The measured spectrum and JENDL-3.3, JENDL-3.2 and EFF-2.4 calculations of the OKTAVIAN experiment are shown in **Fig. 3.62**. It is seen that all the data are almost satisfactory above 0.1 MeV energy region except the energy region between 5 and 10 MeV. The calculation with EFF-2.4 overestimates the experiment by more than 25 % in 5-10 MeV. JENDL-3.3 overestimates the experiment in the region by about 14 %, whereas the calculation with JENDL-3.2 agrees with the experiment within a few %. Since the cross section values of  $^{65}\text{Cu}$  among nuclear data do not largely differ from each other<sup>13)</sup>, the differences among the calculated results can be considered due to the continuum inelastic cross section values of  $^{63}\text{Cu}$ .

### 3.15 Arsenic

The measured spectrum and JENDL-3.3 and JENDL-3.2 calculations of the OKTAVIAN Arsenic experiment are shown in **Fig. 3.63**. Both the calculations are very close to each other and give almost satisfactory predictions except for the energy region below 1 MeV and between 8 and 12 MeV.

### 3.16 Selenium

In **Fig. 3.64**, depicted are the OKTAVIAN measured spectrum and the calculated one with JENDL-3.3, which is the only library currently available for the MCNP-4C calculation. It overestimates the experiment above 12 MeV, whereas below this energy the calculation underestimates the measurement considerably. The cause of this discrepancy is not yet clear.

### 3.17 Zirconium and $\text{Li}_2\text{ZrO}_3$

In **Fig. 3.65**, the measured spectrum and the calculated spectra of the OKTAVIAN experiment with JENDL-3.3, JENDL-3.2, ENDF/B-VI (release 2) and EFF-2.4 are shown. JENDL-3.3 and JENDL-3.2 give satisfactory predictions above 0.7 MeV, whereas below the energy region, there are considerable discrepancies in those calculations. On the contrary, the ENDF/B-VI (release 2) and EFF-2.4 calculations considerably overestimate the experiment above 1 MeV. ENDF/B-VI calculation also considerably underestimates the experiment below 1 MeV. EFF-2.4 predicts the partial spectrum below 1 MeV satisfactorily, where the JENDL calculations cannot give satisfactory predictions. As explained in the reference 15, the modification of the secondary energy distribution of the  $(n,2n)$  cross section in JENDL-3.2 by imitating that of EFF-2.4 improves the agreement with the measurement.

**Figures 3.66 through 3.69** show the comparison between the calculation and measurement for the FNS  $\text{Li}_2\text{ZrO}_3$  experiment. The results of JENDL-3.3 are in good agreement with experiments except below 10 keV for the thin penetration between 76 mm and 177 mm depth.

The photon flux measurement of FNS for  $\text{Li}_2\text{ZrO}_3$  from 101.6 mm penetration is shown in **Fig. 3.70**. The photon peaks from discrete inelastic reactions are well reproduced with JENDL-3.3, while a peak around at 6 MeV is underestimated in JENDL-3.2.

### 3.18 Niobium

Since EFF-2.4 adopts the ENDF/B-VI data for Nb, the JENDL-3.3, JENDL-3.2 and ENDF/B-VI calculations of the OKTAVIAN experiment are shown in **Fig. 3.71** together with the measured spectrum. There is not a large difference between the MCNP-4C and ANISN calculations as shown in **Fig. 3.71**. The agreement of the JENDL-3.3 and JENDL-3.2 calculations with the experiment is similar to that of Zr. Both can predict the experiment well above 1 MeV and overestimate the experiment below 1 MeV. The ENDF/B-

VI overestimates the experiment above 1 MeV, whereas the agreement below 1 MeV is fair. Similarly to the Zr case, the modification of the secondary energy distribution of the  $(n,2n)$  cross section in JENDL-3.2 improves the agreement with the measurement. The photon spectra for Niobium are generally acceptable as shown in **Fig. 3.72**.

### 3.19 Molybdenum

The measured spectrum and the JENDL-3.3, JENDL-3.2, ENDF/B-VI and EFF-2.4 calculations of the OKTAVIAN experiment are shown in **Fig. 3.73**. The JENDL-3.3 and JENDL-3.2 calculations predict the experiment quite well over whole energy region except the slight underestimation around 10 MeV. The ENDF/B-VI calculation also overestimates the experiment between 1 and 4 MeV by about 30 % and underestimates the experiment below 0.7 MeV as found in **Fig. 3.73**. The prediction with EFF-2.4 is better than that of ENDF/B-VI. However, the underestimations between 7 and 13 MeV and below 1 MeV are larger than those of JENDL-3.3 and JENDL-3.2. JENDL-3.3 and JENDL-3.2 presumably need slight modification of the inelastic cross section to solve the underestimation found between 6 and 12 MeV.

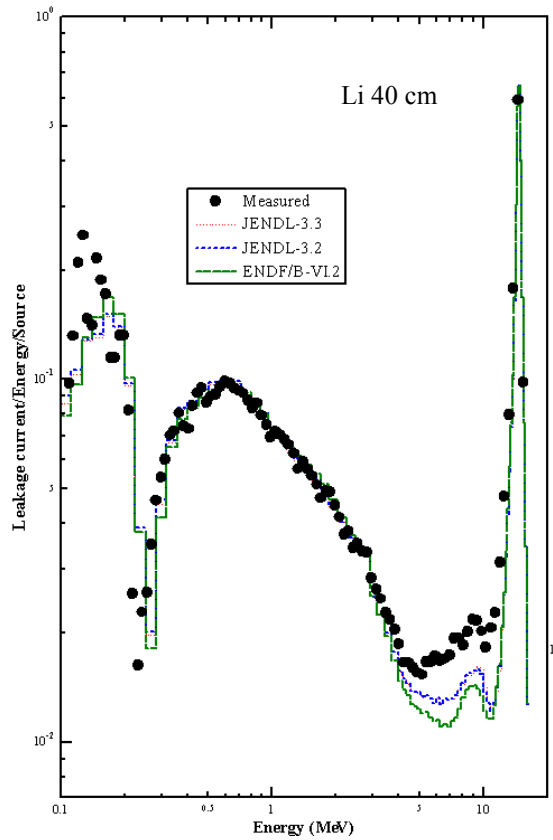
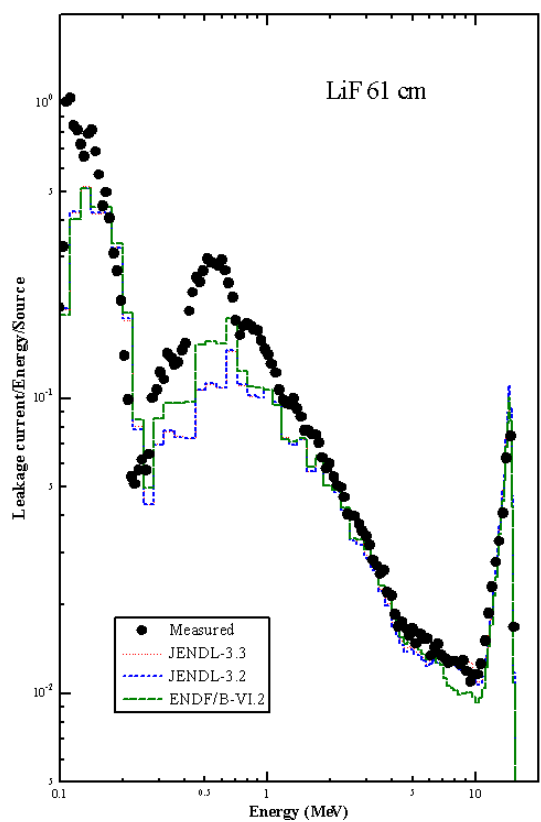
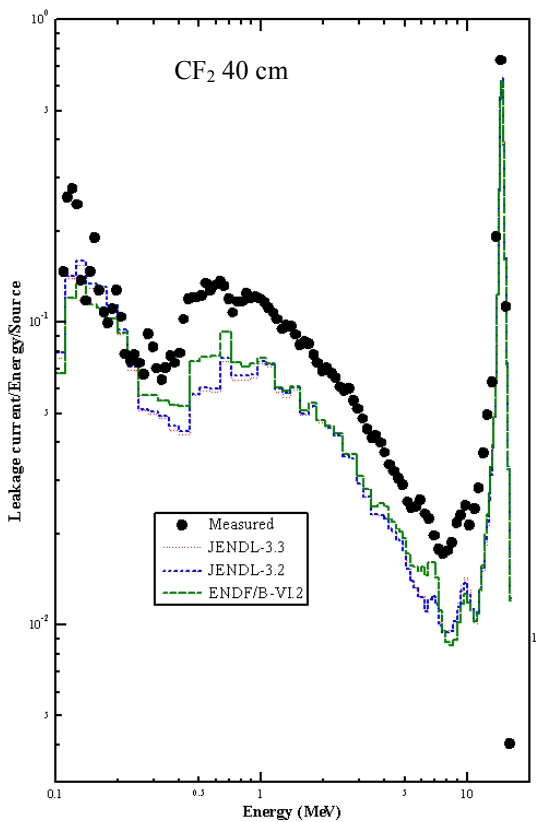
### 3.20 Tungsten

The neutron flux measurement of FNS is shown in **Fig. 3.74**. The calculated neutron spectra above 150 keV slightly underestimate the FNS experiment. For leakage photon measurements of FNS and OKTAVIAN, the profile of photon flux with JENDL-3.3 is generally acceptable compared with that with JENDL-3.2 as shown in **Figs. 3.75** and **3.76**.

The calculations using JENDL-3.3, JENDL-3.2, ENDF/B-VI and EFF-2.4 of the OKTAVIAN experiment are shown in **Fig. 3.77** together with the measured spectrum. The ENDF/B-VI calculation predicts better than those with the other nuclear data. However, there still exists a large underestimation above 5 MeV and slight underestimation below 5 MeV in the ENDF/B-VI calculation. With the JENDL-3.3, the odd spectrum shape around 7 MeV, which is observed in JENDL-3.2, disappears and the agreement below 1 MeV becomes excellent. However, there still remains a considerable underestimation between 1 and 10 MeV. This underestimation could be improved by changing the inelastic scattering cross section values.

### 3.21 Mercury

The neutron flux measurement of FNS is shown in **Fig. 3.78**. The calculated neutron spectra at thickness of 7 and 14 cm are generally acceptable while the calculated values slightly show underestimation. The gamma-ray heating rate measurement of FNS indicates underestimation as shown in **Fig. 3.79**.

**Fig. 3.1** Results of OKTAVIAN Lithium benchmark.**Fig. 3.2** Results of OKTAVIAN LiF benchmark.**Fig. 3.3** Results of OKTAVIAN TEFLOON benchmark.

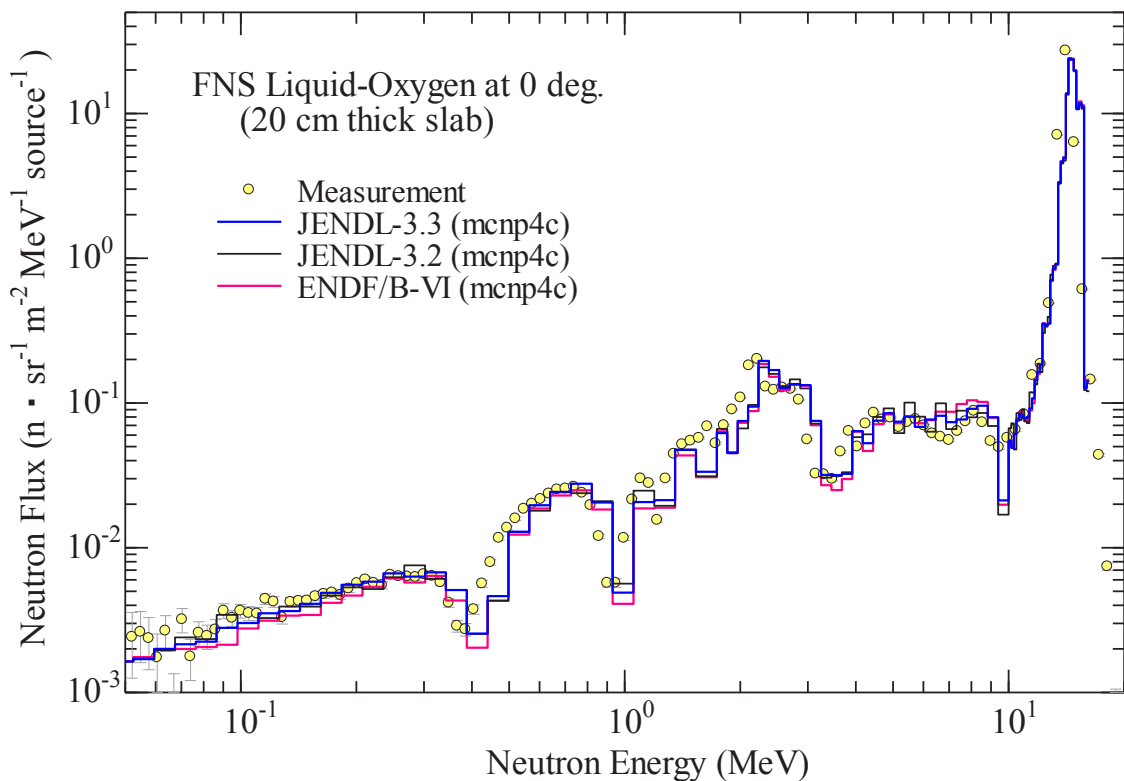
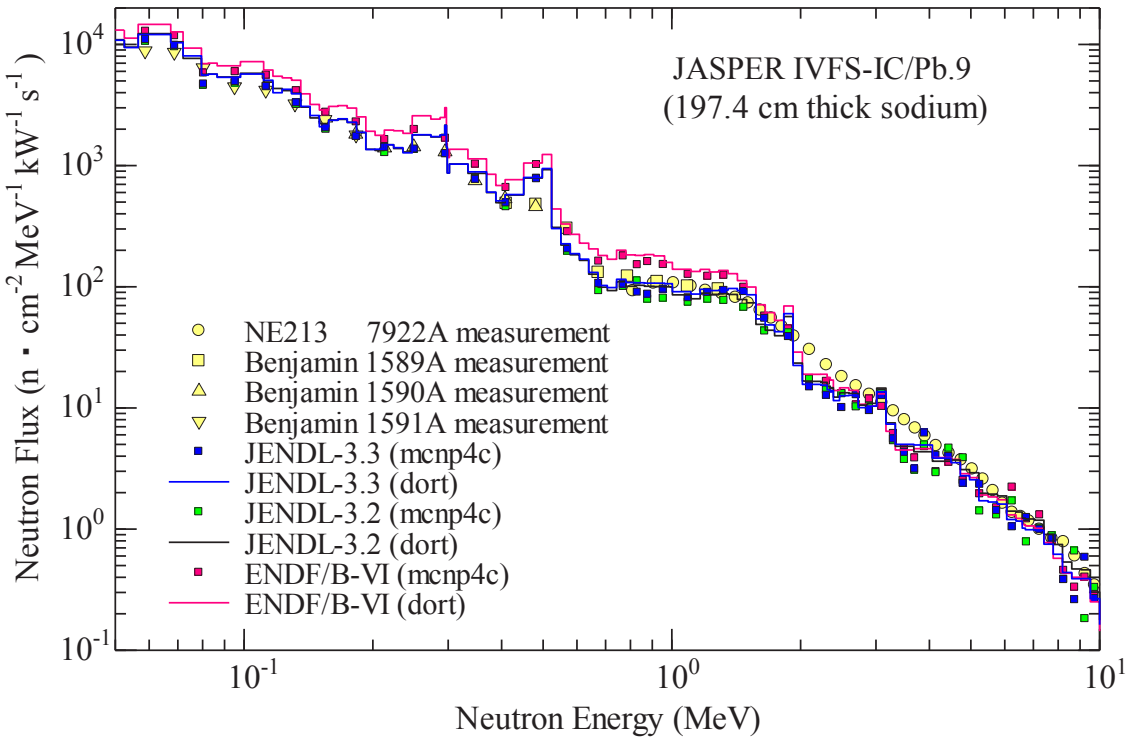
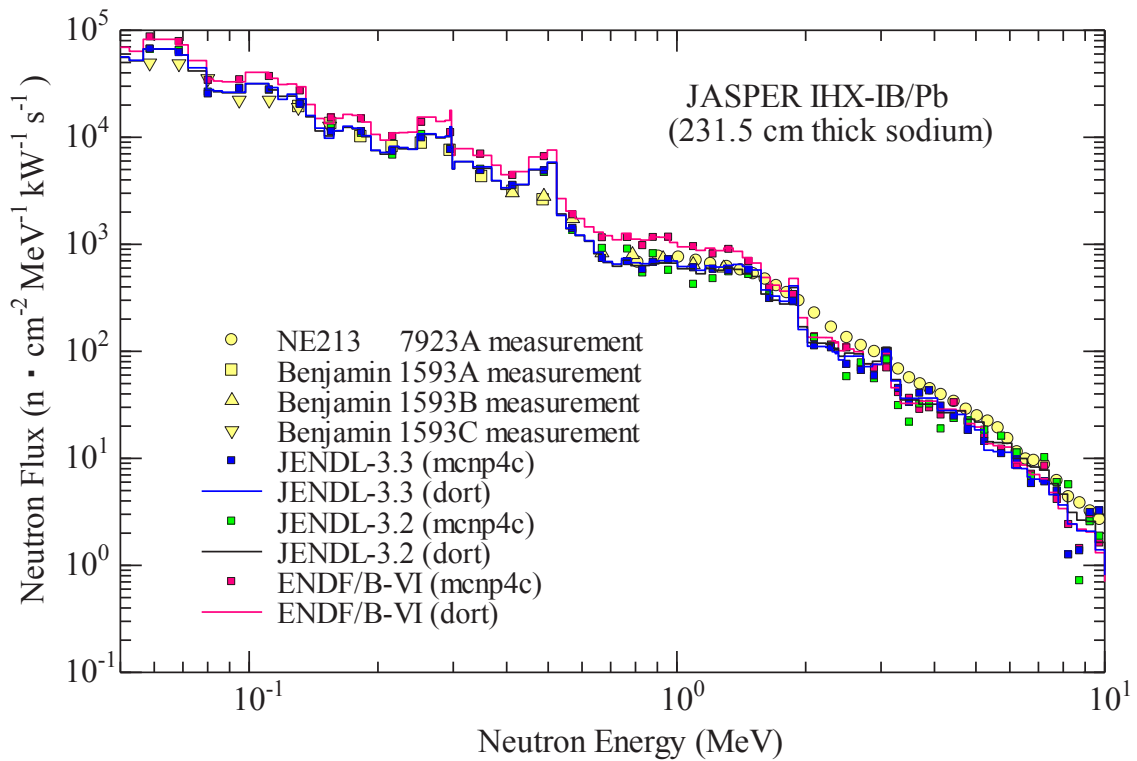


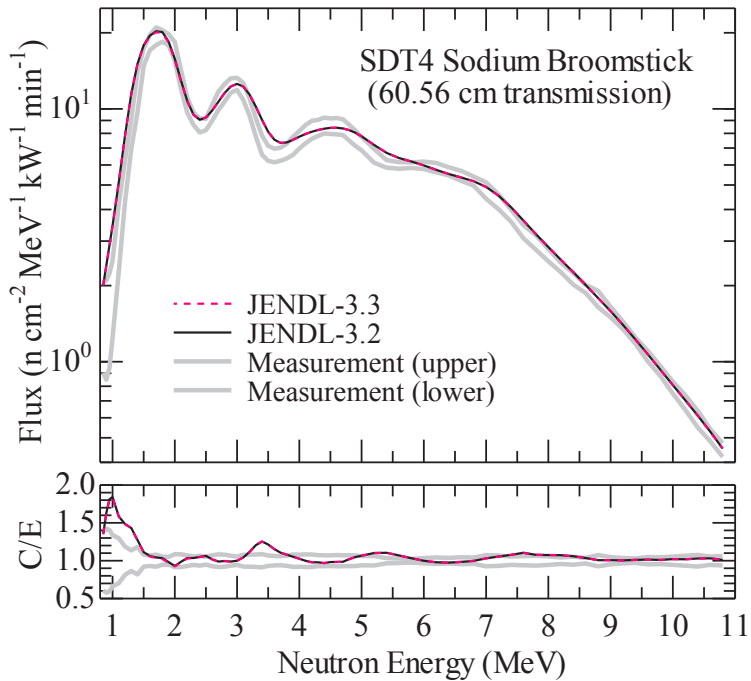
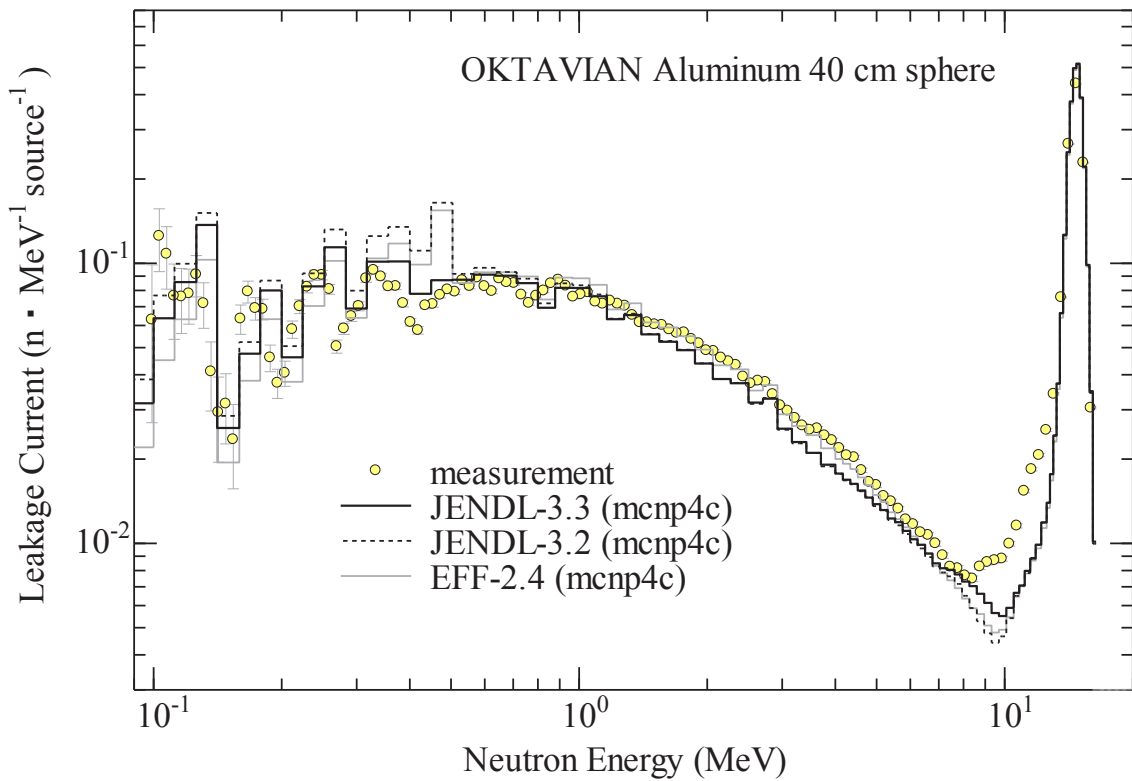
Fig. 3.4 Results of FNS Oxygen benchmark.



**Fig. 3.5** Results of JASPER IVFS-IC/Pb benchmark.



**Fig. 3.6** Results of JASPER IHX-IB/Pb benchmark.

**Fig. 3.7** Results of Sodium SDT4 benchmark.**Fig. 3.8** Results of OKTAVIAN Aluminum benchmark.

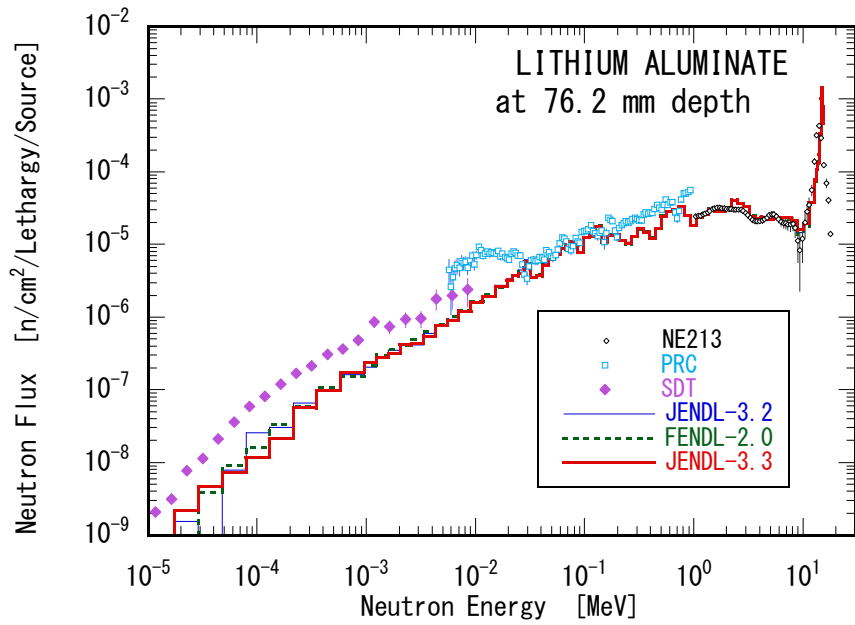


**Fig. 3.9** Results of FNS  $\text{Li}_2\text{AlO}_3$  benchmark at 76.2 mm depth.

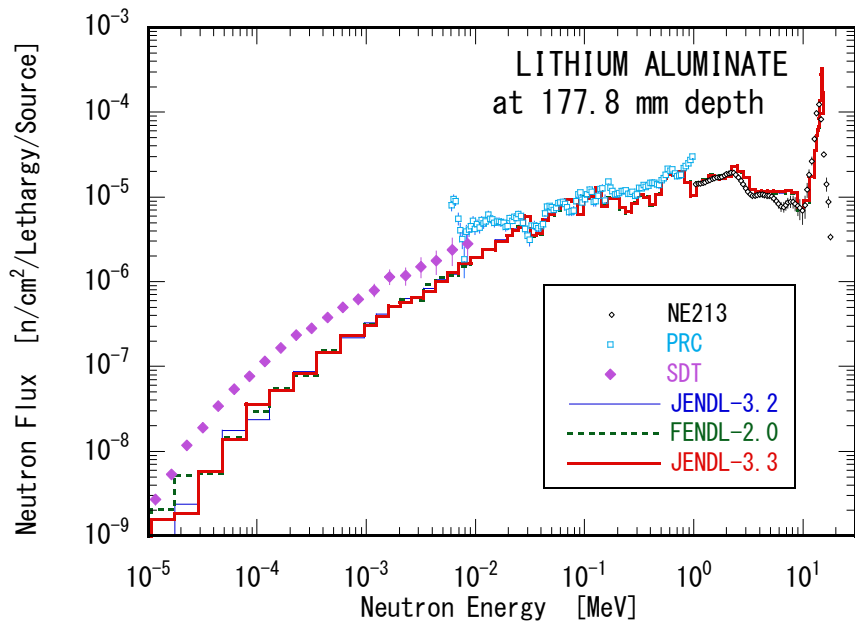


**Fig. 3.10** Results of FNS  $\text{Li}_2\text{AlO}_3$  benchmark at 177.8 mm depth.

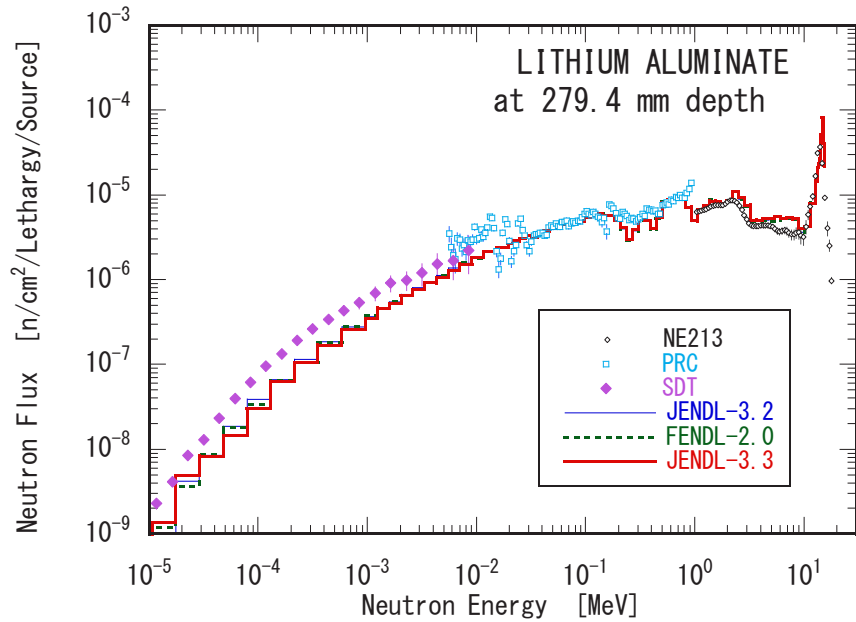


**Fig. 3.11** Results of FNS  $\text{Li}_2\text{AlO}_3$  benchmark at 279.4 mm depth.

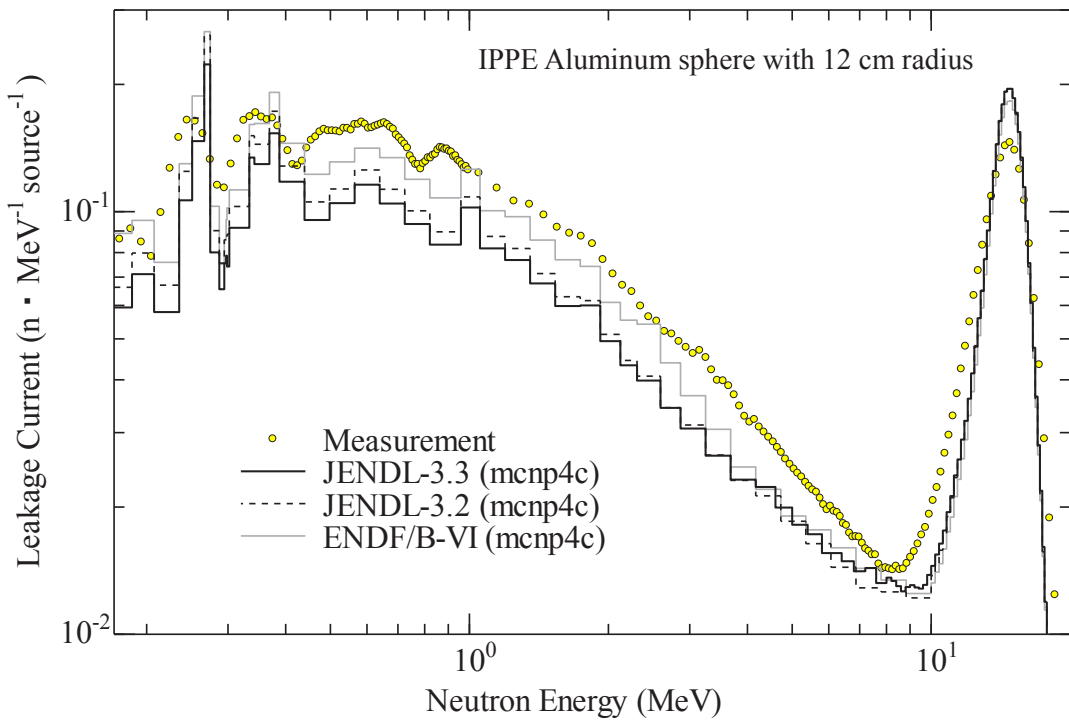


**Fig. 3.12** Results of IPPE Al benchmark from 12 cm radius.

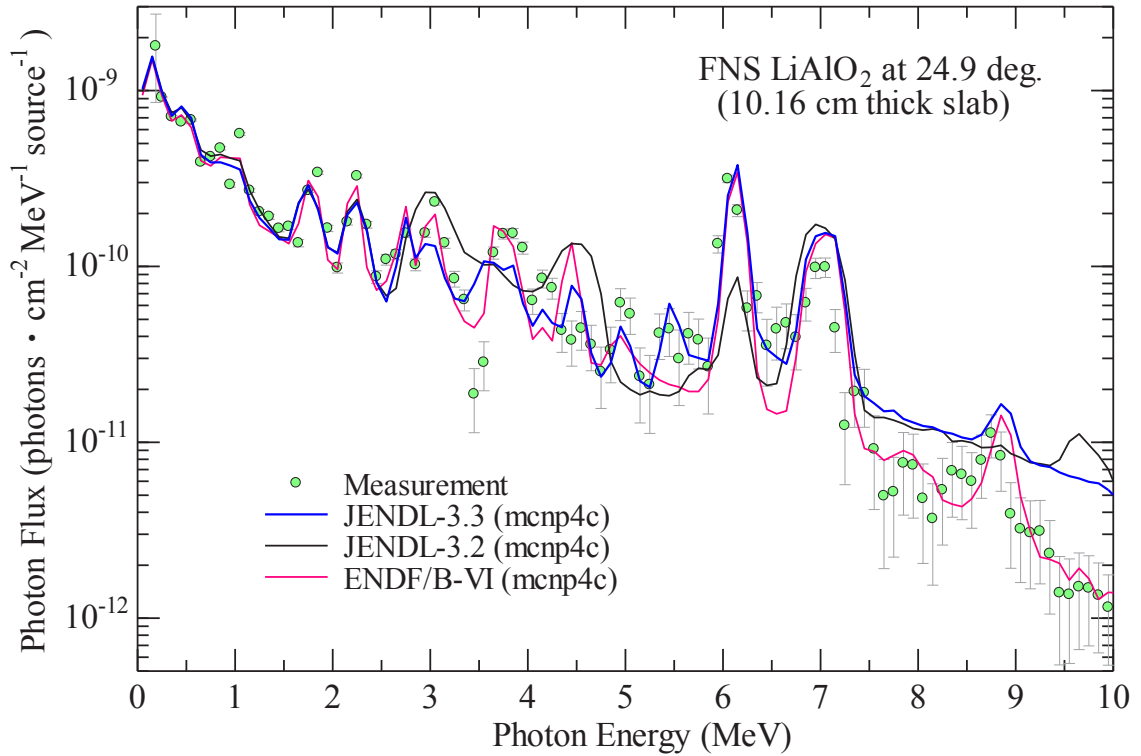


**Fig. 3.13** Photon flux of FNS LiAlO<sub>2</sub> benchmark.

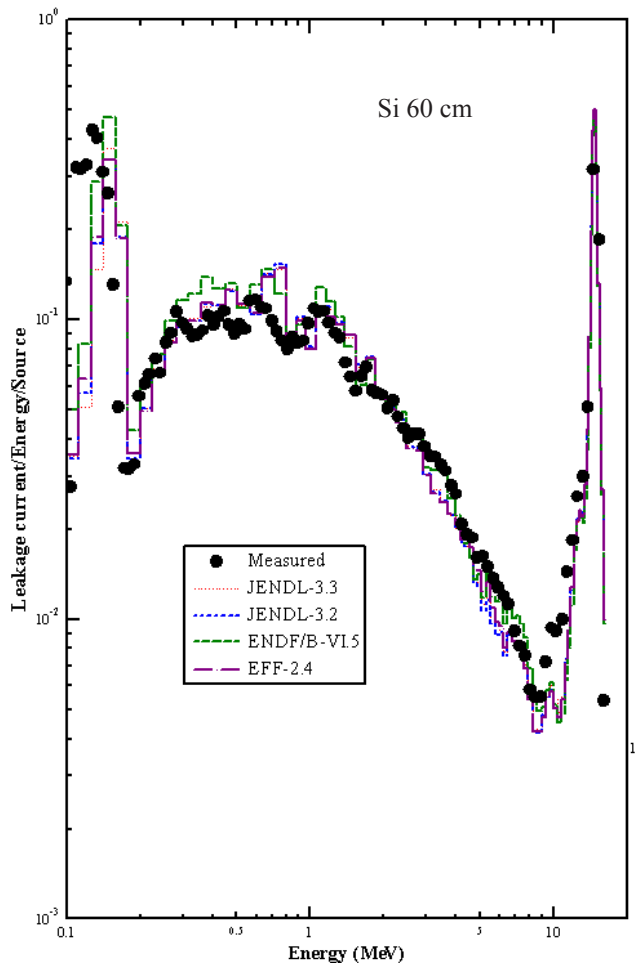


Fig. 3.14 Results of OKTAVIAN Silicon benchmark.

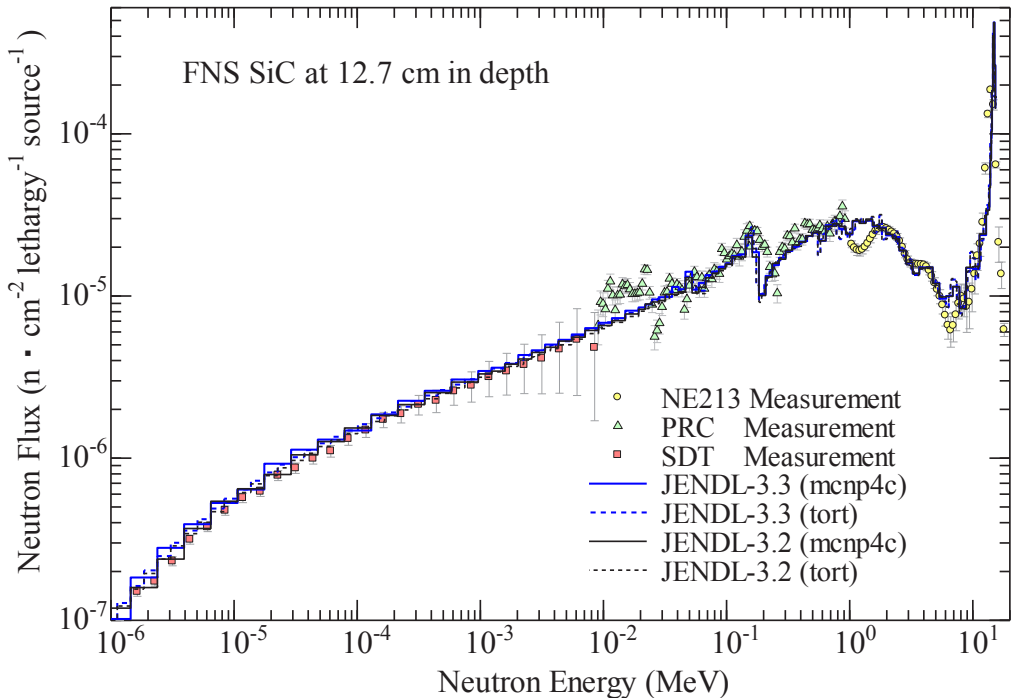
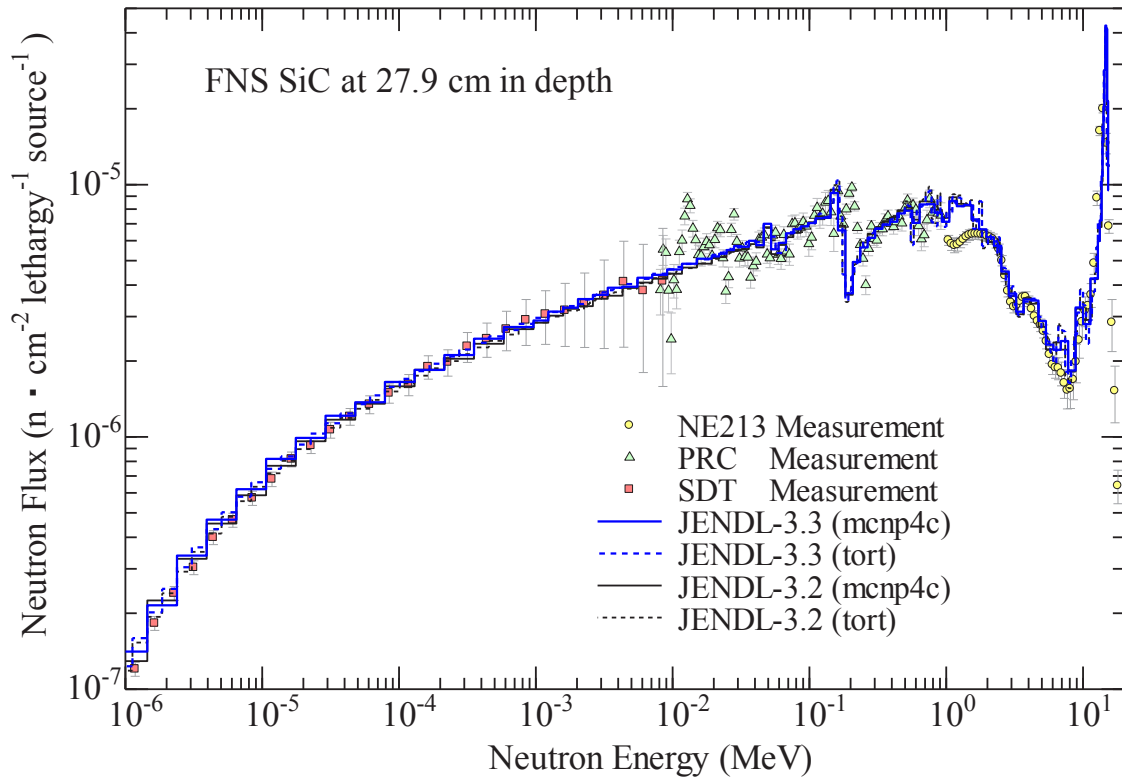
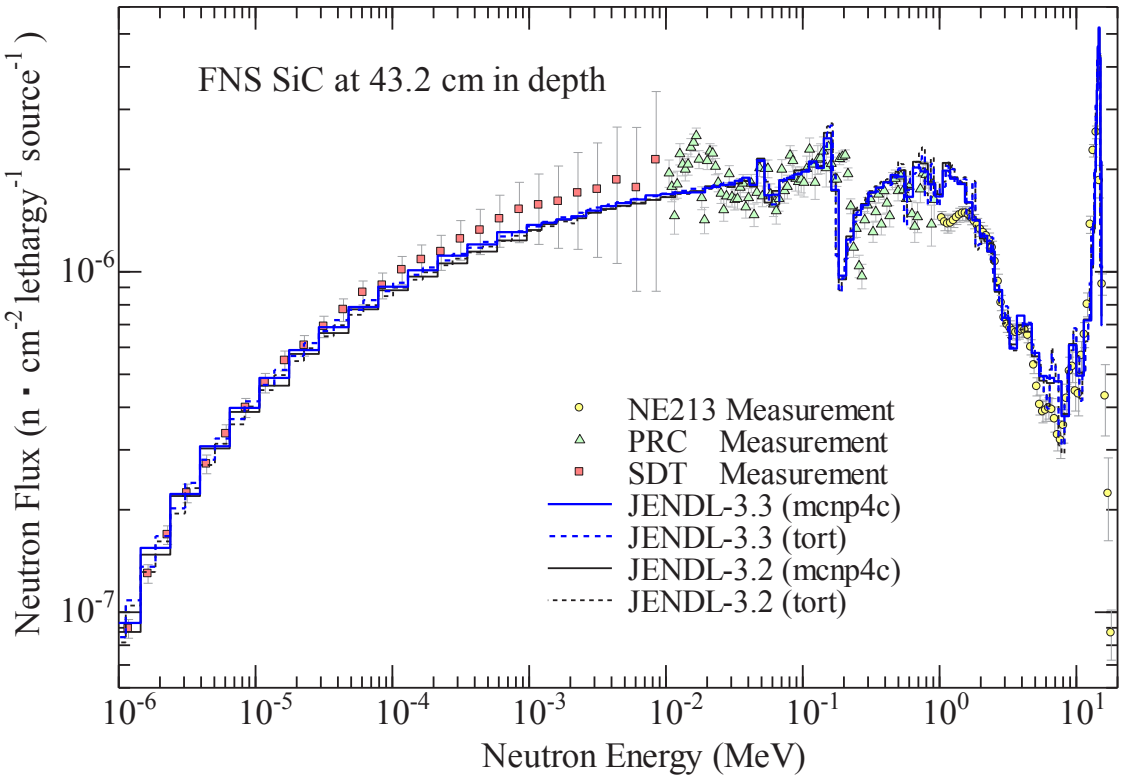


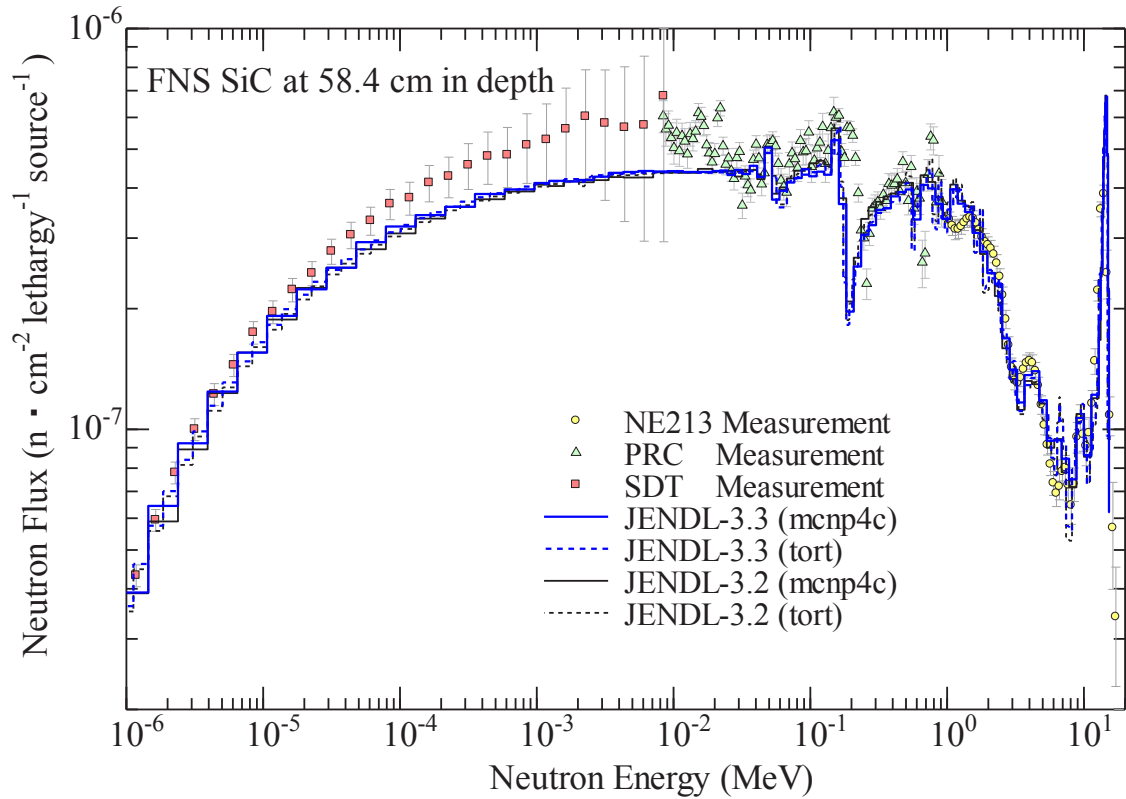
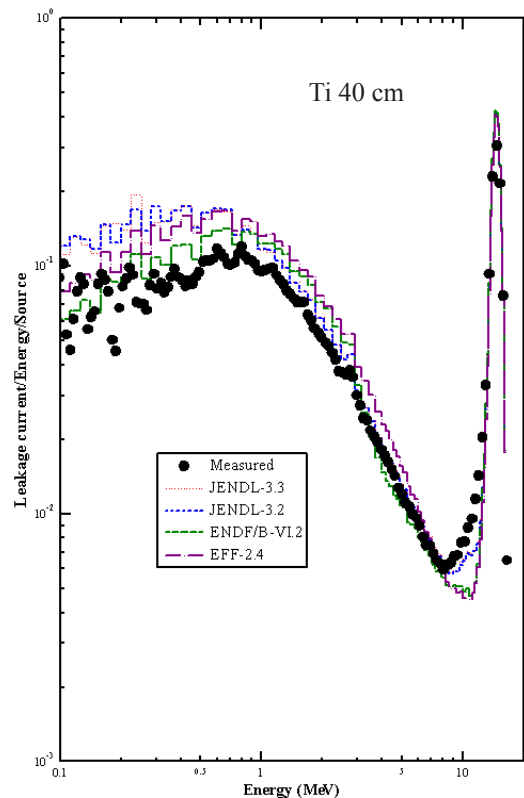
Fig. 3.15 Results of FNS Silicon Carbide benchmark at 12.7 cm depth.



**Fig. 3.16** Results of FNS Silicon Carbide benchmark at 27.9 cm depth.



**Fig. 3.17** Results of FNS Silicon Carbide benchmark at 43.2 cm depth.

**Fig. 3.18** Results of FNS Silicon Carbide benchmark at 58.4 cm depth.**Fig. 3.19** Results of OKTAVIAN Titanium benchmark (1).

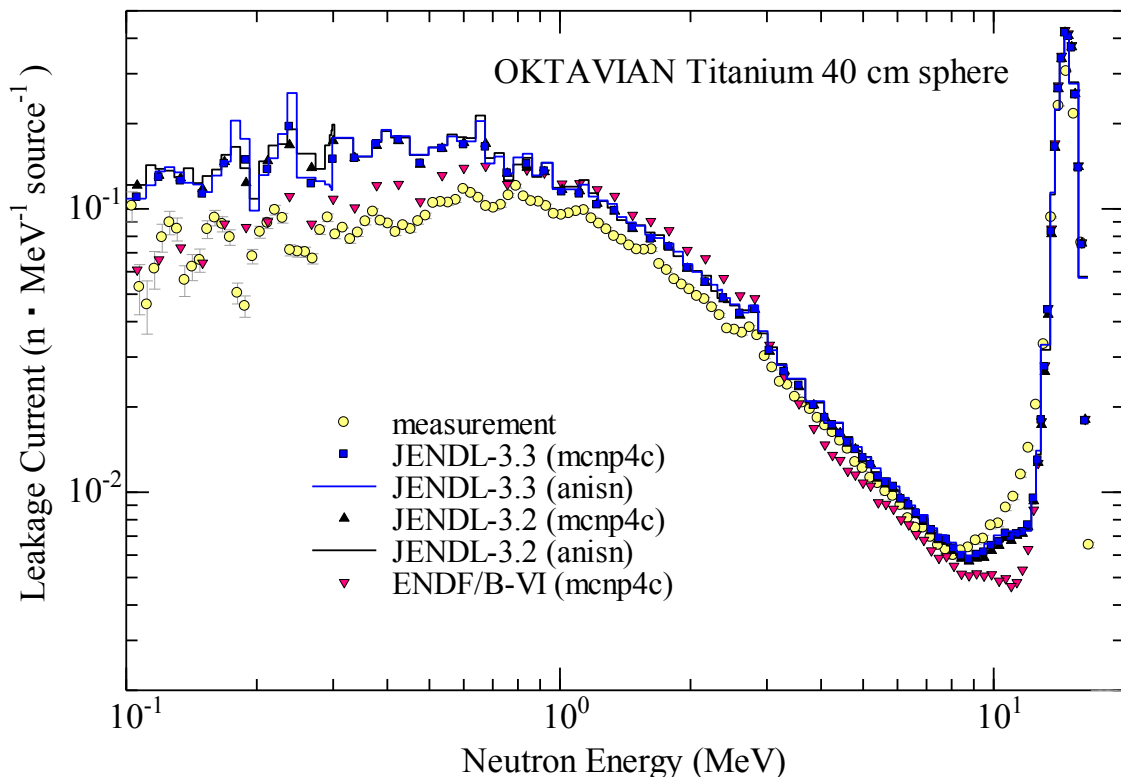


Fig. 3.20 Results of OKTAVIAN Titanium benchmark (2).

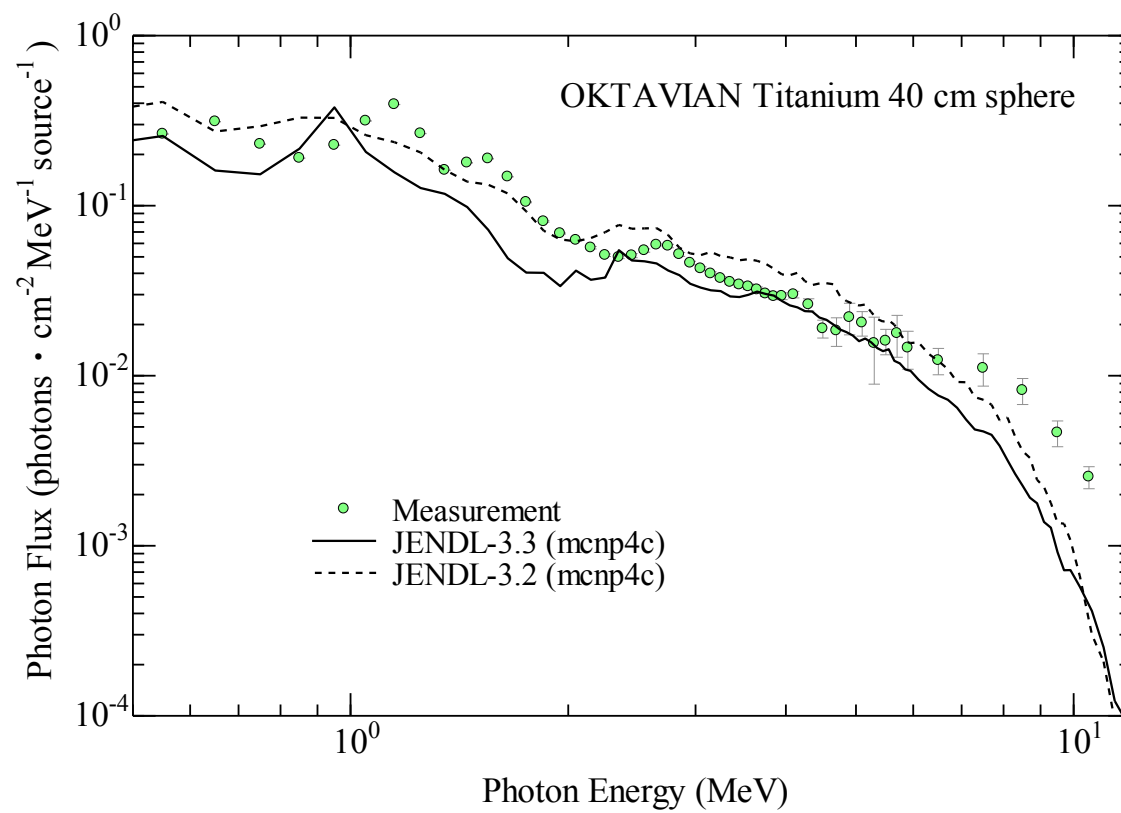


Fig. 3.21 Photon flux of OKTAVIAN Titanium benchmark.

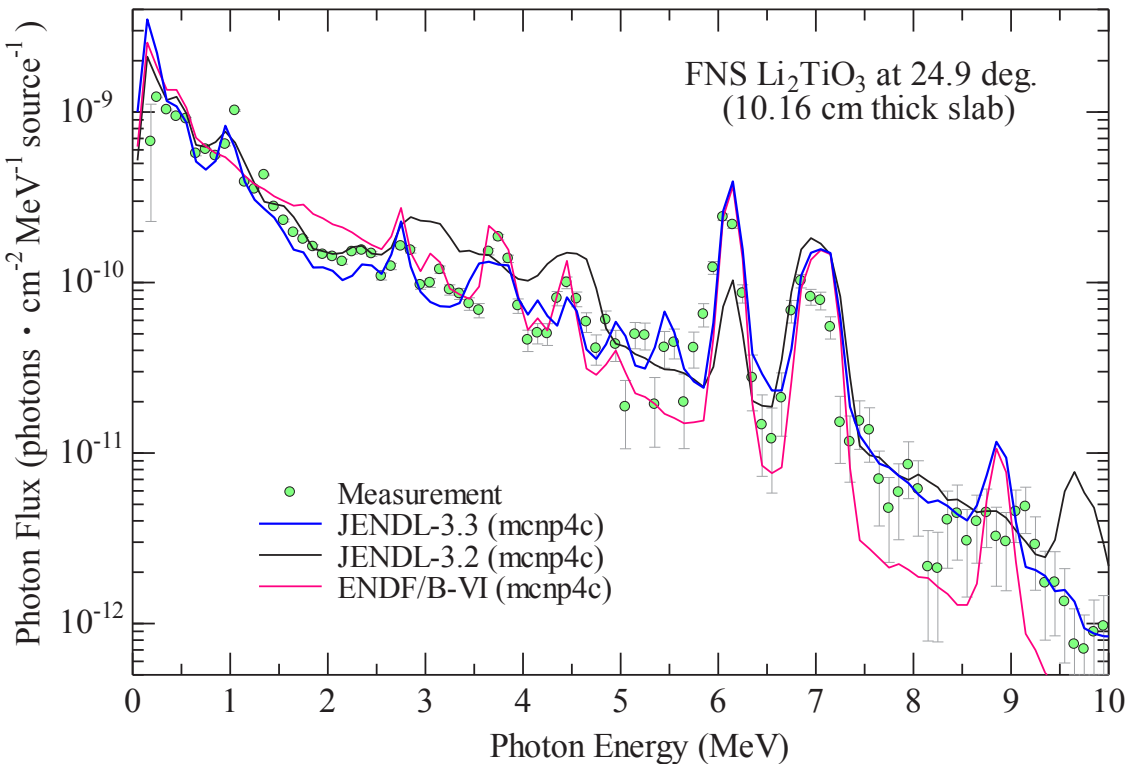
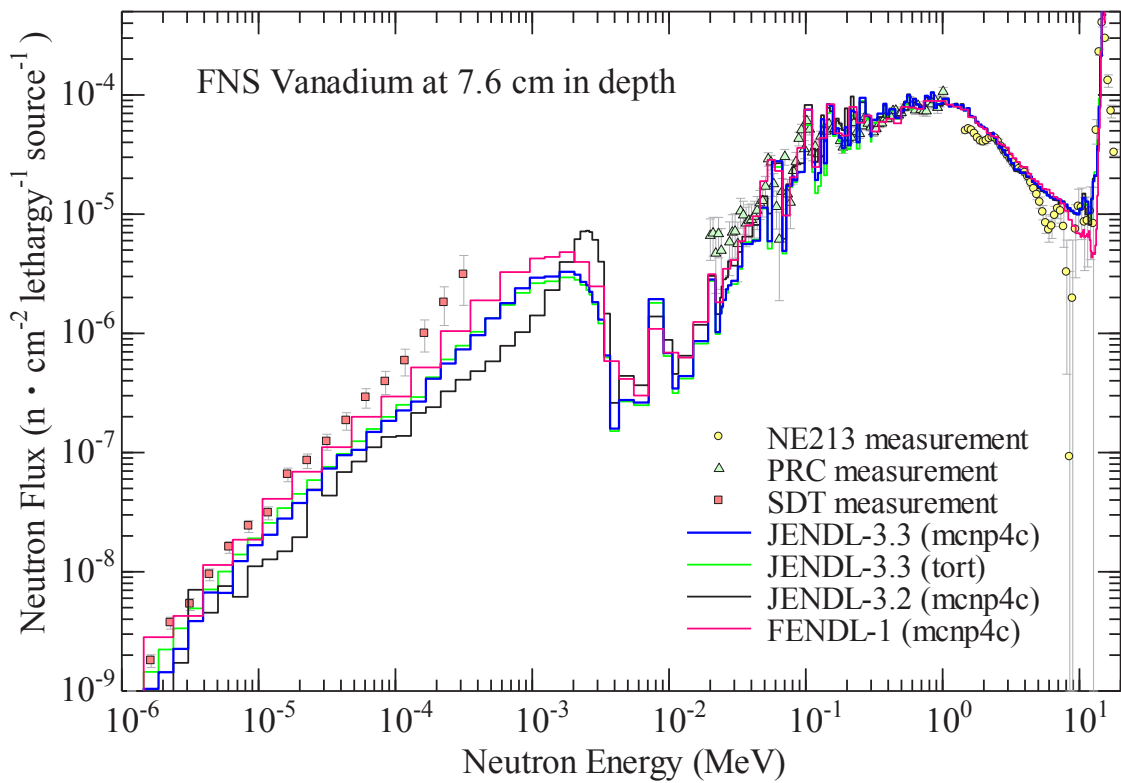
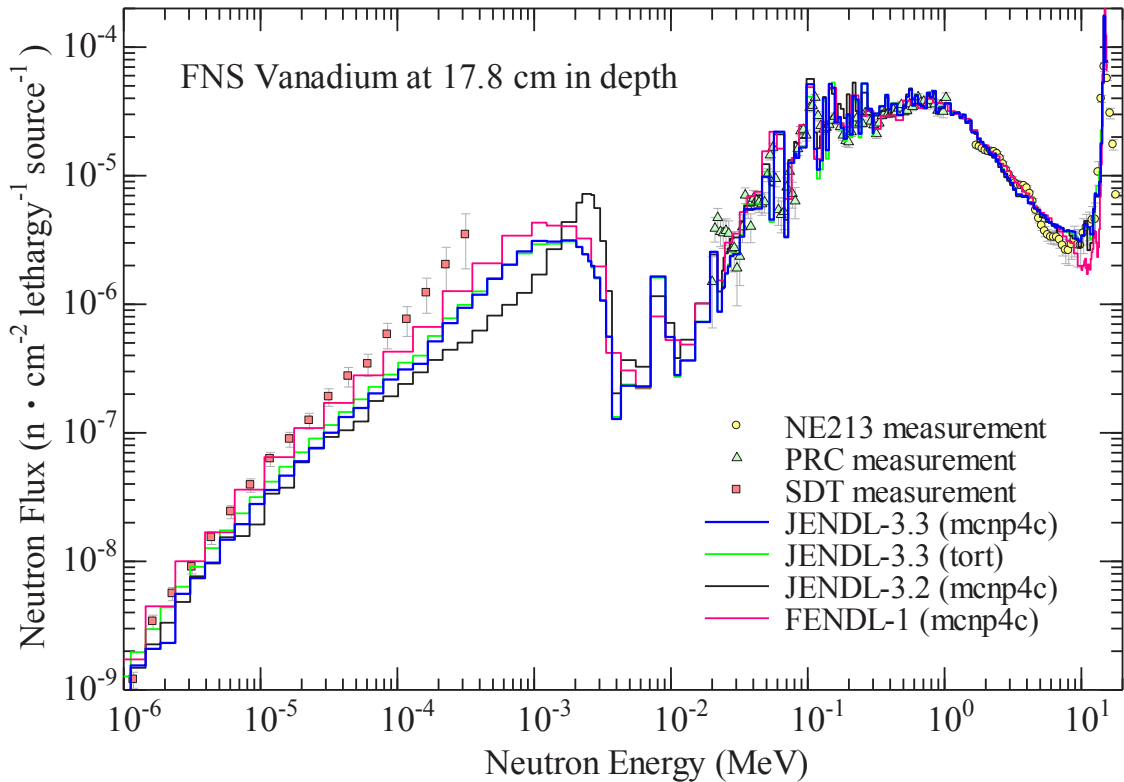
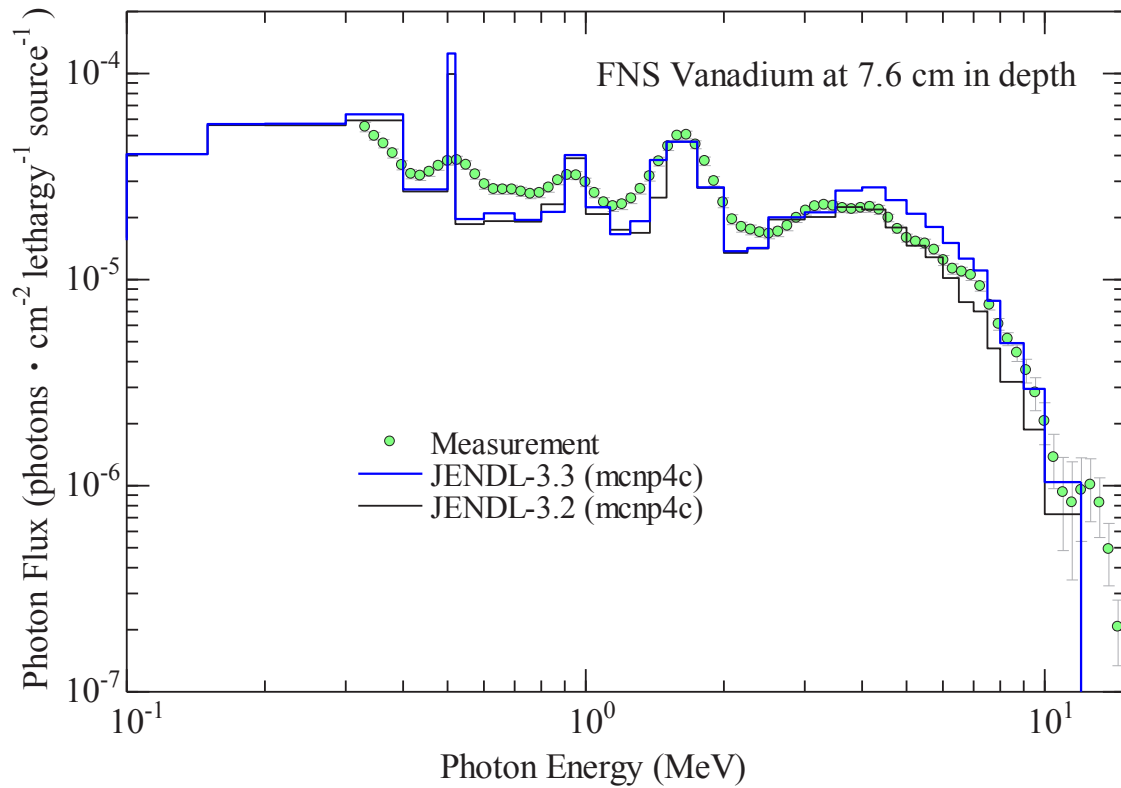
Fig. 3.22 Photon flux of FNS Li<sub>2</sub>TiO<sub>3</sub> benchmark.

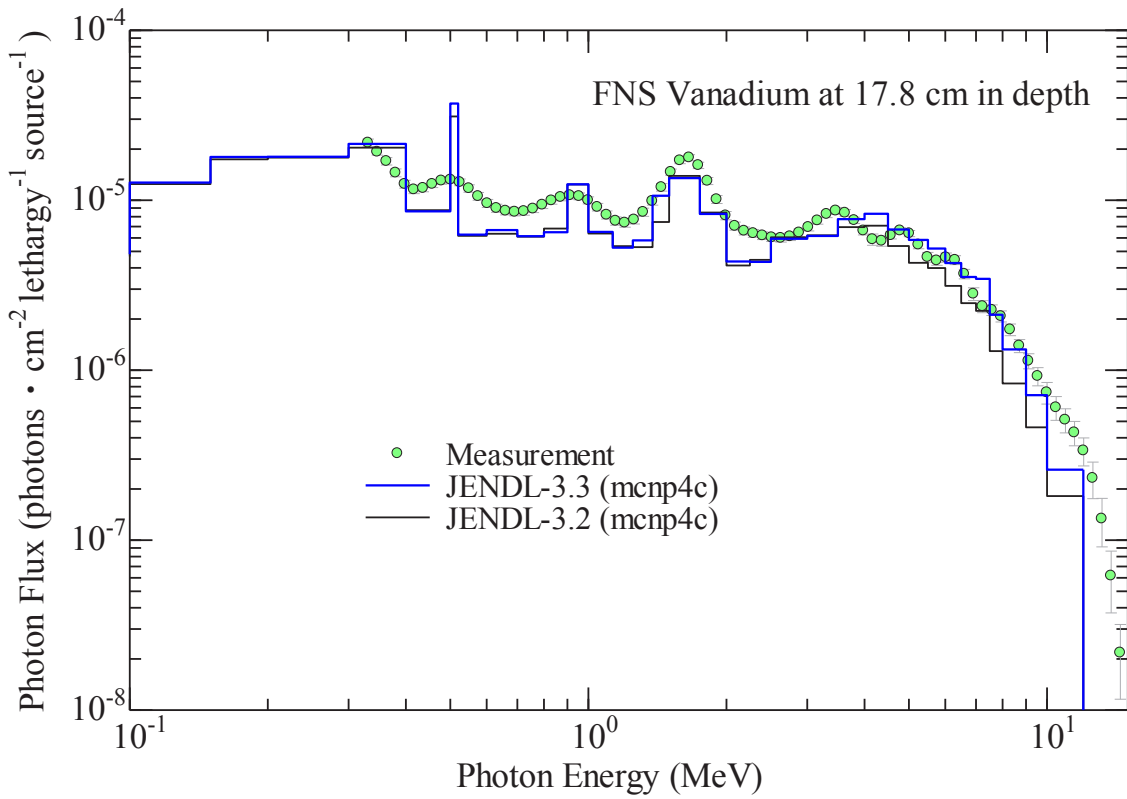
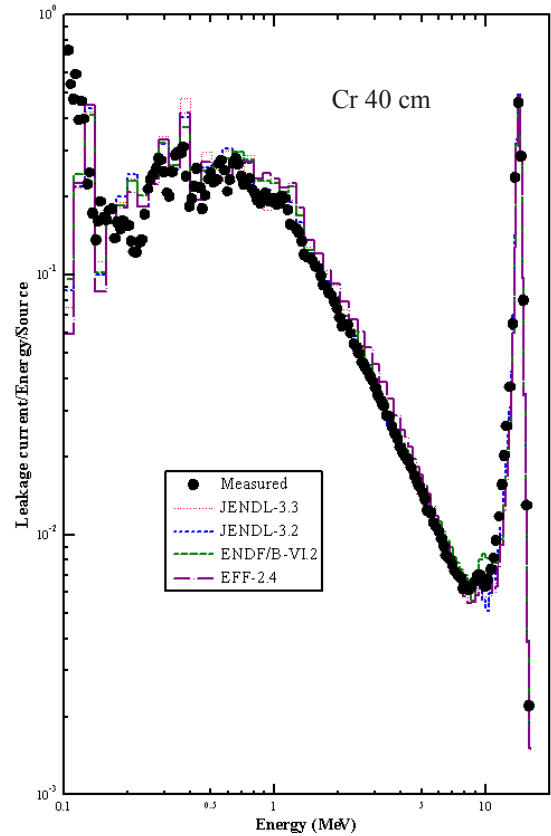
Fig. 3.23 Results of FNS Vanadium benchmark at 7.6 cm depth.



**Fig. 3.24** Results of FNS Vanadium benchmark at 17.8 cm depth.



**Fig. 3.25** Photon flux of FNS Vanadium benchmark at 7.6 cm depth.

**Fig. 3.26** Photon flux of FNS Vanadium benchmark at 17.8 cm depth.**Fig. 3.27** Results of OKTAVIAN Chromium benchmark (1).

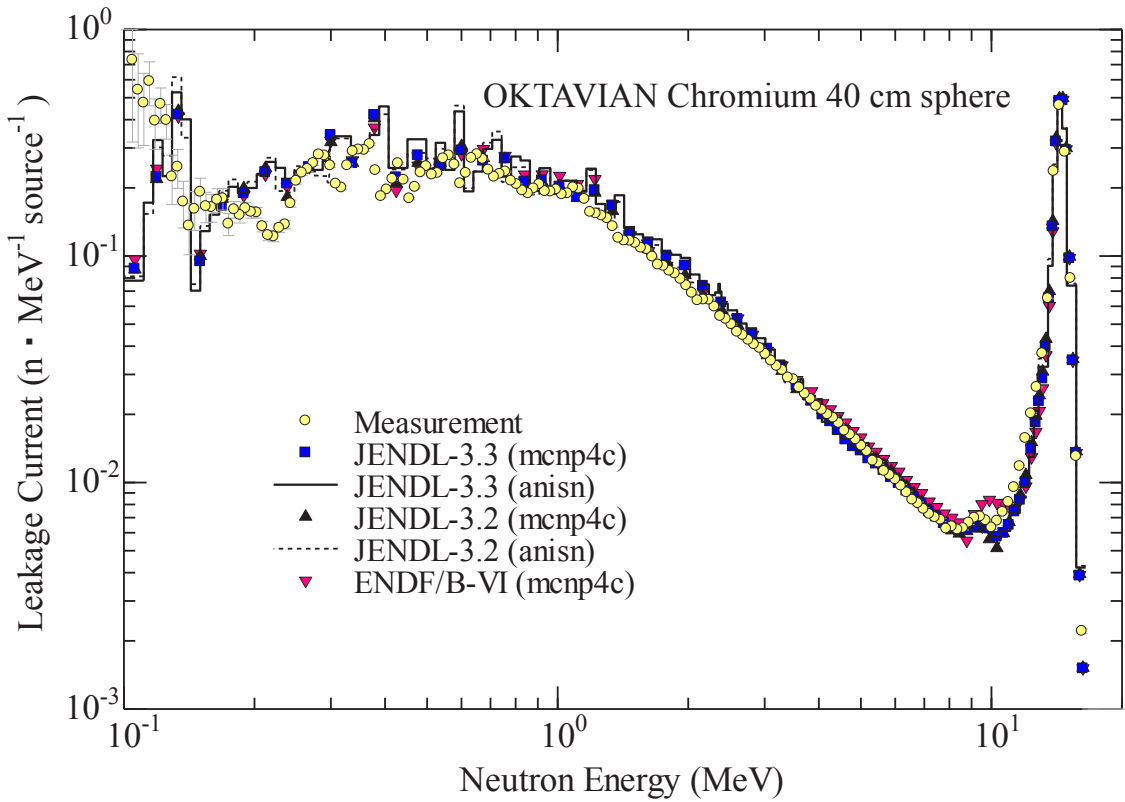


Fig. 3.28 Results of OKTAVIAN Chromium benchmark (2).

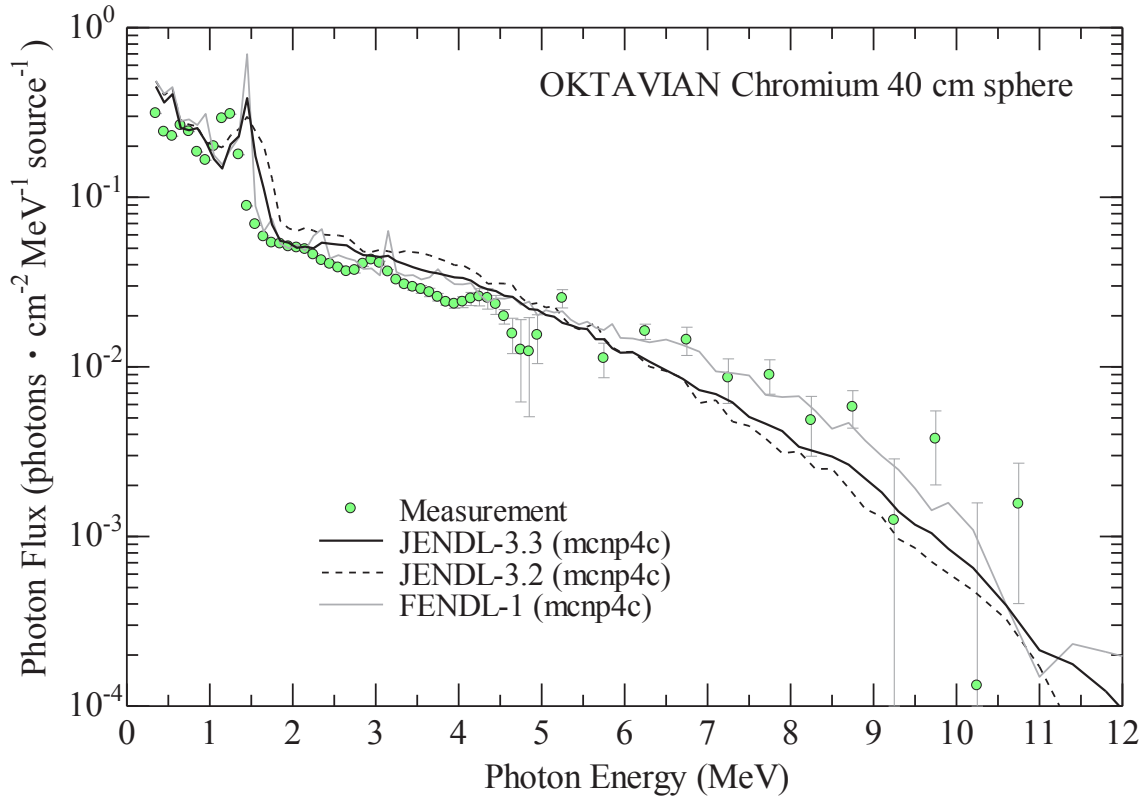
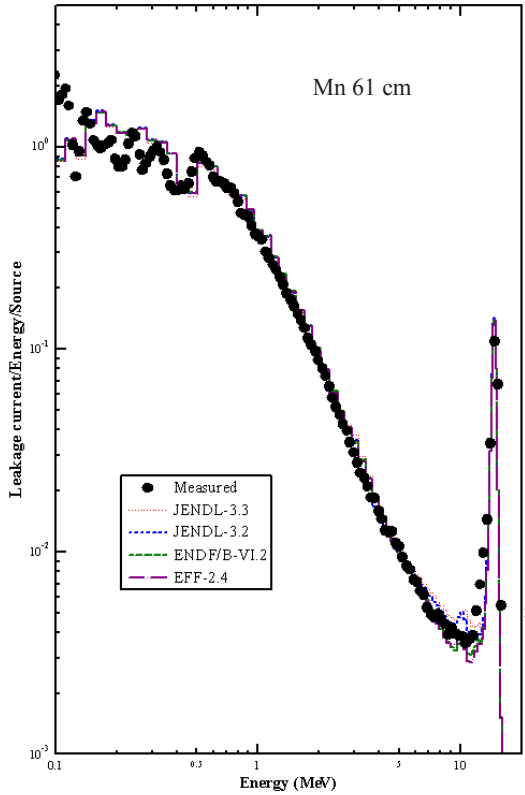
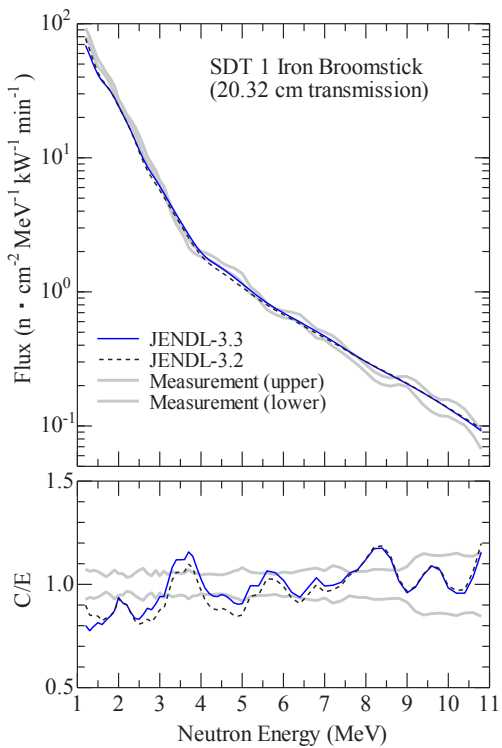
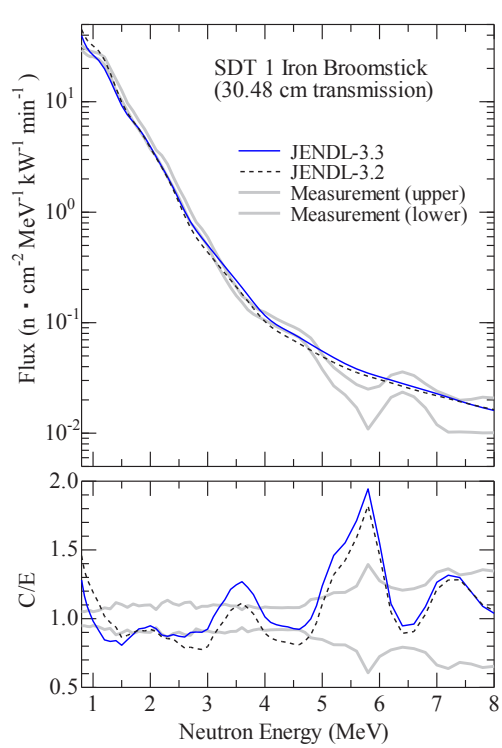
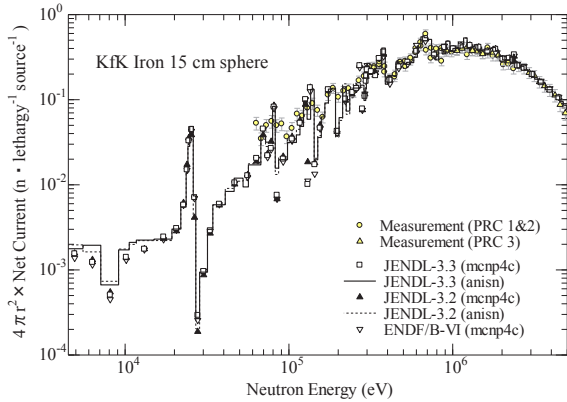
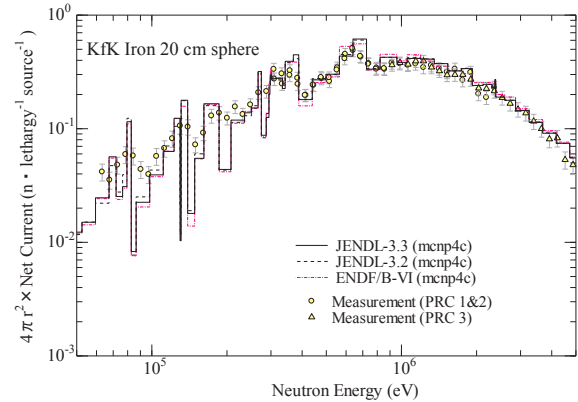
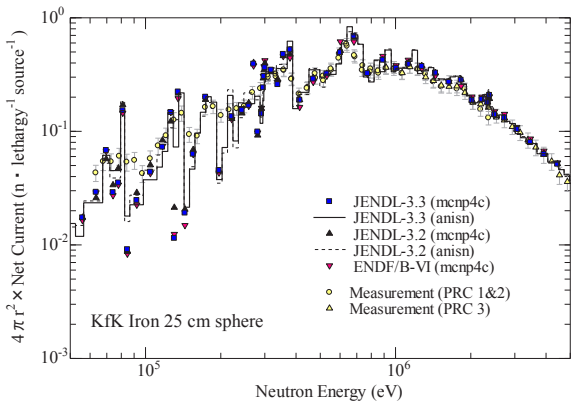
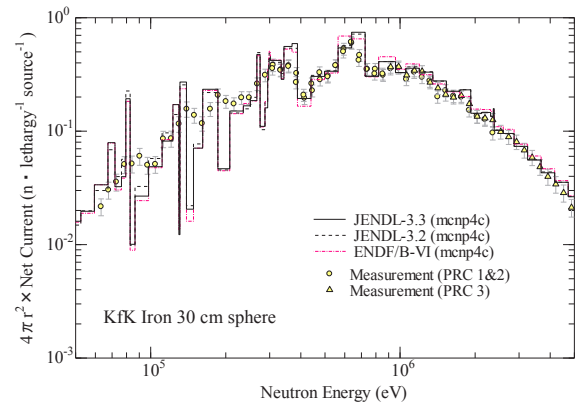
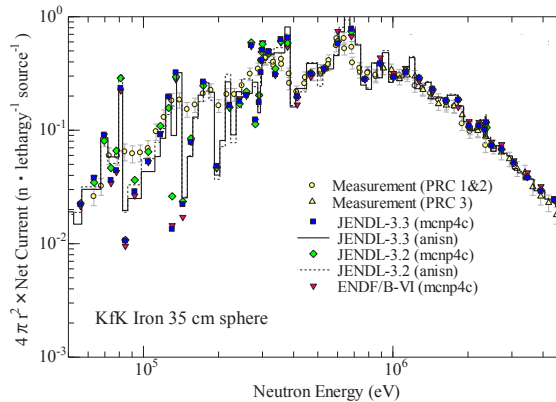
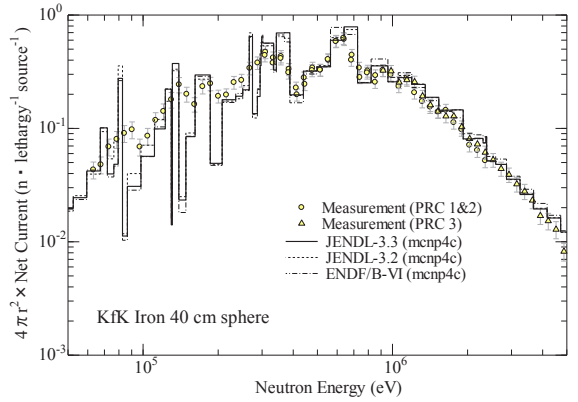
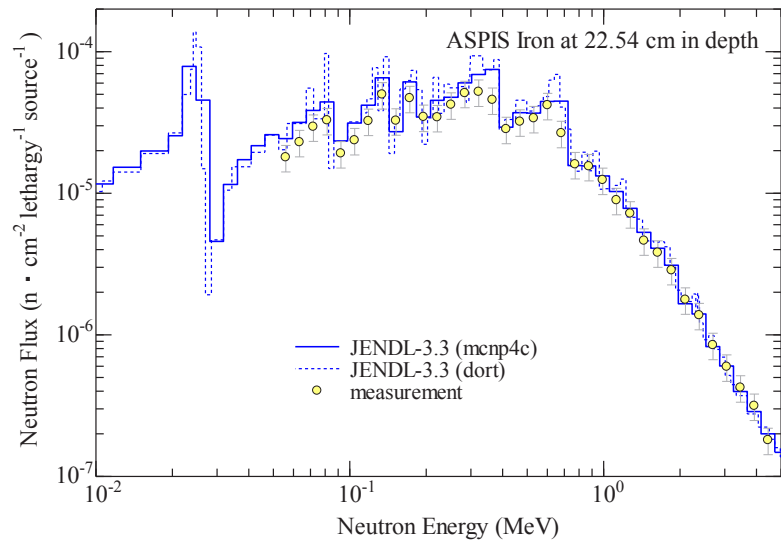
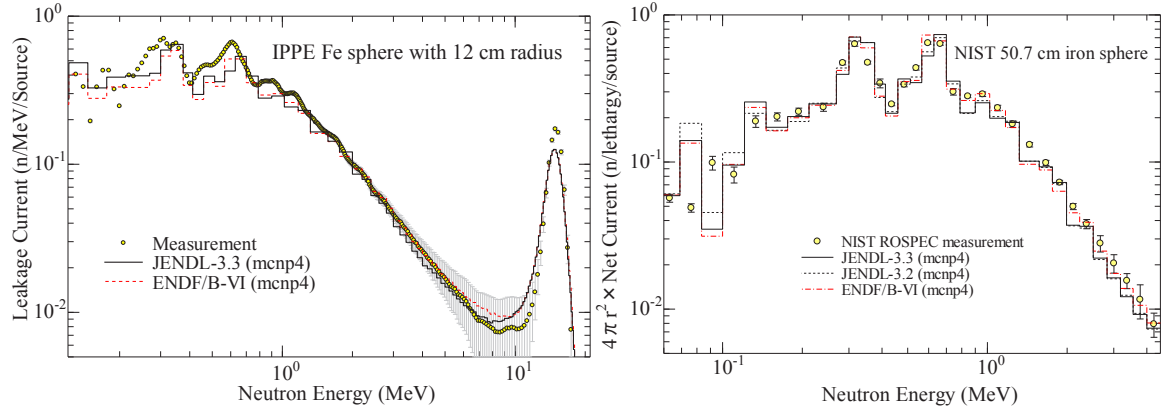
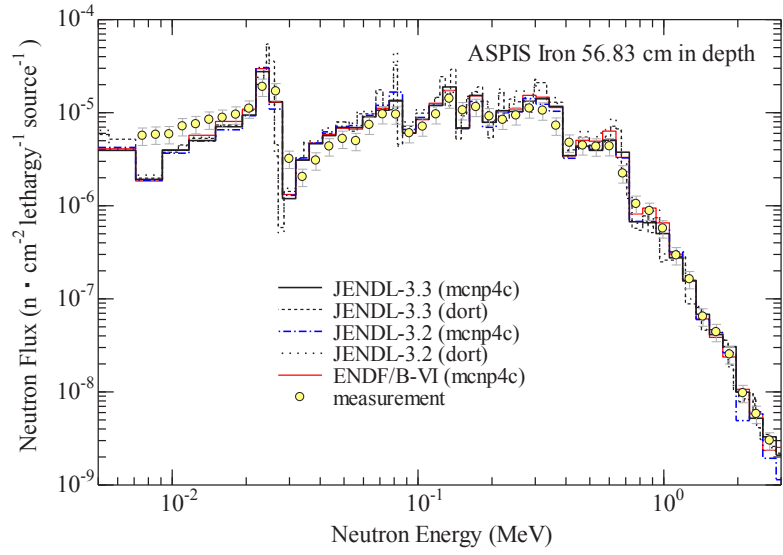


Fig. 3.29 Photon flux of OKTAVIAN Chromium benchmark.

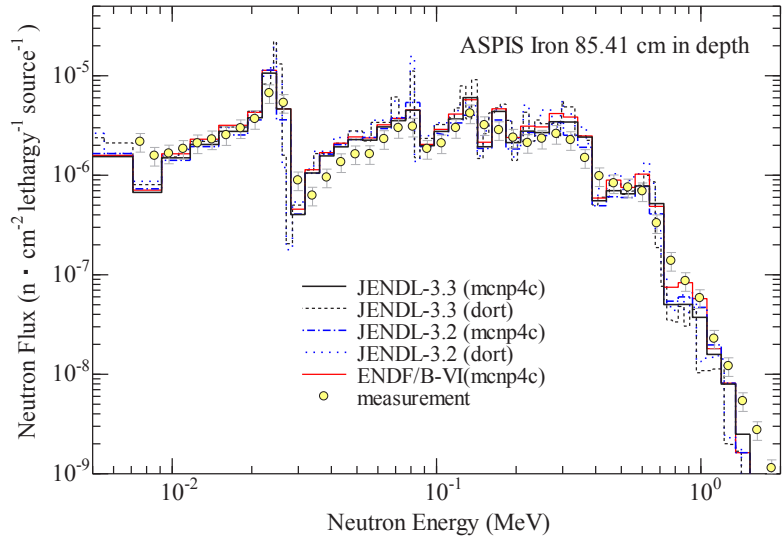
**Fig. 3.30** Results of OKTAVIAN Manganese benchmark.**Fig. 3.31** Results of SDT1 Iron benchmark for 20.32 cm transmission.**Fig. 3.32** Results of SDT1 Iron benchmark for 30.48 cm transmission.

**Fig. 3.33** Results of KfK Iron benchmark for 15 cm sphere.**Fig. 3.34** Results of KfK Iron benchmark for 20 cm sphere.**Fig. 3.35** Results of KfK Iron benchmark for 25 cm sphere.**Fig. 3.36** Results of KfK Iron benchmark for 30 cm sphere.**Fig. 3.37** Results of KfK Iron benchmark for 35 cm sphere.**Fig. 3.38** Results of KfK Iron benchmark for 40 cm sphere.

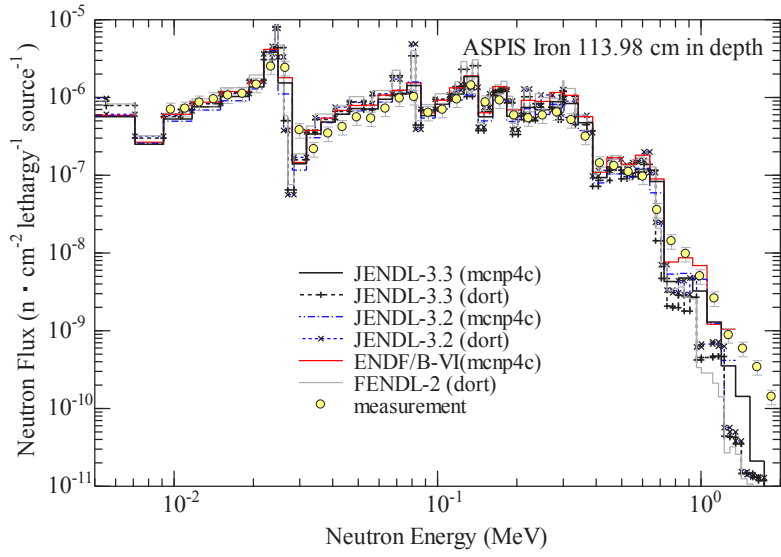
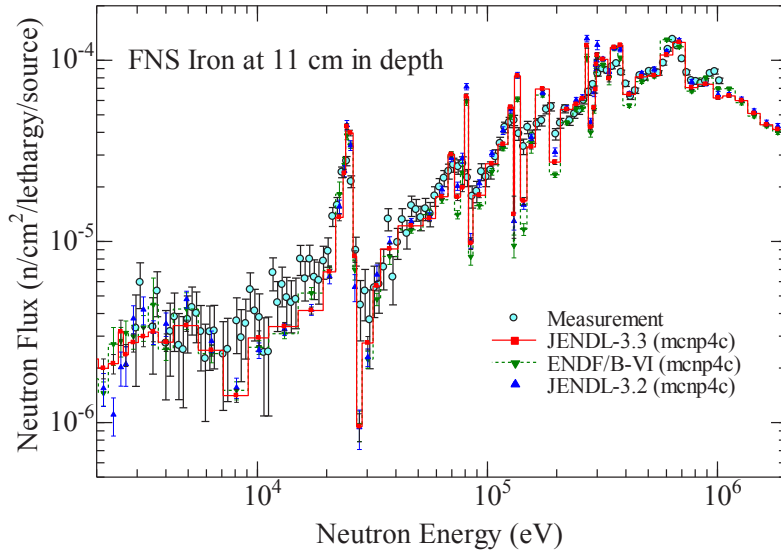


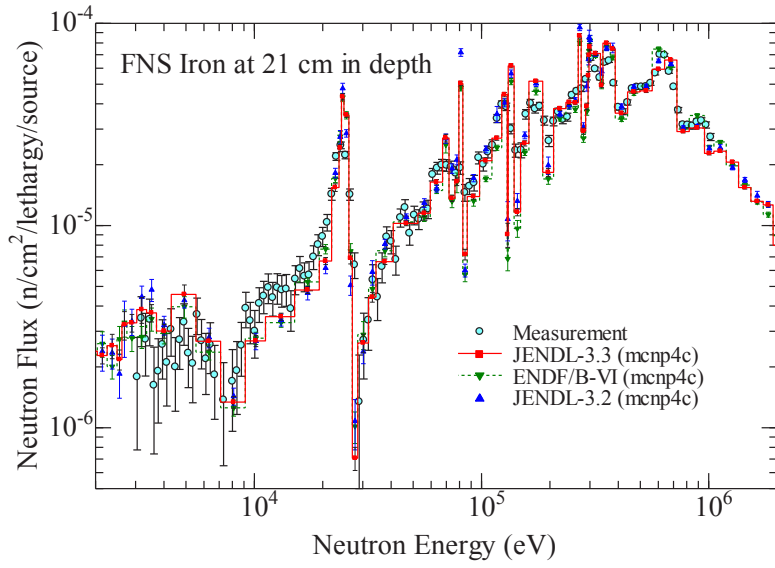
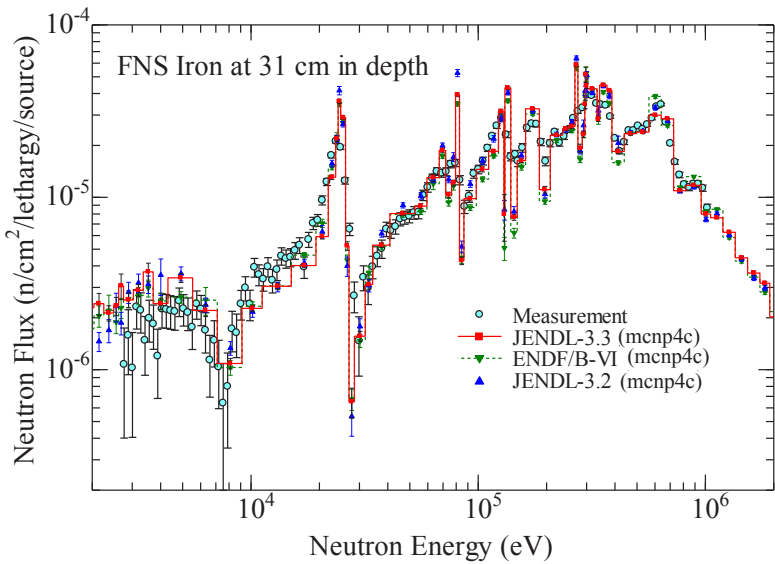


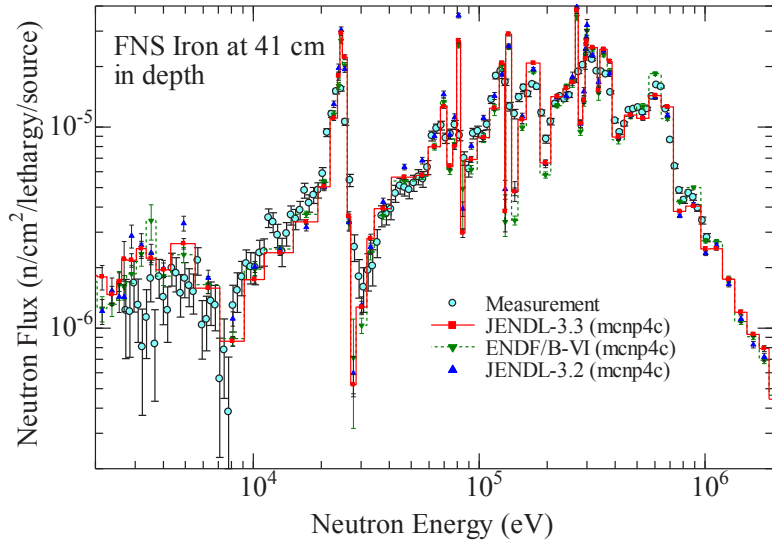
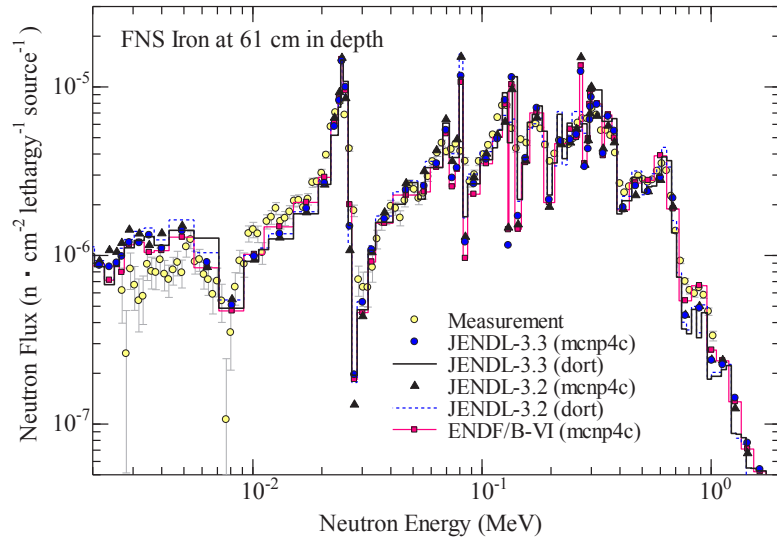
**Fig. 3.42** Results of ASPIS Iron benchmark at 56.83 cm depth.

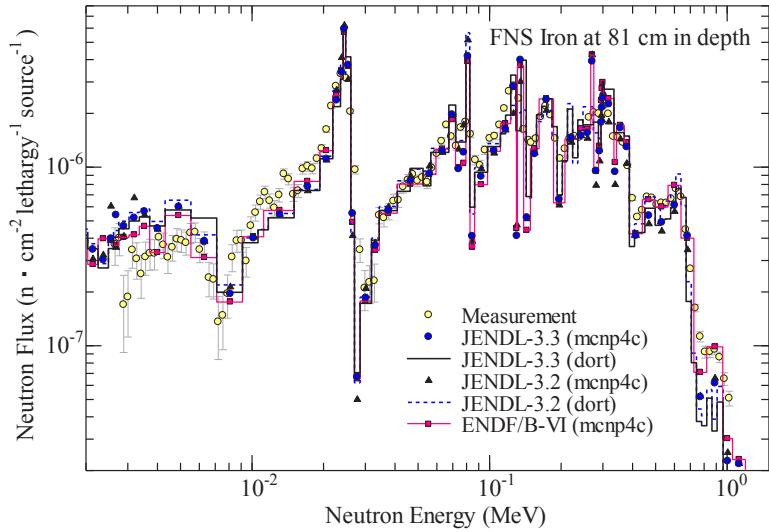
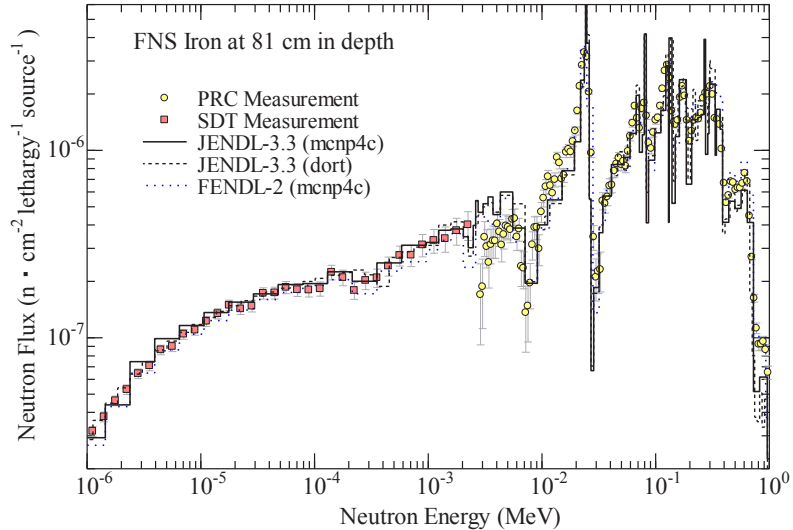
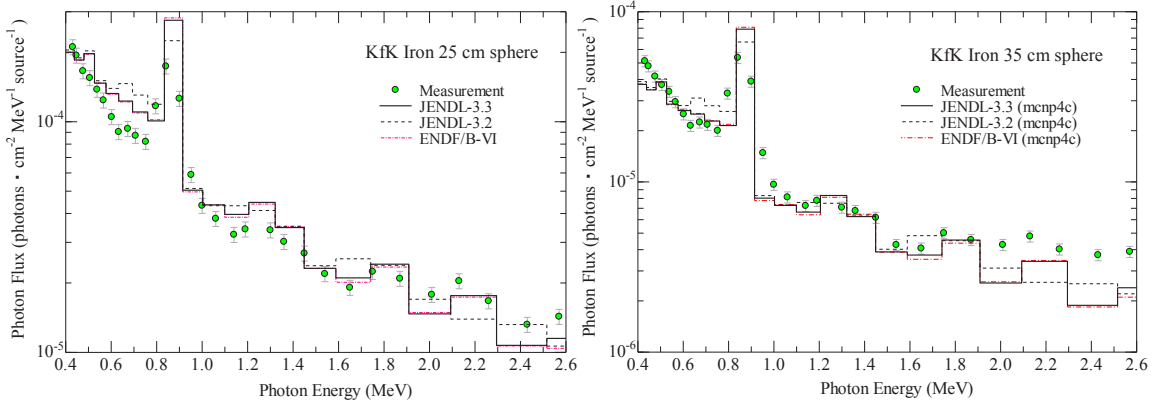


**Fig. 3.43** Results of ASPIS Iron benchmark at 85.41 cm depth.

**Fig. 3.44** Results of ASPIs Iron benchmark at 113.98 cm depth.**Fig. 3.45** Results of FNS Iron benchmark at 11 cm in depth.

**Fig. 3.46** Results of FNS Iron benchmark at 21 cm in depth.**Fig. 3.47** Results of FNS Iron benchmark at 31 cm depth.

**Fig. 3.48** Results of FNS Iron benchmark at 41 cm depth.**Fig. 3.49** Results of FNS Iron benchmark at 61 cm depth.

**Fig. 3.50** Results of FNS Iron benchmark at 81 cm depth (1).**Fig. 3.51** Results of FNS Iron benchmark at 81 cm depth (2).**Fig. 3.52** Photon flux of KfK Iron benchmark for 25 cm sphere.**Fig. 3.53** Photon flux of KfK Iron benchmark for 35 cm sphere.

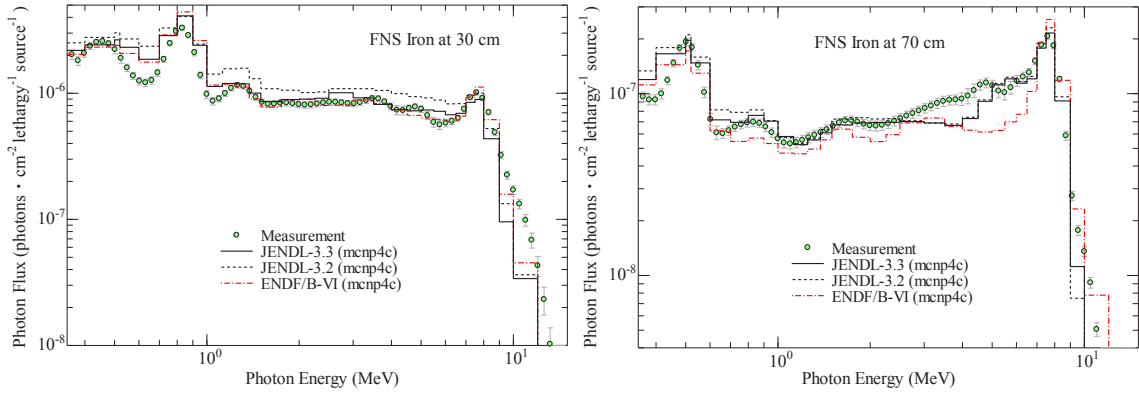


**Fig. 3.54** Photon flux of FNS Iron benchmark at 30 cm in depth.

**Fig. 3.55** Photon flux of FNS Iron benchmark at 70 cm in depth.

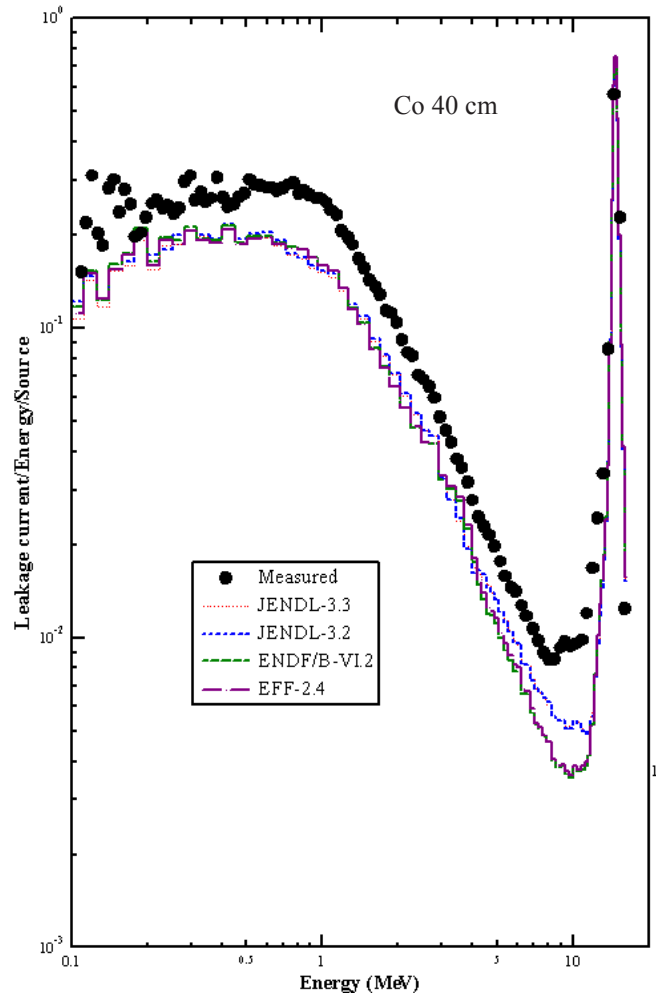


**Fig. 3.56** Results of OKTAVIAN Cobalt benchmark (1).

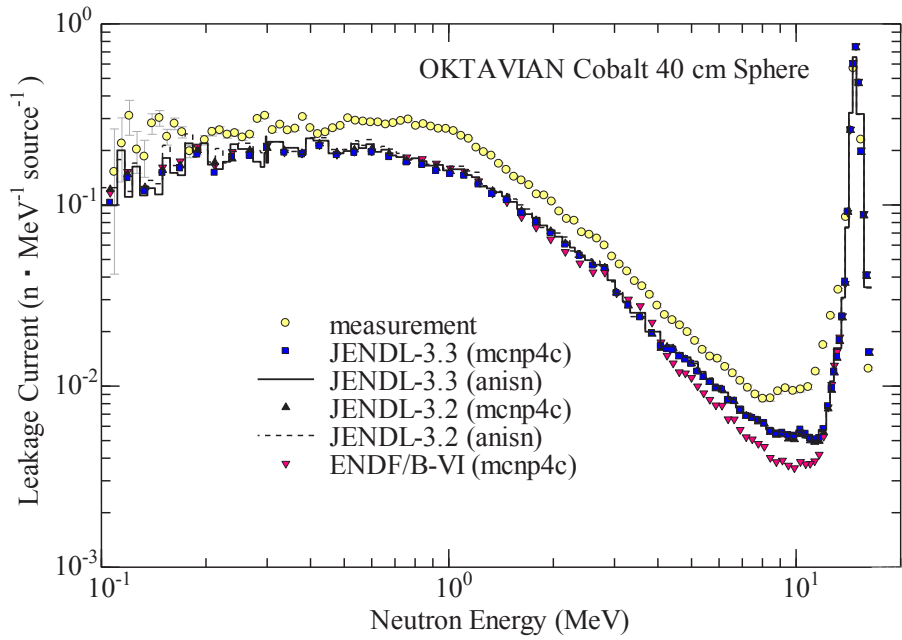


Fig. 3.57 Results of OKTAVIAN Cobalt benchmark (2).

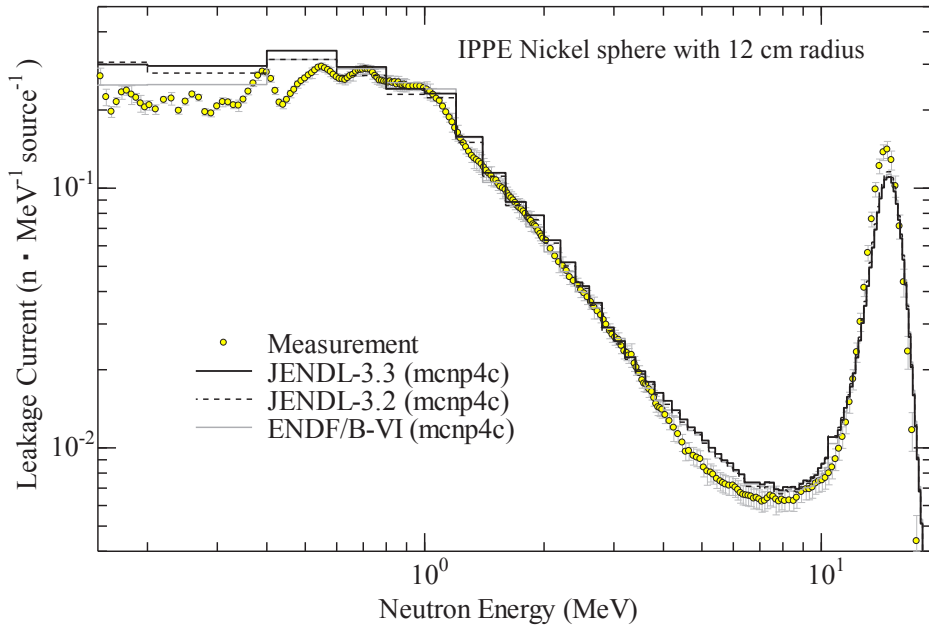


Fig. 3.58 Results of IPPE Nickel benchmark.

**Table 3.1** Calculated results and C/E values of the ORNL iron experiments (JENDL-3.3)

Iron Slab Thickness (cm)	Central Distance behind Slab (cm)	Detector Locations (cm)	Measured Angle with Respect to Centreline (deg.)	Detector Type	Measured Values (E)				Calculated Values (C)				C/E (Calculated/Measured)				
					Bonner Balls (Neutrons/cm <sup>2</sup> /min/W)		Other Detectors	Bonner Balls (Neutrons/cm <sup>2</sup> /min/W)		Other Detectors	Bonner Balls		Other Detectors	Bonner Balls			
					3in.	6in.		3in.	6in.		3in.	6in.		3in.	6in.		
10.287 (4.0in.)	401.32 (158in.)	107.95 (42.5in.)	15	NFE213 Spectrometer	-	-	1.80	-	-	1.96	-	-	-	-	109		
	294.64 (116in.)	294.64 (116in.)	45				0.847			1.09					-	129	
	354.44 (139.5in.)	92.71 (36.5in.)	15	Bonner Ball	0.577	3.54	1.58	-	0.562	4.32	1.80	-	0.97	1.22	1.14		
	254.00 (100in.)	254.00 (100in.)	45		0.411	2.39	1.04	-	0.396	3.02	1.23	-	0.96	1.26	1.18		
	308.10 (12.13in.)	381.00 (150in.)	15	NFE213 Spectrometer	-	-	0.255			0.281					-	1.10	
		279.40 (110in.)	45				0.176			0.164					-	0.93	
	31.115 (12.25in.)	25.40 (10in.)	50	Benjamin Spectrometer			78.3			81.8					-	1.05	
	62.001 (24.4in.)	314.96 (124in.)	83.82 (33in.)	15	Bonner Ball	0.367	1.70	0.600	-	0.335	1.95	0.631	-	0.91	1.15	1.05	
		229.87 (90.5in.)	229.87 (90.5in.)	45			0.245	1.13	0.405	0.254	1.45	0.460	-	1.04	1.28	1.14	
	92.862 (35.56in.)	281.94 (111in.)	76.20 (30in.)	15	Bonner Ball	0.181	0.700	0.227	-	0.149	0.736	0.213	-	0.82	1.05	0.94	
		207.01 (81.5in.)	207.01 (81.5in.)	45			0.128	0.475	0.151	0.129	0.626	0.188	-	1.01	1.32	1.25	

**Table 3.2** Calculated results and C/E values of the ORNL iron experiments (JENDL-3.2)

Iron Slab Thickness (cm)	Detector Locations(cm)			Detector Type	Measured Values (E)			Calculated Values (C)			C/E (Calculated/Measured)				
	Central Distance behind Slab	Radial Distance from Centerline	Measured Angle with Respect to Centerline (deg.)		Bonner Balls (Neutrons/cm/min/W)		Other Detectors	Bonner Balls (Neutrons/cm/min/W)		Other Detectors	Bonner Balls		Other Detectors		
					3in.	6in.		3in.	6in.		3in.	6in.			
10.287 (4.05in.)	401.32 (158in.)	107.95 (42.5in.)	15	NE-213 Spectrometer	-	-	1.80	-	-	1.96	-	-	1.09		
	294.64 (116in.)	294.64 (116in.)	45			0.347				1.10			1.30		
	354.44 (139.5in.)	92.71 (36.5in.)	15	Bonner Ball	0.577	3.54	1.58	0.560	4.33	1.81	0.97	1.22	1.15		
	254.00 (106in.)	254.00 (100in.)	45	Bonner Ball	0.411	2.39	1.04	0.396	3.03	1.24	0.96	1.27	1.19		
	381.00 (12.13in.)	102.87 (40.5in.)	15	NE-213 Spectrometer	-	-	0.255	-	-	0.297	-	-	1.16		
	279.40 (110in.)	279.40 (110in.)	45			0.176				0.174			0.99		
	31.115 (12.25in.)	25.40 (10in.)	30.48 (12in.)	50	Benjamin Spectrometer		78.3			80.9	-	-	1.03		
	314.96 (124in.)	314.96 (124in.)	83.82 (33in.)	15	Bonner Ball	0.367	1.70	0.600	0.341	1.98	0.641	0.93	1.16	1.07	
	62.001 (24.4in.)	229.87 (90.5in.)	229.87 (90.5in.)	45	Bonner Ball	0.245	1.13	0.405	0.259	1.47	0.468	-	1.06	1.30	1.16
	92.862 (35.56in.)	281.94 (111in.)	76.20 (30in.)	15	Bonner Ball	0.181	0.700	0.227	0.156	0.761	0.219	0.86	1.09	0.96	-
	207.01 (81.5in.)	207.01 (81.5in.)	45	Bonner Ball	0.128	0.475	0.151	0.135	0.646	0.193	-	1.05	1.36	1.28	-

**Table 3.3** Calculated results and C/E values of the ORNL iron experiments (ENDF/B-VI)

Iron Slab Thickness (cm)	Detector Locations(cm)			Detector Type	Measured Values (E)			Calculated Values (C)			C/E (Calculated/Measured)		
					Bonner Ball(s)(Neutrons/cm <sup>2</sup> /min/W)		Other Detectors	Bonner Ball(s)(Neutrons/cm <sup>2</sup> /min/W)		Other Detectors	Bonner Balls		Other Detectors
	3in.	6in.	10in.		3in.	6in.		3in.	6in.		3in.	6in.	
10.287 (4.05in.)	401.32 (158in.)	107.95 (42.5in.)	15	NE-213 Spectrometer	-	-	1.80	-	-	2.00	-	-	1.11
	294.64 (116in.)	294.64 (116in.)	45				0.847				1.11		1.31
354.44 (139.5in.)	92.71 (36.5in.)	15		Bonner Ball	0.577	3.54	1.58	0.557	4.39	1.85	-	0.97	1.24
254.00 (100in.)	254.00 (100in.)	45		Bonner Ball	0.411	2.39	1.04	0.394	3.08	1.27		0.96	1.29
30.810 (12.13in.)	381.00 (150in.)	102.87 (40.5in.)	15	NE-213 Spectrometer	-	-	0.255	-	-	0.313	-	-	1.23
	279.40 (110in.)	279.40 (110in.)	45				0.176			0.185			1.05
31.115 (12.25in.)	25.40 (10in.)	30.48 (12in.)	50	Benjamin Spectrometer			78.3			83.2	-	-	1.06
	314.96 (124in.)	83.82 (33in.)	15		0.367	1.70	0.600	0.343	2.05	0.675		0.93	1.21
62.001 (24.41in.)	229.87 (90.5in.)	229.87 (90.5in.)	45	Bonner Ball	0.245	1.13	0.405	0.260	1.53	0.494	-	1.06	1.35
92.862 (35.36in.)	281.94 (111in.)	76.20 (30in.)	15	Bonner Ball	0.181	0.700	0.227	0.158	0.807	0.237	-	0.87	1.15
	207.01 (81.5in.)	207.01 (81.5in.)	45				0.137	0.686	0.209	-	1.07	1.44	1.38

**Table 3.4** Calculated results and C/E values of the ORNL stainless steel experiments (JENDL-3.3)

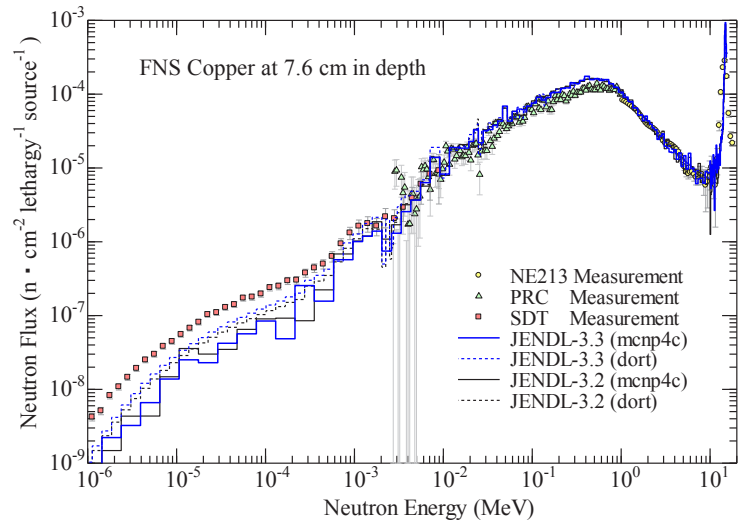
Stainless Steel Slab Thickness (cm)	Detector Locations (cm)			Detector Type	Measured Values (E)			Calculated Values (C)			C/E (Calculated/Measured)
	Central Distance behind Slab	Radial Distance from Centerline	Measured Angle with Respect to Centerline (deg.)		Bonner Balls (Neutrons/cm <sup>2</sup> /min/W)	Other Detectors	Bonner Balls (Neutrons/cm <sup>2</sup> /min/W)	Other Detectors	Bonner Balls	Other Detectors	
345.44 (13.6in.)	92.71 (36.5in.)	15			0.496	2.74	1.28	-	0.492	3.41	1.43
30.91 (12.17in.)	254.00 (100in.)	45	Bonner Ball		0.327	1.77	0.797	-	0.328	2.23	0.902
25.40 (10in.)	30.48 (12in.)	50	Benjamin Spectrometer		-	-	66.6	-	-	71.2	-
											1.07

**Table 3.5** Calculated results and C/E values of the ORNL stainless steel experiments (JENDL-3.2)

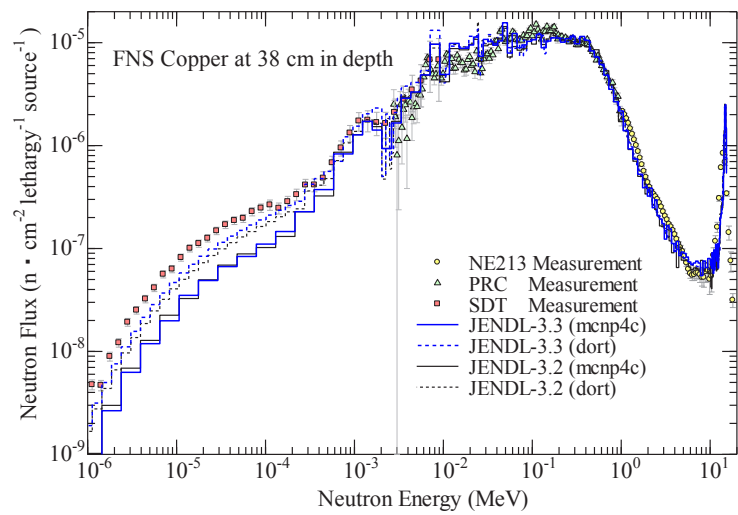
Stainless Steel Slab Thickness (cm)	Detector Locations (cm)			Detector Type	Measured Values (E)			Calculated Values (C)			C/E (Calculated/Measured)
	Central Distance behind Slab	Radial Distance from Centerline	Measured Angle with Respect to Centerline (deg.)		Bonner Balls (Neutrons/cm <sup>2</sup> /min/W)	Other Detectors	Bonner Balls (Neutrons/cm <sup>2</sup> /min/W)	Other Detectors	Bonner Balls	Other Detectors	
345.44 (13.6in.)	92.71 (36.5in.)	15			0.496	2.74	1.28	-	0.495	3.41	1.44
30.91 (12.17in.)	254.00 (100in.)	45	Bonner Ball		0.327	1.77	0.797	-	0.330	2.23	0.907
25.40 (10in.)	30.48 (12in.)	50	Benjamin Spectrometer		-	-	66.6	-	-	70.7	-
											1.06

**Table 3.6** Calculated results and C/E values of the ORNL stainless steel experiments (ENDF/B-VI)

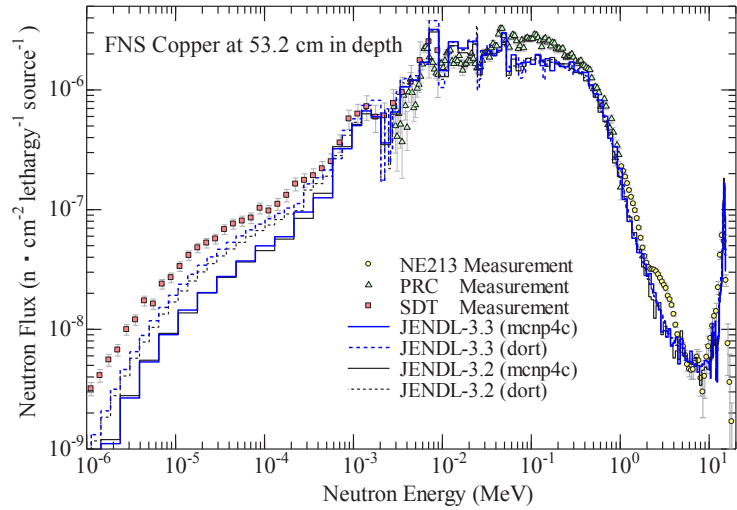
Stainless Steel Slab Thickness (cm)	Detector Locations(cm)			Detector Type	Measured Values (E)			Calculated Values (C)			C/E (Calculated/Measured)
	Central Distance behind Slab	Radial Distance from Centerline	Measured Angle with Respect to Centerline (deg.)		Bonner Balls (Neutrons/cm <sup>2</sup> /min/W)	Other Detectors	Bonner Balls (Neutrons/cm <sup>2</sup> /min/W)	Other Detectors	Bonner Balls	Other Detectors	
345.44 (13.6in.)	92.71 (36.5in.)	15			0.496	2.74	1.28	-	0.486	3.40	1.43
30.91 (12.17in.)	254.00 (100in.)	45	Bonner Ball		0.327	1.77	0.797	-	0.324	2.23	0.906
25.40 (10in.)	30.48 (12in.)	50	Benjamin Spectrometer		-	-	66.6	-	-	71.4	-
											1.07



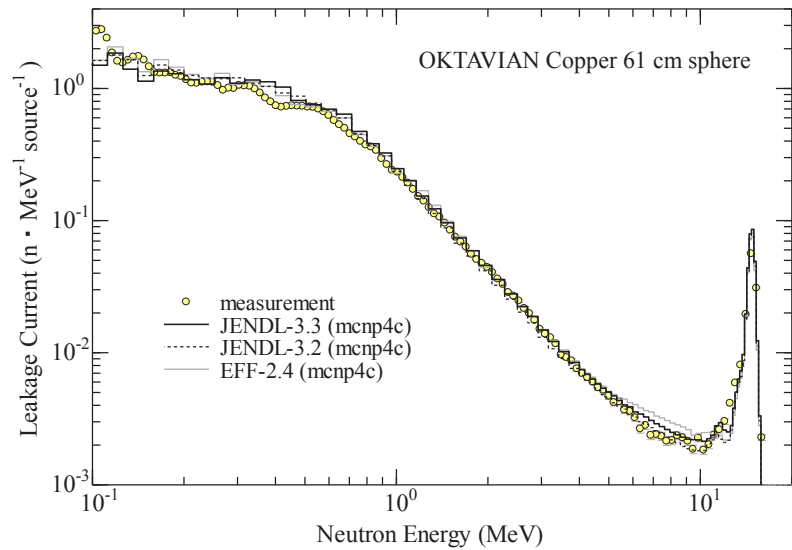
**Fig. 3.59** Results of FNS Copper benchmark at 7.6 cm in depth.



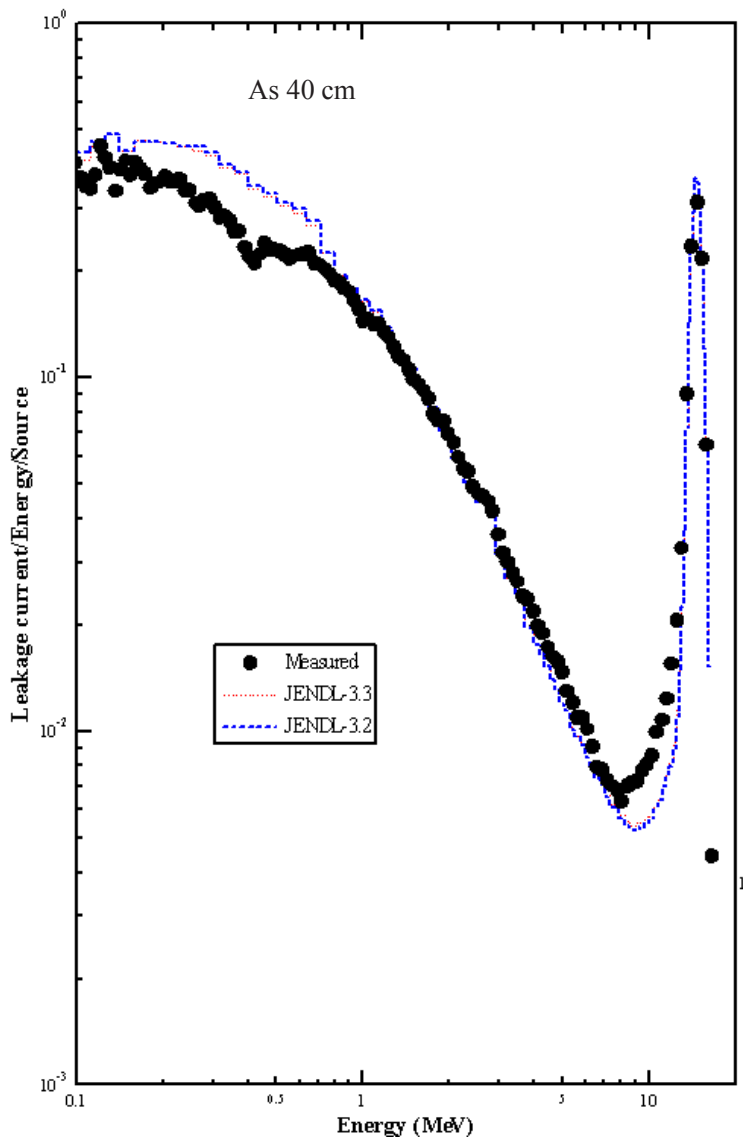
**Fig. 3.60** Results of FNS Copper benchmark at 38 cm in depth.



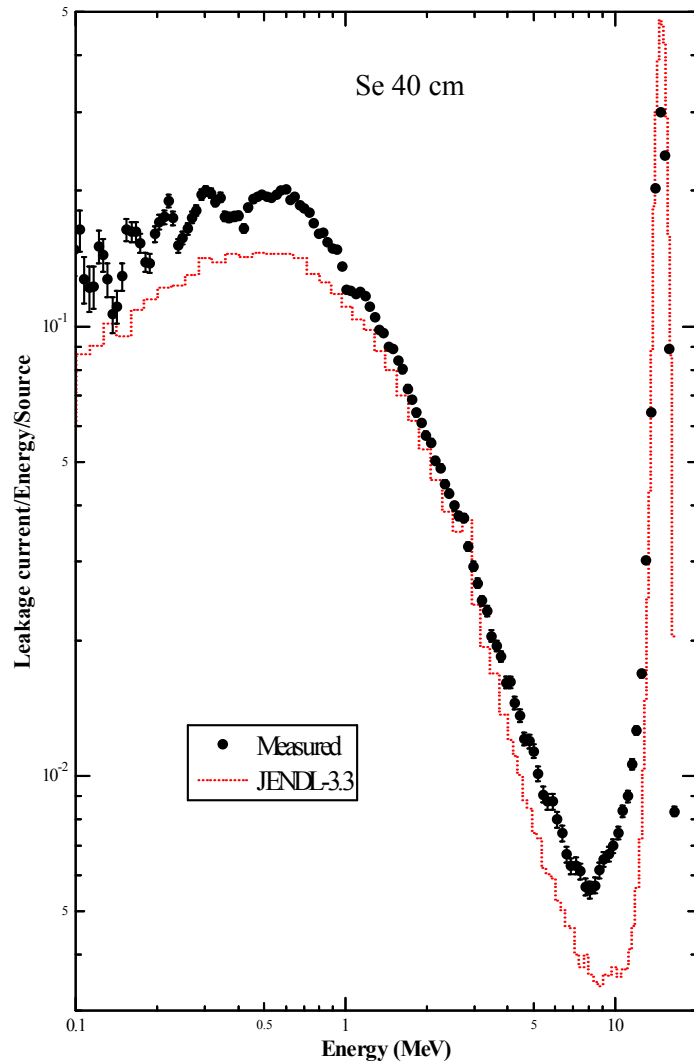
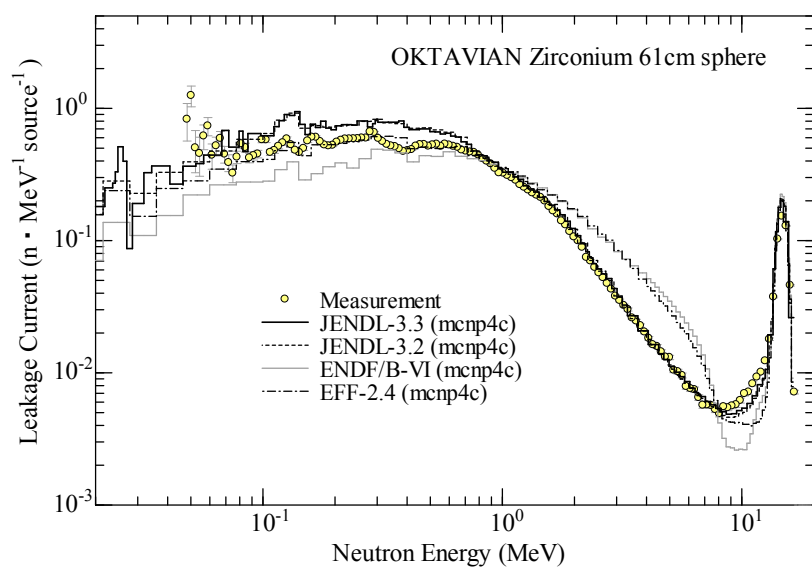
**Fig. 3.61** Results of FNS Copper benchmark at 53.2 cm in depth.

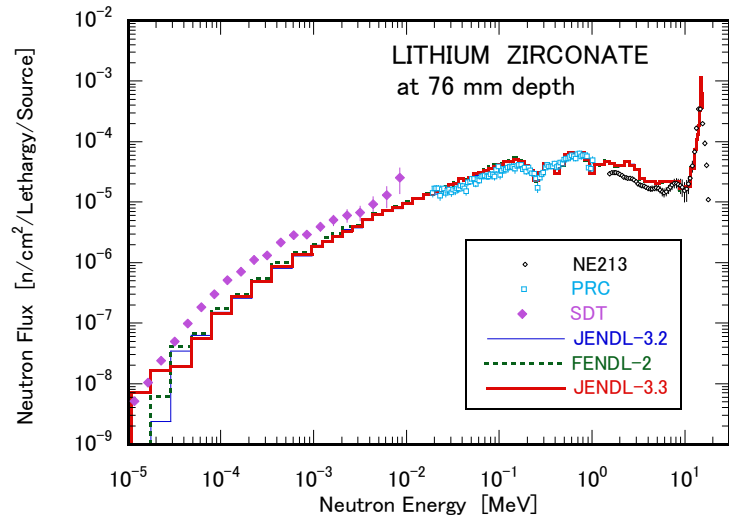


**Fig. 3.62** Results of OKTAVIAN Copper benchmark.

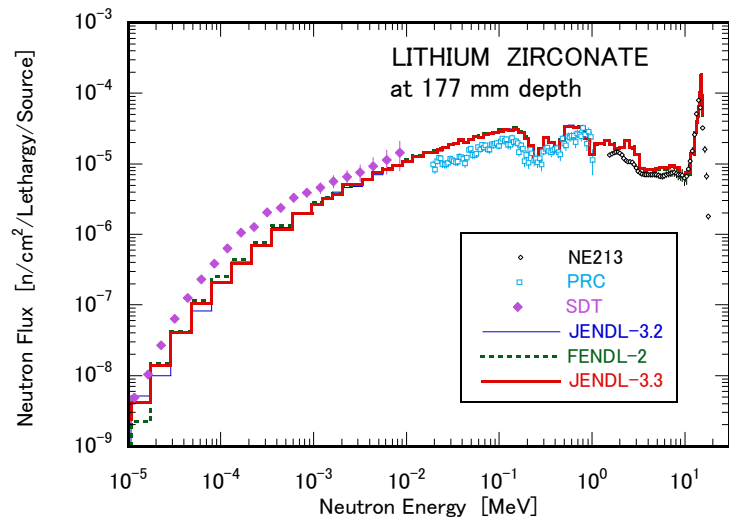


**Fig. 3.63** Results of OKTAVIAN Arsenic benchmark.

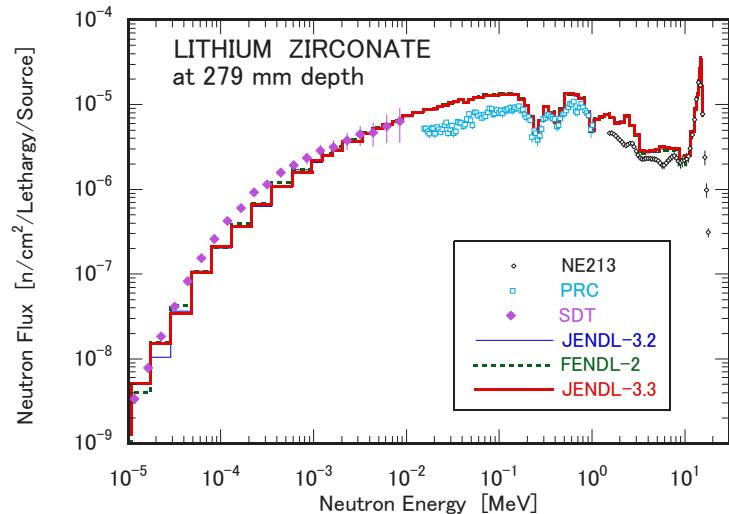
**Fig. 3.64** Results of OKTAVIAN Selenium benchmark.**Fig. 3.65** Results of OKTAVIAN Zirconium benchmark.



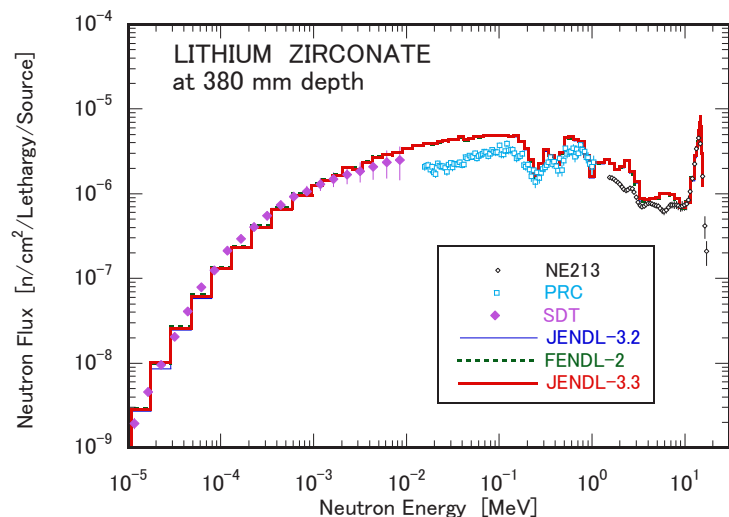
**Fig. 3.66** Results of FNS Li<sub>2</sub>ZrO<sub>3</sub> benchmark at 76 mm in depth.



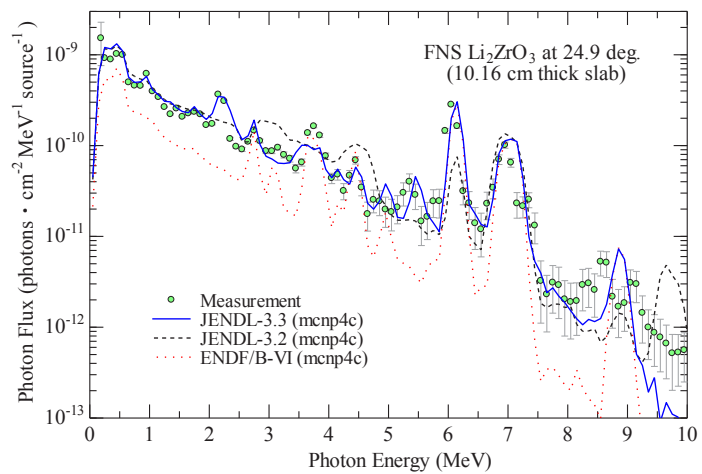
**Fig. 3.67** Results of FNS Li<sub>2</sub>ZrO<sub>3</sub> benchmark at 177 mm in depth.



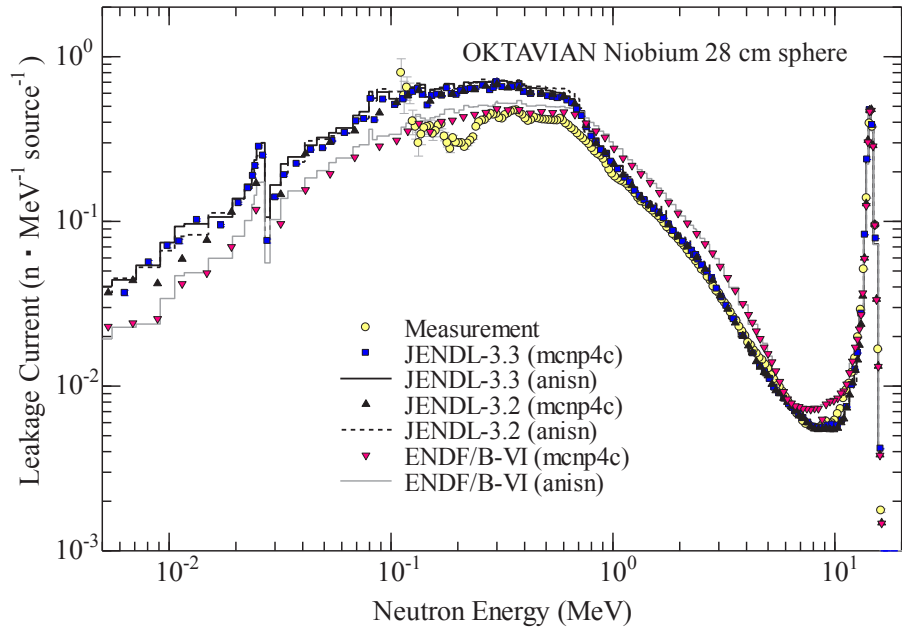
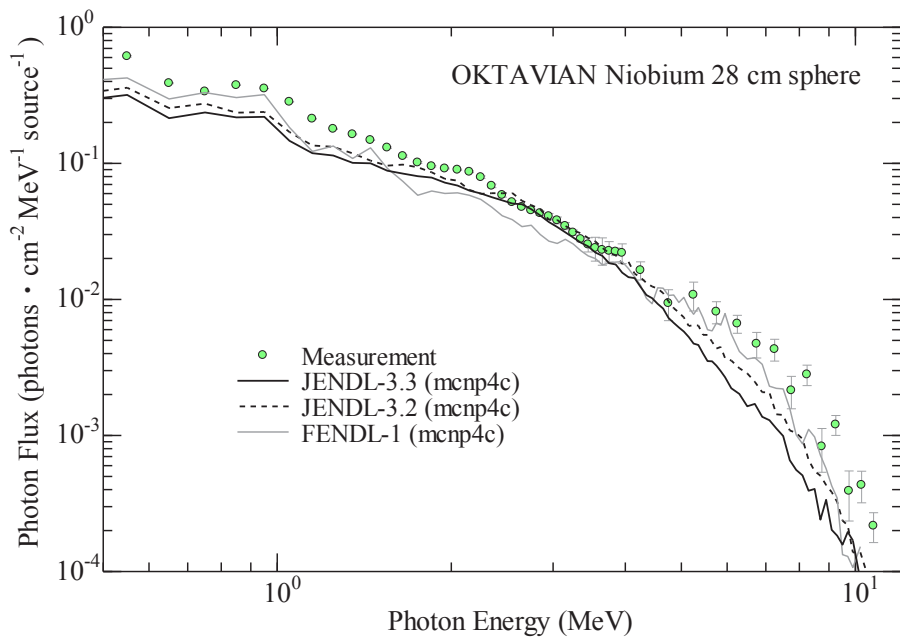
**Fig. 3.68** Results of FNS  $\text{Li}_2\text{ZrO}_3$  benchmark at 279 mm in depth.



**Fig. 3.69** Results of FNS  $\text{Li}_2\text{ZrO}_3$  benchmark at 380 mm in depth.



**Fig. 3.70** Results of FNS  $\text{Li}_2\text{ZrO}_3$  benchmark at 10.16 cm in depth.

**Fig. 3.71** Results of OKTAVIAN Niobium benchmark.**Fig. 3.72** Results of gamma-ray spectrum in the OKTAVIAN Niobium benchmark.

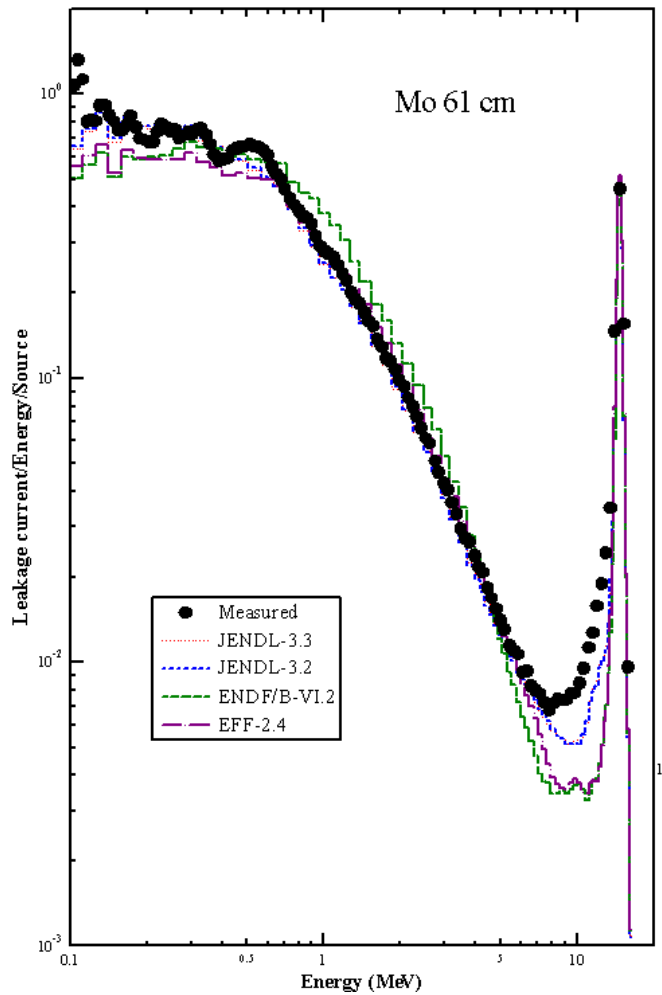


**Fig. 3.73** Results of the OKTAVIAN Molybdenum benchmark.

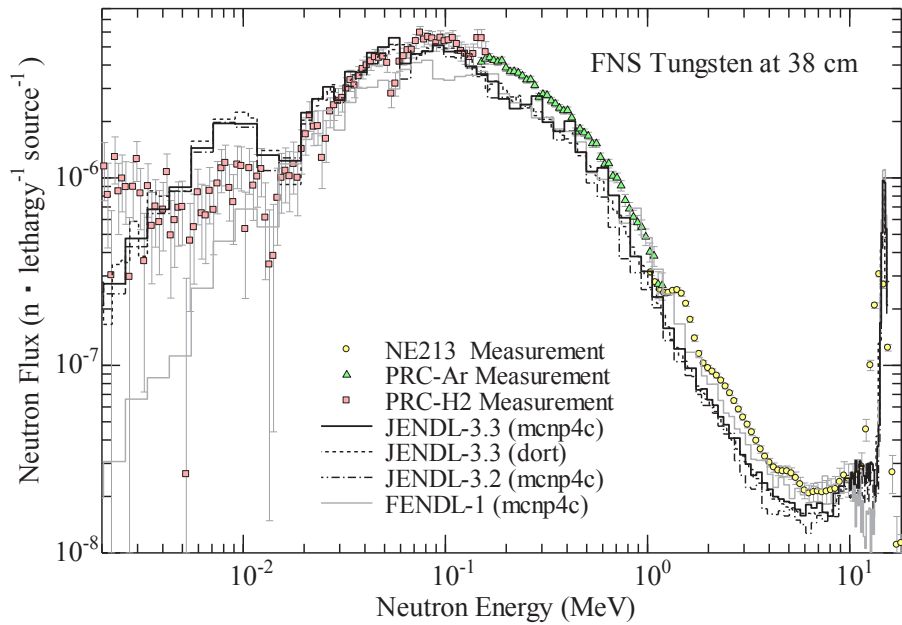


**Fig.3.74** Results of the FNS Tungsten benchmark.

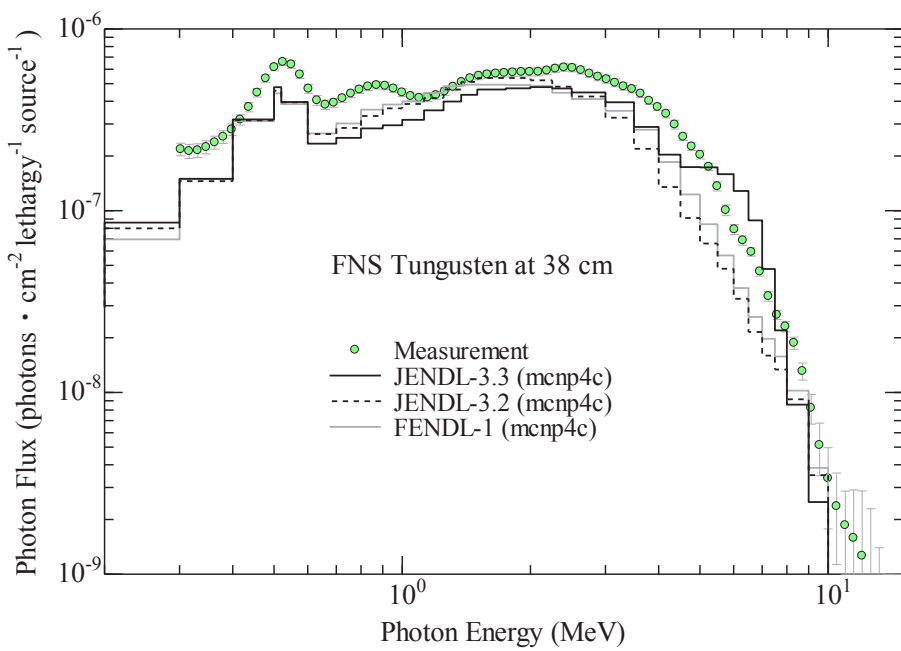


**Fig. 3.75** Results of gamma-ray spectrum of the FNS Tungsten benchmark.

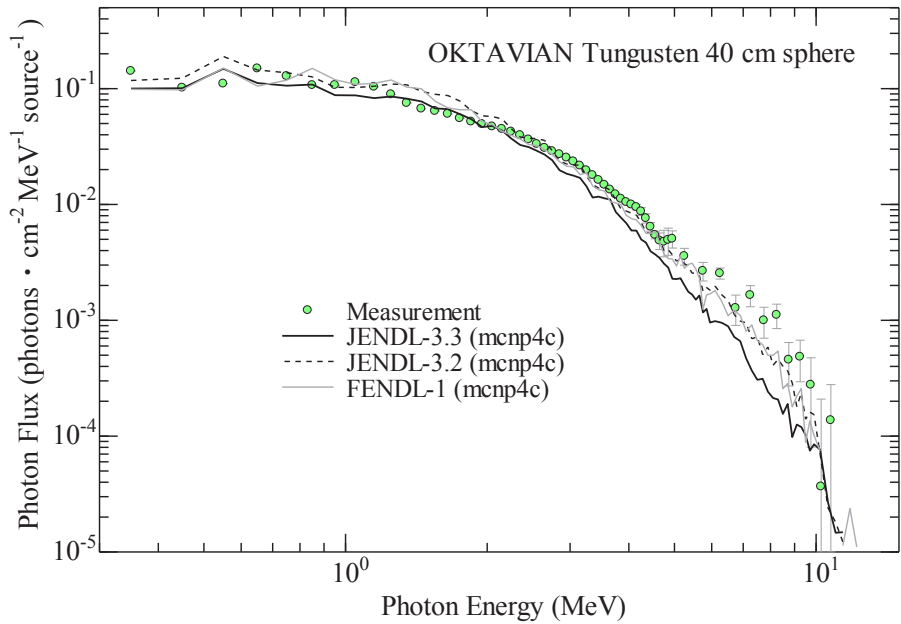


**Fig. 3.76** Results of gamma-ray spectrum of the OKTAVIAN Tungsten benchmark.

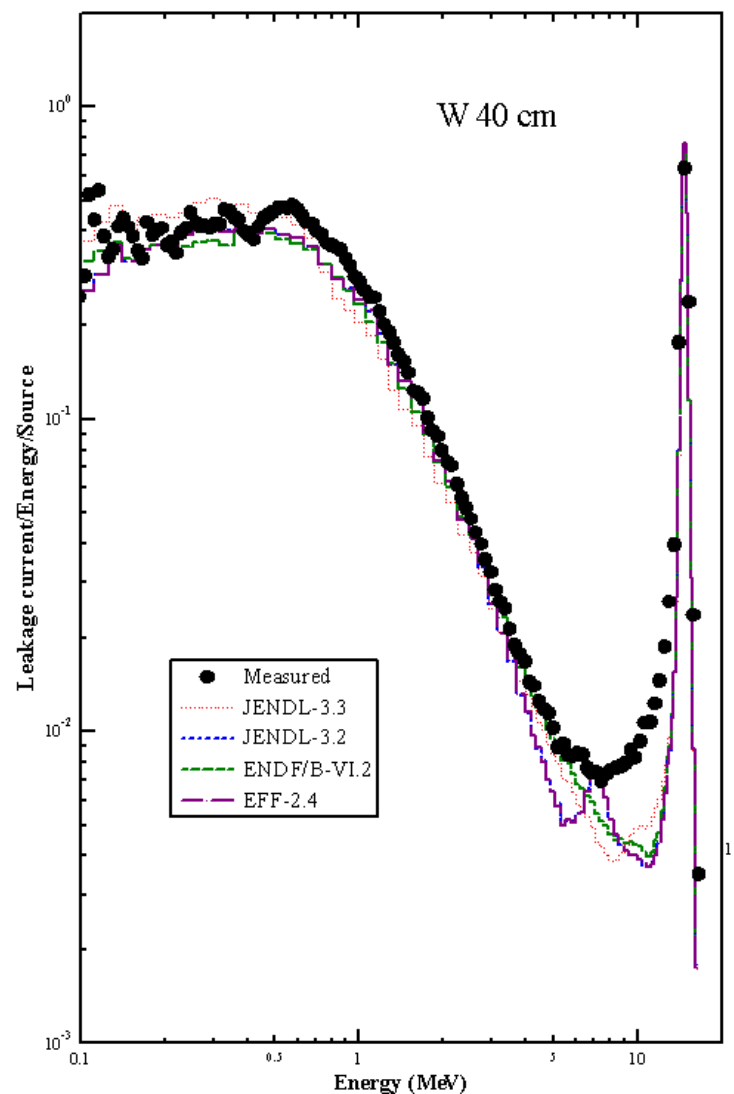


Fig.3.77 Results of OKTAVIAN Tungsten benchmark.

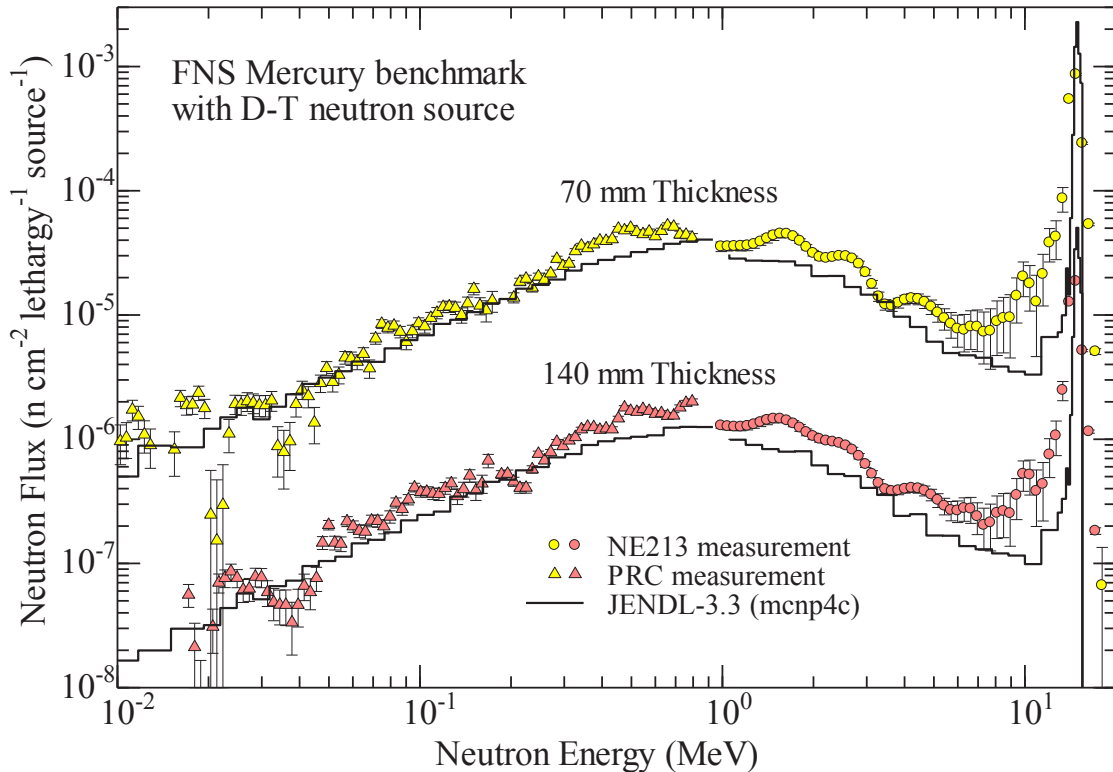


Fig. 3.78 Results of FNS Mercury benchmark.

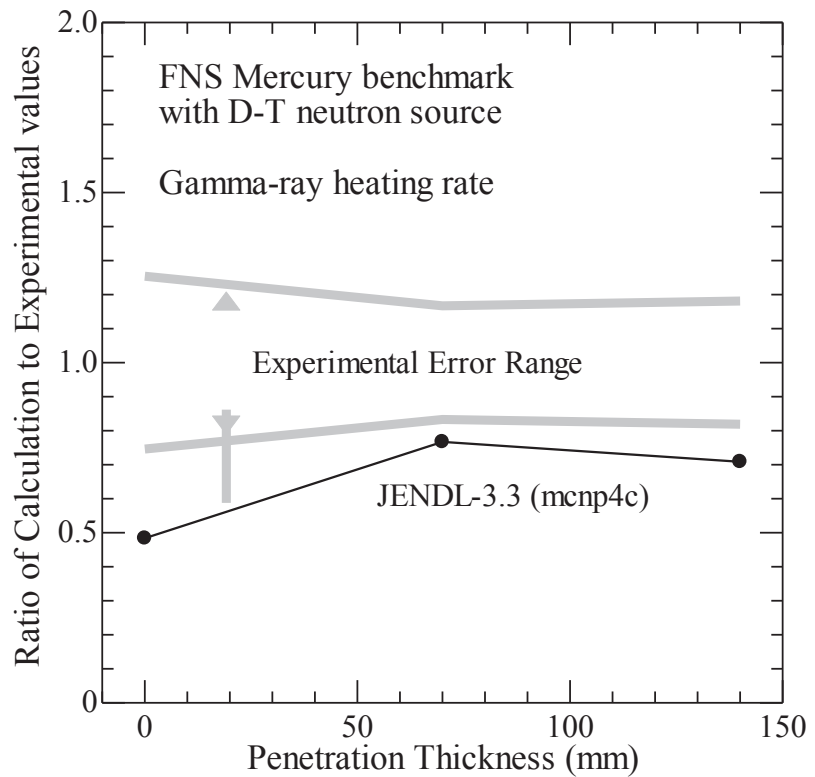


Fig. 3.79 Results of gamma-ray heating rate in the FNS Tungsten benchmark.

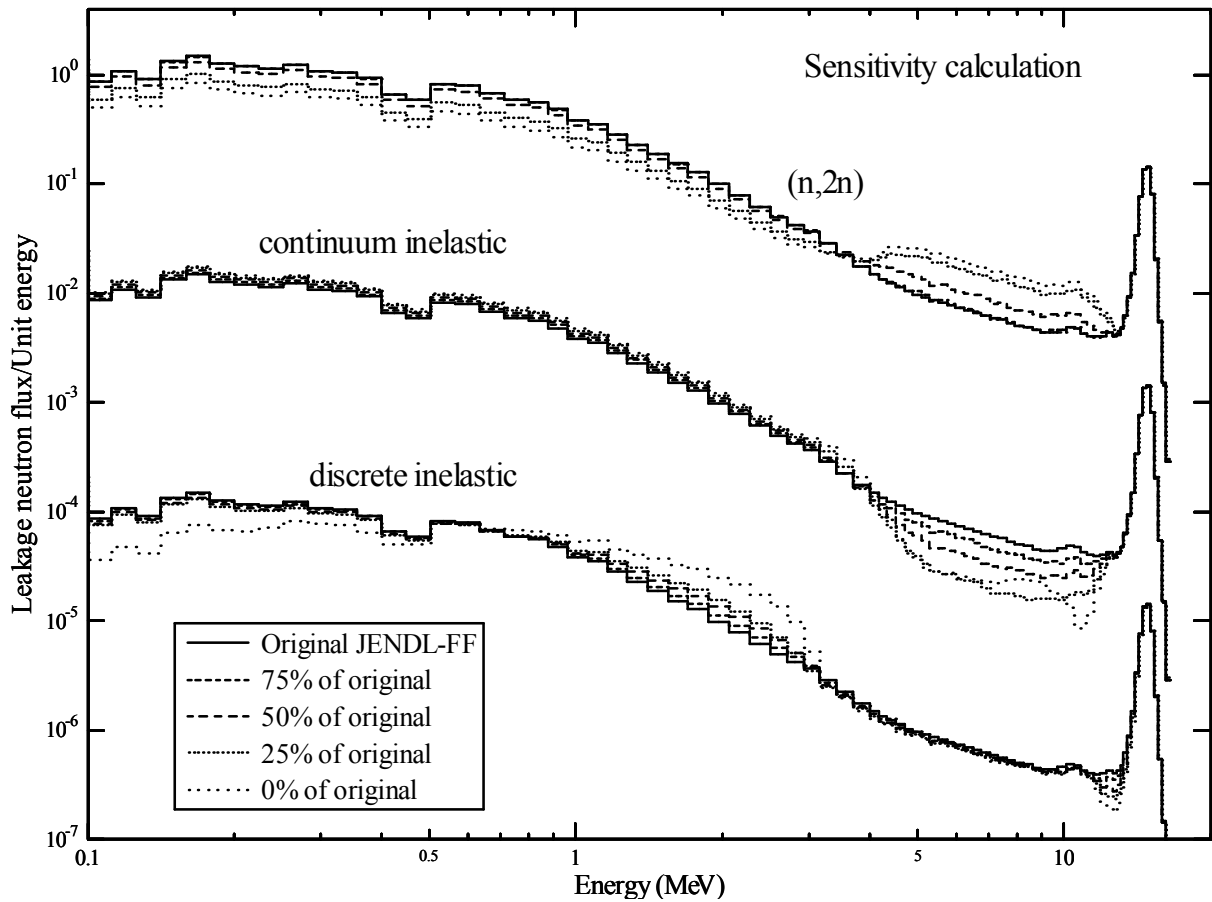
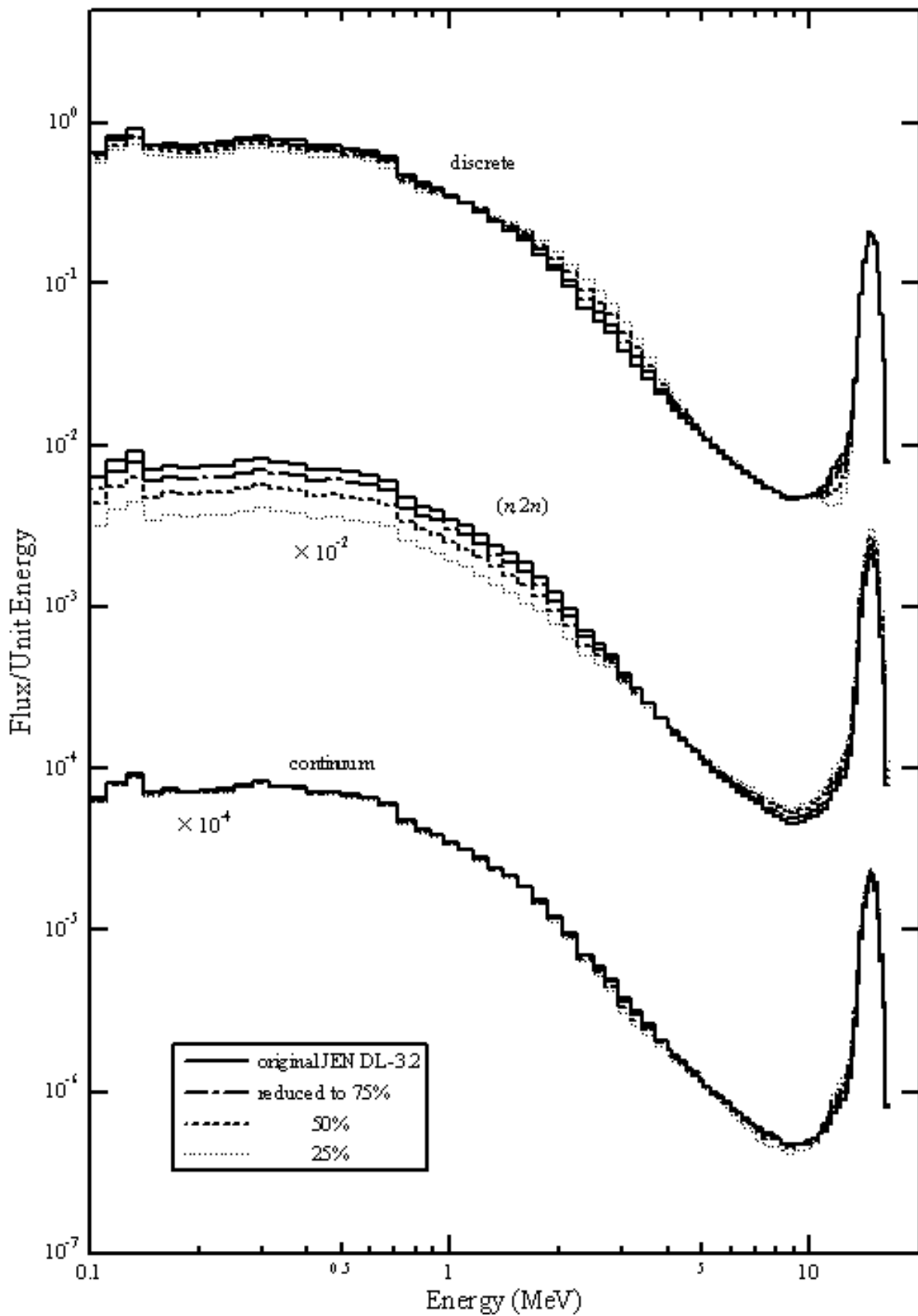


Fig. 4.1 Calculated spectra with the modified Manganese data in the JENDL-3.2 library.



**Fig. 4.2** General dependence of the partial cross section to the energy spectra, which was performed with MCNP-4A with artificial libraries modified from FSXLIB-J3R2.

#### 4. Discussion

It is of great importance to get the dependence of the whole spectrum to each partial cross section of the nuclear data. For this purpose, the partial cross section values in the MCNP-4C library were reduced and the change in the spectrum calculated with the reduced values was compared with the spectrum calculated with the original values. The discrete inelastic, continuum inelastic and total inelastic were taken into account because it turned out from the preliminary calculation that the other cross sections such as  $(n,\alpha)$ ,  $(n,p)$  and  $(n,\gamma)$  cross sections affect the total spectra no more than 0.01 %. The Manganese data in FSXLIB-J3R2 MCNP-4A library was used for this procedure. The cross section values of the discrete inelastic scattering, the continuum inelastic scattering and the  $(n,2n)$  reaction were uniformly reduced to 75 %, 50 % and 25 %, respectively.

The calculated spectra with the modified library are shown in **Fig. 4.1**, from which the change by the modification can be seen. The general dependence of the spectra on the change of the partial cross section is plainly depicted in **Fig. 4.2**. The outline is as the followings.

As the discrete inelastic scattering cross sections are reduced, the dip at 12.5 MeV becomes deeper and the partial spectrum between 1 and 6 MeV becomes abundant. The partial spectrum above about 6 MeV is not sensitive to the change of this cross section. The partial spectrum below 1 MeV is decreased on the contrary. The reduction of the continuum inelastic scattering cross section makes the partial spectrum above 10 MeV abundant. It also makes the spectrum between 4 and 10 MeV slightly large. The spectrum below 4 MeV is not sensitive to the reduction of this cross section. As the  $(n,2n)$  reaction cross section is reduced, both the peak at 14 MeV and the partial spectrum between 4 and 12.5 MeV become larger. The spectrum below 4 MeV becomes considerably lower at the same time. The similar calculations were conducted for some of the samples.

#### 5. Conclusion

An integral test of JENDL-3.3 using the FSXLIB-J3R3 and the MATXS-J33 libraries has been performed for 28 materials in 22 medium-heavy nuclei and the compounds that consist of Lithium, Oxygen, LiF, TEFLON: $(CF_2)_n$ , Sodium, Aluminum,  $Li_2AlO_3$ ,  $LiAlO_2$ , Silicon, SiC, Titanium,  $Li_2TiO_3$ , Vanadium, Chromium, Manganese, Iron, Cobalt, Nickel, SS304, Copper, Arsenic, Selenium, Zirconium,  $Li_2ZrO_3$ , Niobium, Molybdenum, Tungsten and Mercury. The results were generally satisfactory and JENDL-3.3 would be acceptable for shielding applications for fission and fusion reactors. However, some problems in JENDL-3.3 remained, and the improvement should be made in the next release of JENDL.

#### Acknowledgments

Authors are indebted to M. Wada of Startcom Co. Ltd. for his calculations of the FNS benchmarks.

#### References

- 1) K. Shibata, T. Kawano, T. Nakagawa, O. Iwamoto, J. Katakura, T. Fukahori, S. Chiba, A. Hasegawa, T. Murata, H. Matsunobu, T. Ohsawa, Y. Nakajima, T. Yoshida, A. Zukeran, M. Kawai, M. Baba, M. Ishikawa, T. Asami, T. Watanabe, Y. Watanabe, M. Igashira, N. Yamamuro, H. Kitazawa, N. Yamano, H. Takano, "Japanese evaluated nuclear data library version 3 revision-3: JENDL-3.3", *J. Nucl. Sci. Technol.*, **39**[11], 1125-1136 (2002).
- 2) K. Kosako, N. Yamano, T. Fukahori, K. Shibata, A. Hasegawa, "The libraries FSXLIB and MATXS LIB based on JENDL-3.3", *JAERI-Data/Code 2003-011* (2003) 38p.
- 3) J.F. Briesmeister (Ed.), "MCNP - A general Monte Carlo n-particle transport code, version 4C", LA-13709-M, Los Alamos National Laboratory (LANL) (2000) 778p.
- 4) N. Yamano, "On the Integral Test Method for Neutron Nuclear Data Evaluation", *Ann. Nucl. Energy*, **24**[13], 1085-1094 (1997).
- 5) W.W. Engle Jr., "A USER'S MANUAL FOR ANISN: A One Dimensional Discrete Ordinates Transport Code with Anisotropic Scattering", K-1693 (1967).

- 6) W.A. Rhodes, R.L. Childs, "The DORT Two-Dimensional Discrete Ordinates Transport Code", Nucl. Sci. Eng., **99**[1], 88-89 (1988).
- 7) W.A. Rhoades, D.B. Simpson, "The TORT Three-Dimensional Discrete Ordinates Neutron/Photon Transport Code (TORT Version 3)", ORNL/TM-13221 (1998) 205p.
- 8) T. Nakagawa, K. Shibata, S. Chiba, et al., "Japanese evaluated nuclear data library version 3 revision-2: JENDL-3.2", J. Nucl. Sci. Technol., **32**[12], 1259-1271 (1995).
- 9) P.F. Rose, (Ed.), "ENDF-201 ENDF/B-VI Summary Documentation", BNL-NCS-17541 (1991) 457p.
- 10) H.D. Lemmel, et al., "EFF-2.4. The European Fusion File, Summary documentation", IAEA-NDS-170 (1995) 6p.
- 11) S. Ganesan, P.K. McLaughlin, "FENDL/E Evaluated Nuclear Data Library of Neutron Nuclear Interaction Cross-Sections and Photon Production Cross-Sections and Photon-Atom Interaction Cross Sections for Fusion Applications Version 1.0 of May 1994", IAEA-NDS-128 (1995) 10p.
- 12) A.B. Pashchenko, et al., "FENDL-2: An Improved Nuclear Data Library for Fusion Applications", Proc. Int. Conf. on Nuclear Data for Science and Technology, Trieste, Italy, 19-24 May 1997, **59**[2], Part II, 1150 (1997).
- 13) C. Ichihara, S.A. Hayashi, I. Kimura, et al., "Measurement and Analysis of Leakage Neutron Spectra from Spherical Assemblies of Chromium, Manganese and Copper with 14 MeV Neutrons", J. Nucl. Sci. Technol., **37**[4], 358-367 (2000).
- 14) C. Ichihara, S.A. Hayashi, I. Kimura, et al., "Measurement of Leakage Neutron Spectra from a Spherical Pile of Niobium Bombarded with 14 MeV Neutrons and Validation of Its Nuclear Data", J. Nucl. Sci. Technol., **38**[11], 959-966 (2001).
- 15) C. Ichihara, I. Kimura, S.A. Hayashi, et al., "Measurement of Leakage Neutron Spectra from a Spherical Pile of Zirconium Irradiated with 14 MeV Neutrons and Validation of Its Nuclear Data", J. Nucl. Sci. Technol., **40**[6], 417-422 (2003).
- 16) C. Ichihara, I. Kimura, J. Yamamoto, et al., "Measurement and Analysis of Leakage Neutron Spectrum from a Spherical Pile of Silicon with Incident 14 MeV Neutrons", J. Nucl. Sci. Technol., **44**[1], 29-35 (2007).
- 17) K. Sumita, A. Takahashi, T. Iida, et al., "Status of OKTAVIAN and Proposal of OKTAVIAN II", Nucl. Sci. Eng., **106**[3], 249-265 (1990).
- 18) J.F. Briesmeister (ed.), "A General Monte Carlo N-Particle Transport Code, Version 4A", LA-12625-M, (1993).
- 19) R.E. Textor, and V.V. Verbinski, "O5S: A Monte Carlo Code for Calculating Pulse Height Distributions due to Monoenergetic Neutrons Incident on Organic Scintillator", ORNL-4160 (1968).
- 20) D. Kinsey (Ed.), "ENDF/B Summary Documentation", BNL-NCS-17541, 3rd Edition (1979) 594p.
- 21) W. Mannhart, "Status of the Cf-252 fission neutron spectrum evaluation with regard to recent experiments", IAEA-NDS-220/L, 305-336 (1989).
- 22) F. Maekawa, M. Wada, C. Ichihara, Y. Makita, A. Takahashi, Y. Oyama, "Compilation of Benchmark Results for Fusion Related Nuclear Data", JAERI-Data/Code 98-024 (1998) 174p.
- 23) Y. Oyama, S. Yamaguchi, H. Maekawa, "Experimental results of angular neutron flux spectra leaking from slabs of fusion reactor candidate materials, I", JAERI-M 90-092 (1990) 124p.
- 24) F. Maekawa, C. Konno, Y. Kasugai, Y. Oyama, Y. Ikeda, "Data Collection of fusion neutronics benchmark experiment conducted at FNS/JAEA", JAERI-Data/Code 98-021 (1998) 93p.
- 25) Y. Oyama, H. Maekawa, "Spectral Measurement of Angular Neutron Flux on the Restricted Surface of Slab Assemblies by the Time-Of-Flight Method", Nucl. Instrum. Methods, **A245**[1], 173-181 (1986).
- 26) Y. Oyama, H. Maekawa, "Measurement and Analysis of an Angular Neutron Flux on a Beryllium Slab Irradiated with Deuterium-Tritium Neutrons", Nucl. Sci. Eng., **97**, 220-234 (1987).
- 27) Y. Oyama, S. Yamaguchi, H. Maekawa, "Measurement and Analyses of Angular Neutron Flux Spectra on a Graphite and Lithium-Oxide Slabs Irradiated with 14.8 MeV Neutrons", J. Nucl. Sci. Technol., **25**[5], 419-428 (1988).

- 28) Y. Oyama, "Experimental Study of Angular Neutron Flux Spectra on a Slab Surface to Assess Nuclear Data and Calculational Methods for a Fusion Reactor Design", JAERI-M 88-101 (1988) 129p.
- 29) H. Maekawa, Y. Oyama, "Experiment on Angular Neutron Flux Spectra from Lead Slabs Bombarded by D-T Neutrons", Fusion Eng. Design, **18**, 287-291 (1991).
- 30) Y. Oyama, H. Maekawa, K. Kosako, "Measurement and Analyses of Angular Neutron Flux Spectra Leaking from Liquid Nitrogen, Liquid Oxygen and Iron Slabs", Proc. Int. Conf. on Nuclear Data for Science and Technology, Jülich, Germany, 13-17 May 1991, 337-340 (1991).
- 31) Y. Oyama, K. Kosako, H. Maekawa, "Measurement and Calculations of Angular Neutron Flux Spectra from Iron Slabs Bombarded with 14.8 MeV Neutrons", Nucl. Sci. Eng., **115**[1], 24-37 (1993).
- 32) Sub Working Group of Fusion Reactor Physics Subcommittee (Ed.), "Collection of Experimental Data for Fusion Neutronics Benchmark", JAERI-M 94-014 (1994) 302p.
- 33) Y. Oyama, S. Yamaguchi, H. Maekawa, "Experimental Results of Angular Neutron Flux Spectra Leaking from Slabs of Fusion Reactor Candidate Materials (I)", JAERI-M 90-092 (1990) 124p.
- 34) H. Maekawa, Y. Ikeda, Y. Oyama, S. Yamaguchi, K. Tsuda, T. Fukumoto, K. Kosako, M. Yoshizawa, T. Nakamura, "Fusion Blanket Benchmark Experiments on a 60 cm-thick Lithium-Oxide Cylindrecal Assembly", JAERI-M 86-182 (1986) 78p.
- 35) H. Maekawa, S. Yamaguchi, C. Konno, Y. Oyama, Y. Ikeda, K. Sekiyama, K. Kosako, "Benchmark Experiment and Analysis of a Beryllium Cylindrical Assembly", Fusion Technol., **19**[3P2B], 1949-1954 (1991).
- 36) H. Maekawa, Y. Ikeda, Y. Oyama, S. Yamaguchi, K. Tsuda, T. Fukumoto, K. Kosako, M. Yoshizawa, T. Nakamura, "Benchmark Experiments on a 60 cm-thick Graphite Cylindrical Assembly", JAERI-M 88-034 (1988) 65p.
- 37) F. Maekawa, C. Konno, Y. Kasugai, Y. Oyama, Y. Ikeda, "Data Collection of Fusion Neutronics Benchmark Experiment Conducted at FNS/JAERI", JAERI-Data/Code 98-021 (1998) 93p.
- 38) K. Oishi, Y. Ikeda, C. Konno, T. Nakamura, "Measurement and Analysis of Neutron Spectra in a Large Cylindrical Iron Assembly Irradiated by 14 MeV Neutrons", Proc. 7<sup>th</sup> Int. Conf. on Radiation Shielding, Bournemouth, United Kingdom, 12-16 Sep. 1988, 331-340 (1988).
- 39) C. Konno, Y. Ikeda, K. Kosako, Y. Oyama, H. Maekawa, T. Nakamura, E.F. Bennet, "Measurement and Analysis of Low Energy Neutron Spectrum in a Large Cylindrical Iron Assembly Bombarded by 14 MeV Neutrons", Fusion Eng. Des., **18**, 297-303 (1991).
- 40) F. Maekawa, Y. Oyama, "Measurement of Neutron Energy Spectra below 10 keV in an Iron Shield Bombarded by 14 MeV Neutrons and Benchmark Test of Recent Evaluated Nuclear Data Libraries from 14 MeV Down to 1 eV", Nucl. Sci. Eng., **125**[2], 205-217 (1997).
- 41) F. Maekawa, Y. Oyama, C. Konno, M. Wada, Y. Ikeda, "Measurement of Gamma-Ray Spectra and Heating Rates in Iron and Stainless Steel Shields Bombarded by Deuterium-Tritium Neutrons and Validation of Secondary Gamma-Ray Data in Evaluated Nuclear Data Libraries", Nucl. Sci. Eng., **126**[2], 187-200 (1997).
- 42) C. Konno, F. Maekawa, Y. Oyama, Y. Ikeda, H. Maekawa, "Benchmark Experiment on Copper with D-T Neutrons for verification of Neutron Transport and Related Nuclear Data of JENDL-3.1", ISFNT-3, Fusion Eng. Des., **28**, 745-752 (1995).
- 43) F. Maekawa, Y. Oyama, C. Konno, Y. Ikeda, H. Maekawa, "Benchmark Experiment on Copper with D-T Neutrons for Verification of Secondary Gamma-ray Data in JENDL-3.1", ISFNT-3, Fusion Eng. Des., **28**, 753-761 (1995).
- 44) F. Maekawa, Y. Oyama, C. Konno, Y. Ikeda, K. Kosako, H. Maekawa, "Benchmark Experiment on Copper Slab Assembly Bombarded by D-T Neutrons", JAERI-M 94-038 (1994) 77p.
- 45) F. Maekawa, C. Konno, Y. Oyama, M. Wada, Y. Uno, Y. Ikeda, "Benchmark Experiment on Tungsten Assembly Bombarded with D-T Neutrons", Proc. Int. Conf. on Nuclear Data for Science and Technology, Trieste, Italy, 19-24 May, 1997, 1218-1220 (1998).
- 46) C. Konno, F. Maekawa, Y. Ikeda, Y. Oyama, K. Kosako, H. Maekawa, "Bulk Shielding Experiments on

- Large SS316 Assemblies”, Fusion Technol., **21**[3P2B], 2169-2173 (1992).
- 47) F. Maekawa, C. Konno, K. Kosako, Y. Oyama, Y. Ikeda, H. Maekawa, “Analysis of Bulk Shielding Experiments on Large SS316 Assemblies”, Fusion Technol., **21**[3P2B], 2107-2111 (1992).
- 48) C. Konno, F. Maekawa, Y. Oyama, Y. Ikeda, K. Kosako, H. Maekawa, “Bulk Shielding Experiments on Large SS316 Assemblies Bombarded with D-T Neutrons Volume I: Experiment”, JAERI-Research 94-043 (1994) 96p.
- 49) F. Maekawa, C. Konno, K. Kosako, Y. Oyama, Y. Ikeda, H. Maekawa, “Bulk Shielding Experiments on Large SS316 Assemblies Bombarded with D-T Neutrons Volume II: Analysis”, JAERI-Research 94-044 (1994) 143p.
- 50) H. Maekawa, Y. Ikeda, Y. Oyama, S. Yamaguchi, T. Nakamura, “Neutron Yield Monitors for the Fusion Neutronics Source (FNS) – for 80° Beam Line –”, JAERI-M 83-219 (1983) 28p.
- 51) S. Yamaguchi, Y. Oyama, H. Maekawa, “Calculation of Anisotropy Correction Factor for Determination of D-T Neutron Yield by Associated  $\alpha$ -particle Method”, JAERI-M 84-109 (1984) 33p.
- 52) M. Nakagawa, T. Mori., “MORSE-DD; A Monte Carlo Code Using Multi-Group Double Differential Form Cross Section”, JAERI-M 84-126 (1984) 74p.
- 53) J.F. Briesmeister (Ed.), “MCNP - A General Monte Carlo Code for Neutrons and Photon Transport, Version 3B”, RSICC/CCC-200 (1988).
- 54) E.A. Straker, “Experimental Evaluation of Minima in Total Cross Sections of Several Shielding Materials”, ORNL-TM-2242 (1968).
- 55) R.E. Maerker, “SDT1. IRON BROOMSTICK EXPERIMENT – AN EXPERIMENTAL CHECK OF NEUTRON TOTAL CROSS SECTIONS”, ORNL-TM-3867 (ENDF-166) (Revised) (1972) 17p.
- 56) R.E. Maerker, “SDT4. SODIUM BROOMSTICK EXPERIMENT – AN EXPERIMENTAL CHECK OF NEUTRON TOTAL CROSS SECTIONS”, ORNL-TM-3870 (ENDF-169) (Revised) (1972) 16p.
- 57) F.J. Muckenthaler, R.R. Spencer, H.T. Hunter, J.L. Hull, A. Shono, “Measurements for the Jasper Program In-Vessel Fuel Storage Experiment”, ORNL/TM-11989 (1992).
- 58) F.J. Muckenthaler, R.R. Spencer, H.T. Hunter, J.L. Hull, A. Shono, “Measurements for the Jasper Program Intermediate Heat Exchanger Experiment”, ORNL/TM-12064 (1992).
- 59) M.D. Carter, A. Packwood, “The Winfrith Benchmark Experiment in Iron – Experimental Results”, Proc. of the Specialists' Meeting on Sensitivity Studies and Shielding Benchmarks, Paris, Octover 1975, 111-119, OECD (1975).
- 60) H. Werle, F. Kappler, D. Kuhn, “Measurements of Neutron Leakage Spectra from Iron Sphere with a  $^{252}\text{Cf}$  Source in the Center”, NEACRP-U-73, 8 (1976).
- 61) S.H. Jiang, H. Werle, “Measurement and Calculation of Californium-252 Fission Neutron-Induced Gamma Fields in Iron”, Nucl. Sci. Eng., **66**[3], 354-362 (1978).
- 62) H. Bluhm, “A  $\gamma$ -discriminating  $^3\text{He}$ -semiconductor sandwich spectrometer”, Nucl. Instr. Methods, **115**[2], 325-337 (1974).
- 63) S.P. Simakov, A.A. Androsenko, et al., Proc. of 17th Symp. on Fusion Technology, Rome, Sep. 14-18, 1992.
- 64) M. B. Stanka, J. M. Adams, C. M. Eisenhauer, “Proton Recoil Measurements of the  $^{252}\text{Cf}$  Fission Neutron Leakage Spectrum from an Iron Sphere”, Nucl. Sci. Eng., **134**[1], 68-76 (2000).
- 65) R.E. Maerker, F.J. Muckenthaler, “A Benchmark Experiment for Neutron Transport in Iron and Stainless Steel”, Nucl. Sci. Eng., **52**[2], 227-246 (1973).
- 66) M. Kawai, A. Hasegawa, K. Ueki, N. Yamano, K. Sasaki, Y. Matsumoto, M. Takemura, N. Ohtani, K. Sakurai, “Shielding Benchmark Tests of JENDL-3”, JAERI-1330 (1994) 129p.
- 67) K. Kosako, F. Maekawa, Y. Oyama, et al., “FSXLIB-J3R2: A Continuous Energy Cross Section Library for MCNP Based on JENDL-3.2”, JAERI-Data/Code 94-020 (1994) 42p.
- 68) J. S. Hendricks, S. C. Frankle and J. D. Court, “ENDF/B-VI Data for MCNP and errata”, LA-12891, Los Alamos National Laboratory (1994) 45p.
- 69) L. Petrizzi, “Final report on task NDB 1.2: processing EFF-2.4 with ACER of NJOY to produce an

- MCNP working library”, EFF-DOC-412 (1994).
- 70) H.D. Lemmel, “EFF-2.4, The European Fusion File 1994, including revisions up to May 1995, Summary Documentation”, IAEA-NDS-170 (1995) 6p.
  - 71) R.E. MacFarlane, D.W. Muir, “The NJOY Nuclear Data Processing System, Version 91”, Los Alamos National Laboratory report LA-12740-M (1994) 573p.
  - 72) R. E. MacFarlane, “TRANSX 2: A Code for Interfacing MATXS Cross-Section Libraries to Nuclear Transport Codes”, Los Alamos National Laboratory report LA-12312-MS (1992).

## Appendix A

### A.1 OKTAVIAN Benchmark

Source spectrum for each sample measurement is presented in **Table A-1.1** to **A-1.5**. Detailed information is described in JAERI-M 94-014 (1994).

**Table A-1.1** Neutron source for Cr and Nb samples

E-up(MeV)	E-low(MeV)	Spectrum/E	Error
1.6400E+01	1.6110E+01	1.5500E-03	2.5690E-05
1.6110E+01	1.5826E+01	9.0773E-02	1.9711E-04
1.5826E+01	1.5546E+01	9.7170E-02	2.0940E-04
1.5546E+01	1.5271E+01	9.7170E-02	2.0940E-04
1.5271E+01	1.5000E+01	1.0386E-01	2.1356E-04
1.5000E+01	1.4735E+01	7.0180E-01	5.8550E-04
1.4735E+01	1.4474E+01	7.0180E-01	5.8550E-04
1.4474E+01	1.4218E+01	7.0180E-01	5.8550E-04
1.4218E+01	1.3976E+01	6.6878E-01	5.6545E-04
1.3976E+01	1.3720E+01	8.7110E-02	2.1220E-04
1.3720E+01	1.3477E+01	8.7110E-02	2.1220E-04
1.3477E+01	1.3239E+01	8.7110E-02	2.1220E-04
1.3239E+01	1.3005E+01	7.6017E-02	1.9417E-04
1.3005E+01	1.2775E+01	1.8800E-02	1.0120E-04
1.2775E+01	1.2549E+01	1.8800E-02	1.0120E-04
1.2549E+01	1.2182E+01	1.8800E-02	1.0120E-04
1.2182E+01	1.1825E+01	9.9915E-03	7.6089E-05
1.1825E+01	1.1479E+01	9.4410E-03	7.4520E-05
1.1479E+01	1.1143E+01	7.5283E-03	6.7374E-05
1.1143E+01	1.0817E+01	6.1620E-03	6.2270E-05
1.0817E+01	1.0500E+01	5.7357E-03	5.9935E-05
1.0500E+01	1.0089E+01	4.2850E-03	5.1990E-05
1.0089E+01	9.6930E+00	3.9533E-03	5.0448E-05
9.6930E+00	9.3140E+00	3.4870E-03	4.8280E-05
9.3140E+00	8.9490E+00	3.3404E-03	4.7968E-05
8.9490E+00	8.5980E+00	3.2660E-03	4.7810E-05
8.5980E+00	8.2610E+00	2.6541E-03	4.3248E-05
8.2610E+00	7.9380E+00	2.5643E-03	4.2596E-05
7.9380E+00	7.6270E+00	2.3900E-03	4.1390E-05
7.6270E+00	7.3270E+00	2.4175E-03	4.1895E-05
7.3270E+00	7.0410E+00	2.4570E-03	4.2620E-05
7.0410E+00	6.7650E+00	2.6431E-03	4.4790E-05
6.7650E+00	6.5000E+00	2.7400E-03	4.5920E-05
6.5000E+00	6.2420E+00	2.8383E-03	4.7705E-05
6.2420E+00	5.9950E+00	2.8895E-03	4.8418E-05
5.9950E+00	5.7570E+00	3.0810E-03	5.0900E-05

5.7570E+00	5.5290E+00	3.2179E-03	5.2555E-05
5.5290E+00	5.3100E+00	3.3880E-03	5.4610E-05
5.3100E+00	5.0990E+00	3.8220E-03	5.8957E-05
5.0990E+00	4.8970E+00	3.9940E-03	6.0680E-05
4.8970E+00	4.7030E+00	4.3624E-03	6.3631E-05
4.7030E+00	4.5160E+00	4.4374E-03	6.4240E-05
4.5160E+00	4.3370E+00	4.6430E-03	6.5910E-05
4.3370E+00	4.1650E+00	4.8690E-03	6.7759E-05
4.1650E+00	4.0000E+00	5.0720E-03	6.9420E-05
4.0000E+00	3.6990E+00	5.4928E-03	7.3258E-05
3.6990E+00	3.4190E+00	6.3891E-03	8.0679E-05
3.4190E+00	3.1620E+00	7.1277E-03	8.6915E-05
3.1620E+00	2.9240E+00	7.8656E-03	9.2877E-05
2.9240E+00	2.7040E+00	9.2892E-03	1.0293E-04
2.7040E+00	2.5000E+00	1.0065E-02	1.0977E-04
2.5000E+00	2.2700E+00	1.0417E-02	1.1492E-04
2.2700E+00	2.0610E+00	1.1573E-02	1.2565E-04
2.0610E+00	1.8710E+00	1.2463E-02	1.3442E-04
1.8710E+00	1.6980E+00	1.3683E-02	1.4635E-04
1.6980E+00	1.5420E+00	1.5145E-02	1.6143E-04
1.5420E+00	1.4000E+00	1.6340E-02	1.7472E-04
1.4000E+00	1.2750E+00	1.7588E-02	1.8955E-04
1.2750E+00	1.1620E+00	1.9631E-02	2.0853E-04
1.1620E+00	1.0580E+00	2.0224E-02	2.1962E-04
1.0580E+00	9.6400E-01	2.0057E-02	2.2861E-04
9.6400E-01	8.7800E-01	2.1538E-02	2.4843E-04
8.7800E-01	8.0000E-01	2.1923E-02	2.6279E-04
8.0000E-01	7.1300E-01	2.3004E-02	2.9009E-04
7.1300E-01	6.3500E-01	2.3099E-02	3.1558E-04
6.3500E-01	5.6600E-01	2.3501E-02	3.5279E-04
5.6600E-01	5.0400E-01	2.2115E-02	3.8901E-04
5.0400E-01	4.4900E-01	2.2021E-02	4.4994E-04
4.4900E-01	4.0000E-01	2.1675E-02	5.3812E-04
4.0000E-01	3.5600E-01	2.3087E-02	6.7952E-04
3.5600E-01	3.1700E-01	1.9493E-02	7.8944E-04
3.1700E-01	2.8300E-01	1.9610E-02	1.0328E-03
2.8300E-01	2.5200E-01	2.0557E-02	1.4119E-03
2.5200E-01	2.2400E-01	1.9221E-02	1.8633E-03
2.2400E-01	2.0000E-01	2.2746E-02	2.5999E-03
2.0000E-01	1.7800E-01	2.4311E-02	4.3017E-03
1.7800E-01	1.5900E-01	8.0320E-03	7.6760E-03
1.5900E-01	1.4100E-01	2.7573E-02	1.3768E-02
1.4100E-01	1.2600E-01	4.8382E-02	2.3796E-02
1.2600E-01	1.1200E-01	1.8406E-01	4.9709E-02
1.1200E-01	1.0000E-01	7.5022E-02	6.5763E-01
1.0000E-01	7.7400E-02	2.5353E-02	2.1295E-01

**Table A-1.2** Neutron source for Li, CF, Si and Co samples

E-up(MeV)	E-low(MeV)	Spectrum/E	Error
2.0660E+01	1.9072E+01	3.0020E-05	2.1670E-05
1.9072E+01	1.7605E+01	5.6830E-05	2.5540E-05
1.7605E+01	1.6252E+01	4.7200E-03	1.3400E-04
1.6252E+01	1.5002E+01	2.4940E-01	9.9810E-04
1.5002E+01	1.3849E+01	5.2050E-01	1.5070E-03
1.3849E+01	1.2784E+01	1.4840E-02	2.6770E-04
1.2784E+01	1.1801E+01	6.0490E-03	1.8050E-04
1.1801E+01	1.0894E+01	3.7650E-03	1.5010E-04
1.0894E+01	1.0056E+01	2.9730E-03	1.3720E-04
1.0056E+01	9.2831E+00	2.2570E-03	1.2380E-04
9.2831E+00	8.5694E+00	2.2200E-03	1.2700E-04
8.5694E+00	7.9106E+00	2.0990E-03	1.2670E-04
7.9106E+00	7.3024E+00	2.1010E-03	1.3250E-04
7.3024E+00	6.7410E+00	1.8620E-03	1.3150E-04
6.7410E+00	6.2227E+00	2.1120E-03	1.4400E-04
6.2227E+00	5.7443E+00	2.4780E-03	1.5880E-04
5.7443E+00	5.3026E+00	2.3330E-03	1.5810E-04
5.3026E+00	4.8949E+00	2.9080E-03	1.7690E-04
4.8949E+00	4.5186E+00	3.3630E-03	1.9290E-04
4.5186E+00	4.1712E+00	3.9850E-03	2.1310E-04
4.1712E+00	3.8505E+00	4.0670E-03	2.2250E-04
3.8505E+00	3.5545E+00	4.8750E-03	2.5040E-04
3.5545E+00	3.2812E+00	5.1890E-03	2.6840E-04
3.2812E+00	3.0289E+00	5.9380E-03	2.9000E-04
3.0289E+00	2.7960E+00	1.2340E-02	4.0670E-04
2.7960E+00	2.5811E+00	1.4390E-02	4.4510E-04
2.5811E+00	2.3826E+00	8.4500E-03	3.6040E-04
2.3826E+00	2.1994E+00	8.8990E-03	3.7930E-04
2.1994E+00	2.0303E+00	9.5500E-03	4.0660E-04
2.0303E+00	1.8742E+00	1.0770E-02	4.4660E-04
1.8742E+00	1.7301E+00	1.0410E-02	4.5940E-04
1.7301E+00	1.5971E+00	1.1540E-02	4.9970E-04
1.5971E+00	1.4743E+00	1.2960E-02	5.4700E-04
1.4743E+00	1.3610E+00	1.3850E-02	5.8500E-04
1.3610E+00	1.2563E+00	1.4460E-02	6.2000E-04
1.2563E+00	1.1598E+00	1.5890E-02	6.7310E-04
1.1598E+00	1.0706E+00	1.6750E-02	7.2210E-04
1.0706E+00	9.8827E-01	1.4410E-02	7.1640E-04
9.8827E-01	9.1229E-01	1.6700E-02	7.8360E-04
9.1229E-01	8.4215E-01	1.5960E-02	7.9430E-04
8.4215E-01	7.7740E-01	1.6830E-02	8.4200E-04
7.7740E-01	7.1763E-01	1.5240E-02	8.5490E-04
7.1763E-01	6.6246E-01	1.6440E-02	9.2530E-04

6.6246E-01	6.1153E-01	1.5950E-02	9.7040E-04
6.1153E-01	5.6451E-01	1.5910E-02	1.0300E-03
5.6451E-01	5.2111E-01	1.5770E-02	1.1020E-03
5.2111E-01	4.8104E-01	1.6610E-02	1.2250E-03
4.8104E-01	4.4406E-01	1.5040E-02	1.3090E-03
4.4406E-01	4.0992E-01	1.5510E-02	1.4540E-03
4.0992E-01	3.7840E-01	1.4920E-02	1.5940E-03
3.7840E-01	3.4931E-01	1.6120E-02	1.8000E-03
3.4931E-01	3.2245E-01	1.1110E-02	1.8980E-03
3.2245E-01	2.9766E-01	1.3930E-02	2.2140E-03
2.9766E-01	2.7478E-01	1.5620E-02	2.6050E-03
2.7478E-01	2.5365E-01	1.3920E-02	3.0030E-03
2.5365E-01	2.3415E-01	1.0760E-02	3.4810E-03
2.3415E-01	2.1615E-01	7.4050E-03	4.1610E-03
2.1615E-01	1.9953E-01	1.9500E-02	5.4190E-03
1.9953E-01	1.8419E-01	9.9410E-03	6.2520E-03
1.8419E-01	1.7003E-01	5.3210E-03	7.4010E-03
1.7003E-01	1.5696E-01	3.4450E-03	9.2120E-03
1.5696E-01	1.4489E-01	4.5760E-03	1.3060E-02

**Table A-1.3** Neutron source for LiF, Mn, Cu, Mo and W samples

E-up(MeV)	E-low(MeV)	Spectrum/E	Error
2.0250E+01	1.8323E+01	4.1604E-05	2.8206E-05
1.8323E+01	1.6579E+01	1.8377E-04	3.8514E-05
1.6579E+01	1.5002E+01	1.5737E-01	7.7008E-04
1.5002E+01	1.3574E+01	4.5675E-01	1.3844E-03
1.3574E+01	1.2282E+01	1.0450E-02	3.0268E-04
1.2282E+01	1.1113E+01	4.3496E-03	1.5756E-04
1.1113E+01	1.0056E+01	2.9156E-03	1.3709E-04
1.0056E+01	9.0989E+00	2.4579E-03	1.3125E-04
9.0989E+00	8.2330E+00	2.0759E-03	1.2786E-04
8.2330E+00	7.4496E+00	1.9946E-03	1.3034E-04
7.4496E+00	6.7406E+00	2.2241E-03	1.4179E-04
6.7406E+00	6.0992E+00	2.7010E-03	1.5982E-04
6.0992E+00	5.5188E+00	3.0866E-03	1.7645E-04
5.5188E+00	4.9936E+00	3.4930E-03	1.9272E-04
4.9936E+00	4.5184E+00	4.2977E-03	2.1699E-04
4.5184E+00	4.0884E+00	5.1424E-03	2.4283E-04
4.0884E+00	3.6993E+00	6.2483E-03	2.7428E-04
3.6993E+00	3.3473E+00	7.2319E-03	3.0114E-04
3.3473E+00	3.0288E+00	8.4660E-03	3.3186E-04
3.0288E+00	2.7405E+00	1.1263E-02	3.8757E-04
2.7405E+00	2.4797E+00	1.3306E-02	4.3255E-04
2.4797E+00	2.2438E+00	1.2220E-02	4.3696E-04
2.2438E+00	2.0302E+00	1.4665E-02	4.9555E-04

2.0302E+00	1.8370E+00	1.5282E-02	5.3113E-04
1.8370E+00	1.6622E+00	1.6998E-02	5.8528E-04
1.6622E+00	1.5040E+00	1.9228E-02	6.5062E-04
1.5040E+00	1.3609E+00	2.1076E-02	7.1556E-04
1.3609E+00	1.2314E+00	2.1579E-02	7.6681E-04
1.2314E+00	1.1142E+00	2.4778E-02	8.6033E-04
1.1142E+00	1.0082E+00	2.5688E-02	9.2480E-04
1.0082E+00	9.1225E-01	2.5161E-02	9.7352E-04
9.1225E-01	8.2544E-01	2.6299E-02	1.0523E-03
8.2544E-01	7.4689E-01	2.7335E-02	1.1375E-03
7.4689E-01	6.7581E-01	2.7047E-02	1.2230E-03
6.7581E-01	6.1150E-01	2.8167E-02	1.3454E-03
6.1150E-01	5.5331E-01	2.9344E-02	1.4818E-03
5.5331E-01	5.0065E-01	2.7781E-02	1.5900E-03
5.0065E-01	4.5301E-01	2.8920E-02	1.7535E-03
4.5301E-01	4.0990E-01	2.0157E-02	1.7663E-03
4.0990E-01	3.7089E-01	2.4503E-02	2.0231E-03
3.7089E-01	3.3560E-01	2.2206E-02	2.2469E-03
3.3560E-01	3.0366E-01	2.0674E-02	2.5817E-03
3.0366E-01	2.7476E-01	2.1334E-02	3.0172E-03
2.7476E-01	2.4862E-01	2.5633E-02	3.5871E-03
2.4862E-01	2.2496E-01	1.5833E-02	4.1818E-03
2.2496E-01	2.0355E-01	1.2905E-02	5.3208E-03
2.0355E-01	1.8418E-01	2.8252E-02	7.0255E-03
1.8418E-01	1.6665E-01	1.2097E-02	8.4314E-03
1.6665E-01	1.5079E-01	8.9529E-03	1.1089E-02
1.5079E-01	1.3644E-01	1.3480E-02	1.5890E-02

**Table A-1.4** Neutron source for Ti, As, Se and Zr samples

E-up(MeV)	E-low(MeV)	Spectrum/E	Error
2.0250E+01	1.8323E+01	4.4181E-05	2.5769E-05
1.8323E+01	1.6579E+01	4.2393E-04	4.3350E-05
1.6579E+01	1.5002E+01	1.9303E-01	7.6692E-04
1.5002E+01	1.3574E+01	3.6457E-01	1.1044E-03
1.3574E+01	1.2282E+01	2.4613E-02	2.9718E-04
1.2282E+01	1.1113E+01	4.9241E-03	1.4285E-04
1.1113E+01	1.0056E+01	3.2094E-03	1.2358E-04
1.0056E+01	9.0989E+00	2.8306E-03	1.2206E-04
9.0989E+00	8.2330E+00	2.4498E-03	1.1989E-04
8.2330E+00	7.4496E+00	2.4894E-03	1.2544E-04
7.4496E+00	6.7406E+00	2.5919E-03	1.3347E-04
6.7406E+00	6.0992E+00	2.8817E-03	1.4640E-04
6.0992E+00	5.5188E+00	3.3637E-03	1.6394E-04
5.5188E+00	4.9936E+00	3.7746E-03	1.8047E-04
4.9936E+00	4.5184E+00	4.5837E-03	1.9981E-04

4.5184E+00	4.0884E+00	5.2122E-03	2.1704E-04
4.0884E+00	3.6993E+00	5.9427E-03	2.3712E-04
3.6993E+00	3.3473E+00	7.2659E-03	2.6475E-04
3.3473E+00	3.0288E+00	7.6316E-03	2.7967E-04
3.0288E+00	2.7405E+00	1.6848E-02	4.0664E-04
2.7405E+00	2.4797E+00	1.3068E-02	3.8121E-04
2.4797E+00	2.2438E+00	1.1394E-02	3.7853E-04
2.2438E+00	2.0302E+00	1.2312E-02	4.1170E-04
2.0302E+00	1.8370E+00	1.3777E-02	4.5335E-04
1.8370E+00	1.6622E+00	1.4832E-02	4.9331E-04
1.6622E+00	1.5040E+00	1.7403E-02	5.5505E-04
1.5040E+00	1.3609E+00	1.7641E-02	5.8536E-04
1.3609E+00	1.2314E+00	2.0237E-02	6.4946E-04
1.2314E+00	1.1142E+00	2.1794E-02	7.0447E-04
1.1142E+00	1.0082E+00	2.1165E-02	7.3652E-04
1.0082E+00	9.1225E-01	2.2380E-02	7.9710E-04
9.1225E-01	8.2544E-01	2.3318E-02	8.5907E-04
8.2544E-01	7.4689E-01	2.2985E-02	9.0490E-04
7.4689E-01	6.7581E-01	2.3898E-02	9.7392E-04
6.7581E-01	6.1150E-01	2.2434E-02	1.0159E-03
6.1150E-01	5.5331E-01	2.1737E-02	1.0594E-03
5.5331E-01	5.0065E-01	1.9280E-02	1.0860E-03
5.0065E-01	4.5301E-01	2.0324E-02	1.1755E-03
4.5301E-01	4.0990E-01	1.8183E-02	1.2518E-03
4.0990E-01	3.7089E-01	2.0341E-02	1.4063E-03
3.7089E-01	3.3560E-01	1.6691E-02	1.4899E-03
3.3560E-01	3.0366E-01	1.8165E-02	1.6835E-03
3.0366E-01	2.7476E-01	1.9851E-02	1.9031E-03
2.7476E-01	2.4862E-01	1.3409E-02	2.0303E-03
2.4862E-01	2.2496E-01	1.5415E-02	2.3966E-03
2.2496E-01	2.0355E-01	2.1325E-02	2.8783E-03
2.0355E-01	1.8418E-01	1.5454E-02	3.2590E-03
1.8418E-01	1.6665E-01	1.7205E-03	3.9672E-03
1.6665E-01	1.5079E-01	2.4666E-02	4.9074E-03
1.5079E-01	1.3644E-01	2.7922E-03	5.5913E-03
1.3644E-01	1.2346E-01	2.5256E-02	7.1728E-03
1.2346E-01	1.1171E-01	1.1217E-02	8.4900E-03
1.1171E-01	1.0108E-01	2.6195E-02	1.0583E-02
1.0108E-01	9.1461E-02	8.9674E-04	1.3379E-02
9.1461E-02	8.2757E-02	1.9367E-02	1.7886E-02
8.2757E-02	7.4882E-02	2.9003E-02	2.3915E-02
7.4882E-02	6.7756E-02	6.2452E-02	3.3441E-02
6.7756E-02	6.1308E-02	6.7532E-03	4.6473E-02
6.1308E-02	5.5474E-02	7.1192E-02	6.8983E-02
5.5474E-02	5.0195E-02	4.4422E-03	1.0281E-01

**Table A-1.5** Neutron source for Al sample

E-up(MeV)	E-low(MeV)	Spectrum/E	Error
2.0250E+01	1.8323E+01	9.9863E-06	1.2403E-05
1.8323E+01	1.6579E+01	3.4531E-04	2.2176E-05
1.6579E+01	1.5002E+01	1.8720E-01	4.2728E-04
1.5002E+01	1.3574E+01	4.3484E-01	6.8764E-04
1.3574E+01	1.2282E+01	1.6027E-02	1.4078E-04
1.2282E+01	1.1113E+01	3.9675E-03	7.6307E-05
1.1113E+01	1.0056E+01	2.4064E-03	6.3499E-05
1.0056E+01	9.0989E+00	1.9953E-03	6.0413E-05
9.0989E+00	8.2330E+00	1.7263E-03	5.9832E-05
8.2330E+00	7.4496E+00	1.7344E-03	6.2936E-05
7.4496E+00	6.7406E+00	1.7674E-03	6.5876E-05
6.7406E+00	6.0992E+00	2.1480E-03	7.3132E-05
6.0992E+00	5.5188E+00	2.2482E-03	7.7259E-05
5.5188E+00	4.9936E+00	2.6730E-03	8.6051E-05
4.9936E+00	4.5184E+00	3.2443E-03	9.8297E-05
4.5184E+00	4.0884E+00	3.8202E-03	1.1115E-04
4.0884E+00	3.6993E+00	4.5713E-03	1.2592E-04
3.6993E+00	3.3473E+00	5.1770E-03	1.3442E-04
3.3473E+00	3.0288E+00	5.5489E-03	1.4159E-04
3.0288E+00	2.7405E+00	1.2099E-02	2.0165E-04
2.7405E+00	2.4797E+00	1.0724E-02	2.0145E-04
2.4797E+00	2.2438E+00	9.0526E-03	1.9837E-04
2.2438E+00	2.0302E+00	9.7660E-03	2.1614E-04
2.0302E+00	1.8370E+00	1.0933E-02	2.3681E-04
1.8370E+00	1.6622E+00	1.1597E-02	2.5463E-04
1.6622E+00	1.5040E+00	1.2747E-02	2.7876E-04
1.5040E+00	1.3609E+00	1.3571E-02	3.0612E-04
1.3609E+00	1.2314E+00	1.4991E-02	3.4093E-04
1.2314E+00	1.1142E+00	1.6866E-02	3.8191E-04
1.1142E+00	1.0082E+00	1.6849E-02	4.0266E-04
1.0082E+00	9.1225E-01	1.8996E-02	4.3563E-04
9.1225E-01	8.2544E-01	1.8726E-02	4.6913E-04
8.2544E-01	7.4689E-01	1.9462E-02	5.0676E-04
7.4689E-01	6.7581E-01	1.8177E-02	5.3054E-04
6.7581E-01	6.1150E-01	1.7867E-02	5.6692E-04
6.1150E-01	5.5331E-01	1.6650E-02	5.9958E-04
5.5331E-01	5.0065E-01	1.8173E-02	6.6321E-04
5.0065E-01	4.5301E-01	1.5406E-02	6.9459E-04
4.5301E-01	4.0990E-01	1.3230E-02	7.5697E-04
4.0990E-01	3.7089E-01	1.6158E-02	8.8218E-04
3.7089E-01	3.3560E-01	1.4749E-02	9.7977E-04
3.3560E-01	3.0366E-01	1.6028E-02	1.1379E-03
3.0366E-01	2.7476E-01	1.2984E-02	1.2752E-03

2.7476E-01	2.4862E-01	1.1491E-02	1.4620E-03
2.4862E-01	2.2496E-01	1.6120E-02	1.8274E-03
2.2496E-01	2.0355E-01	9.5960E-03	2.1554E-03
2.0355E-01	1.8418E-01	1.0837E-02	2.6678E-03
1.8418E-01	1.6665E-01	1.7461E-02	3.5145E-03
1.6665E-01	1.5079E-01	1.7692E-03	4.4141E-03
1.5079E-01	1.3644E-01	6.7201E-03	5.9123E-03
1.3644E-01	1.2346E-01	2.3163E-03	8.1416E-03

# 国際単位系 (SI)

表1. SI 基本単位

基本量	SI 基本単位	
	名称	記号
長さ	メートル	m
質量	キログラム	kg
時間	秒	s
電流	アンペア	A
熱力学温度	ケルビン	K
物質量	モル	mol
光度	カンデラ	cd

表2. 基本単位を用いて表されるSI組立単位の例

組立量	SI組立単位	
	名称	記号
面積	平方メートル	m <sup>2</sup>
体積	立方メートル	m <sup>3</sup>
速度	メートル毎秒	m/s
加速度	メートル毎秒毎秒	m/s <sup>2</sup>
波数	毎メートル	m <sup>-1</sup>
密度、質量密度	キログラム毎立方メートル	kg/m <sup>3</sup>
面積密度	キログラム毎平方メートル	kg/m <sup>2</sup>
比體積	立方メートル毎キログラム	m <sup>3</sup> /kg
電流密度	アンペア毎平方メートル	A/m <sup>2</sup>
磁界の強さ	アンペア毎メートル	A/m
量濃度 <sup>(a)</sup> 、濃度	モル毎立方メートル	mol/m <sup>3</sup>
質量濃度	キログラム毎立方メートル	kg/m <sup>3</sup>
輝度	カンデラ毎平方メートル	cd/m <sup>2</sup>
屈折率 <sup>(b)</sup>	(数字の) 1	1
比透磁率 <sup>(b)</sup>	(数字の) 1	1

(a)量濃度(amount concentration)は臨床化学の分野では物質濃度(substance concentration)ともよばれる。

(b)これらは無次元あるいは次元をもつ量であるが、そのことを表す単位記号である数字の1は通常は表記しない。

表3. 固有の名称と記号で表されるSI組立単位

組立量	SI組立単位		
	名称	記号	他のSI単位による表し方
平面角	ラジアン <sup>(b)</sup>	rad	1 <sup>(b)</sup>
立体角	ステラジアン <sup>(b)</sup>	sr <sup>(c)</sup>	1 <sup>(b)</sup>
周波数	ヘルツ <sup>(d)</sup>	Hz	1/s
力	ニュートン	N	m kg s <sup>-2</sup>
圧力、応力	パスカル	Pa	N/m <sup>2</sup>
エネルギー、仕事、熱量	ジュール	J	m <sup>2</sup> kg s <sup>-2</sup>
仕事率、工率、放射束	ワット	W	m <sup>2</sup> kg s <sup>-3</sup>
電荷、電気量	クーロン	C	s A
電位差(電圧)、起電力	ボルト	V	m <sup>2</sup> kg s <sup>-3</sup> A <sup>-1</sup>
静電容量	ファラード	F	C/V
電気抵抗	オーム	Ω	m <sup>2</sup> kg s <sup>-3</sup> A <sup>-2</sup>
コンダクタンス	ジーメンス	S	A/V
磁束密度	ウェーバ	Wb	Vs
磁束密度	テスラ	T	Wb/m <sup>2</sup>
インダクタンス	ヘンリー	H	kg s <sup>2</sup> A <sup>-1</sup>
セルシウス温度	セルシウス度 <sup>(e)</sup>	°C	Wb/A
光照度	ルーメン	lm	cd sr <sup>(e)</sup>
放射性核種の放射能 <sup>(f)</sup>	ベクレル <sup>(d)</sup>	Bq	lm/m <sup>2</sup>
吸収線量、比エネルギー分与、カーマ	グレイ	Gy	m <sup>2</sup> s <sup>-2</sup>
線量当量、周辺線量当量、方向線量当量、個人線量当量	シーベルト <sup>(g)</sup>	Sv	J/kg
酸素活性	カタール	kat	m <sup>2</sup> s <sup>-2</sup>

(a)SI接頭語は固有の名称と記号を持つ組立単位と組み合わせても使用できる。しかし接頭語を付した単位はもはやコヒーレントではない。

(b)ラジアンとステラジアンは数字の1に対する単位の特別な名称で、量についての情報をつたえるために使われる。実際には、使用する時には記号rad及びsrが用いられるが、習慣として組立単位としての記号である数字の1は明示されない。

(c)測光学ではステラジアンという名称と記号srを表し方の中に、そのまま維持している。

(d)ヘルツは周期現象についてのみ、ベクレルは放射性核種の統計的過程についてのみ使用される。

(e)セルシウス度はケルビンの特別な名称で、セルシウス温度を表すために使用される。セルシウス度とケルビンの単位の大きさは同じである。したがって、温度差や温度間隔を表す數値はどちらの単位で表しても同じである。

(f)放射性核種の放射能(activity referred to a radionuclide)は、しばしば誤った用語で“radioactivity”と記される。(g)単位シーベルト(PV,2002,70,205)についてはCIPM勧告2(CI-2002)を参照。

表4. 単位の中に固有の名称と記号を含むSI組立単位の例

組立量	SI組立単位		
	名称	記号	SI基本単位による表し方
粘度	パスカル秒	Pa s	m <sup>1</sup> kg s <sup>-1</sup>
力のモーメント	ニュートンメートル	N m	m <sup>2</sup> kg s <sup>2</sup>
表面張力	ニュートン毎メートル	N/m	kg s <sup>-2</sup>
角速度	ラジアン毎秒	rad/s	m <sup>-1</sup> s <sup>-1</sup> =s <sup>-1</sup>
角加速度	ラジアン毎秒毎秒	rad/s <sup>2</sup>	m <sup>-1</sup> s <sup>-2</sup> =s <sup>-2</sup>
熱流密度、放射照度	ワット毎平方メートル	W/m <sup>2</sup>	kg s <sup>-3</sup>
熱容量、エンントロピー	ジュール毎ケルビン	J/K	m <sup>2</sup> kg s <sup>-2</sup> K <sup>-1</sup>
比熱容量、比エンントロピー	ジュール毎キログラム毎ケルビン	J/(kg K)	m <sup>2</sup> s <sup>-2</sup> K <sup>-1</sup>
比エネルギー	ジュール毎キログラム	J/kg	m <sup>2</sup> s <sup>-2</sup>
熱伝導率	ワット毎メートル毎ケルビン	W/(m K)	m kg s <sup>-3</sup> K <sup>-1</sup>
体積エネルギー	ジュール毎立方メートル	J/m <sup>3</sup>	m <sup>1</sup> kg s <sup>-2</sup>
電界の強さ	ボルト毎メートル	V/m	m kg s <sup>-3</sup> A <sup>-1</sup>
電荷密度	クーロン毎立方メートル	C/m <sup>3</sup>	m <sup>3</sup> s A
表面電荷密度	クーロン毎平方メートル	C/m <sup>2</sup>	m <sup>2</sup> s A
電束密度、電気変位	クーロン毎平方メートル	C/m <sup>2</sup>	m <sup>2</sup> s A
誘電率	ファラード毎メートル	F/m	m <sup>3</sup> kg s <sup>-4</sup> A <sup>2</sup>
透過率	ヘンリー毎メートル	H/m	m kg s <sup>-2</sup> A <sup>2</sup>
モルエネルギー	ジュール毎モル	J/mol	m <sup>2</sup> kg s <sup>-2</sup> mol <sup>1</sup>
モルエントロピー、モル熱容量	ジュール毎モル毎ケルビン	J/(mol K)	m <sup>2</sup> kg s <sup>-2</sup> K <sup>-1</sup> mol <sup>1</sup>
照射線量(X線及びγ線)	クーロン毎キログラム	C/kg	kg <sup>-1</sup> s A
吸収線量率	グレイ毎秒	Gy/s	m <sup>-2</sup> s <sup>-3</sup>
放射強度	ワット毎メートル毎ステラジアン	W/sr	m <sup>1</sup> m <sup>2</sup> kg s <sup>-3</sup> =m <sup>2</sup> kg s <sup>-3</sup>
放射輝度	ワット毎平方メートル毎ステラジアン	W/(m <sup>2</sup> sr)	m <sup>2</sup> m <sup>2</sup> kg s <sup>-3</sup> =kg s <sup>-3</sup>
酵素活性濃度	カタール毎立方メートル	kat/m <sup>3</sup>	m <sup>-3</sup> s <sup>-1</sup> mol

表5. SI接頭語

乗数	名称	記号	乗数	名称	記号
10 <sup>24</sup>	ヨタ	Y	10 <sup>-1</sup>	デシ	d
10 <sup>21</sup>	ゼタ	Z	10 <sup>-2</sup>	センチ	c
10 <sup>18</sup>	エクサ	E	10 <sup>-3</sup>	ミリ	m
10 <sup>15</sup>	ペタ	P	10 <sup>-6</sup>	マイクロ	μ
10 <sup>12</sup>	テラ	T	10 <sup>-9</sup>	ナノ	n
10 <sup>9</sup>	ギガ	G	10 <sup>-12</sup>	ピコ	p
10 <sup>6</sup>	メガ	M	10 <sup>-15</sup>	フェムト	f
10 <sup>3</sup>	キロ	k	10 <sup>-18</sup>	アト	a
10 <sup>2</sup>	ヘクト	h	10 <sup>-21</sup>	ゼット	z
10 <sup>1</sup>	デカ	da	10 <sup>-24</sup>	ヨクト	y

表6. SIに属さないが、SIと併用される単位

名称	記号	SI単位による値
分	min	1 min=60 s
時	h	1 h=60 min=3600 s
日	d	1 d=24 h=86 400 s
度	°	1°=(π/180) rad
分	'	1'=(1/60)°=(π/10 800) rad
秒	"	1"=(1/60)'=(π/648 000) rad
ヘクタール	ha	1 ha=1 hm <sup>2</sup> =10 <sup>4</sup> m <sup>2</sup>
リットル	L	1 L=1 l=1 dm <sup>3</sup> =10 <sup>3</sup> cm <sup>3</sup> =10 <sup>-3</sup> m <sup>3</sup>
トン	t	1 t=10 <sup>3</sup> kg

表7. SIに属さないが、SIと併用される単位で、SI単位で表される数値が実験的に得られるもの

名称	記号	SI単位で表される数値
電子ボルト	eV	1 eV=1.602 176 53(14)×10 <sup>-19</sup> J
ダルトン	Da	1 Da=1.660 538 86(28)×10 <sup>-27</sup> kg
統一原子質量単位	u	1 u=1 Da
天文単位	ua	1 ua=1.495 978 706 91(6)×10 <sup>11</sup> m

表8. SIに属さないが、SIと併用されるその他の単位

名称	記号	SI単位で表される数値
バール	bar	1 bar=0.1MPa=100 kPa=10 <sup>5</sup> Pa
水銀柱ミリメートル	mmHg	1 mmHg≈133.322Pa
オングストローム	Å	1 Å=0.1nm=100pm=10 <sup>-10</sup> m
海里	M	1 M=1852m
ノット	b	1 b=100fm <sup>2</sup> =(10 <sup>-12</sup> cm) <sup>2</sup> =10 <sup>-28</sup> m <sup>2</sup>
ノット	kn	1 kn=(1852/3600)m/s
ネバール	Np	SI単位との数値的な関係は、対数量の定義に依存。
デシベル	dB	

表9. 固有の名称をもつCGS組立単位

名称	記号	SI単位で表される数値
エルグ	erg	1 erg=10 <sup>-7</sup> J
ダイーン	dyn	1 dyn=10 <sup>-5</sup> N
ボアズ	P	1 P=1 dyn s cm <sup>-2</sup> =0.1Pa s
ストークス	St	1 St=1cm <sup>2</sup> s <sup>-1</sup> =10 <sup>4</sup> m <sup>2</sup> s <sup>-1</sup>
スチルブ	sb	1 sb=1cd cm <sup>-2</sup> =10 <sup>4</sup> cd m <sup>-2</sup>
フォート	ph	1 ph=1cd sr cm <sup>-2</sup> =10 <sup>4</sup> lx
ガル	Gal	1 Gal=1cm s <sup>-2</sup> =10 <sup>-2</sup> ms <sup>-2</sup>
マックスウェル	Mx	1 Mx=1G cm <sup>2</sup> =10 <sup>8</sup> Wb
ガウス	G	1 G=1Mx cm <sup>-2</sup> =10 <sup>-4</sup> T
エルステッド <sup>(a)</sup>	Oe	1 Oe△(10 <sup>3</sup> /4 π) A m <sup>-1</sup>

(a)3元系のCGS単位系とSIでは直接比較できないため、等号「△」は対応関係を示すものである。

表10. SIに属さないその他の単位の例

名称	記号	SI単位で表される数値
キュリ	Ci	1 Ci=3.7×10 <sup>10</sup> Bq
レントゲン	R	1 R=2.58×10 <sup>-4</sup> C/kg
ラド	rad	1 rad=1cGy=10 <sup>-2</sup> Gy
レム	rem	1 rem=1cSv=10 <sup>-2</sup> Sv
ガンマ	γ	1 γ=1nT=10 <sup>-9</sup> T
フェルミ	f	1 フェルミ=1 fm=10 <sup>-15</sup> m
メートル系カラット	Torr	1 Torr=(101 325/760) Pa
標準大気圧	atm	1 atm=101 325 Pa
カロリ	cal	1 cal=4.1858J (15°Cカロリー), 4.1868J (ITカロリー), 4.184J (熱化学カロリー)
ミクロ	μ	1 μ=1μm=10 <sup>-6</sup> m

